Microfluidic Technologies for High-Throughput Screening Applications

Thesis by

Todd Thorsen

In Partial Fulfillment of the Requirements

For the Degree of

Doctor in Philosophy

California Institute of Technology

Pasadena, California

2003

(Defended September 23, 2002)

Acknowledgements

I came to Caltech with what many people described as “crazy ideas.” Coming from a Masters degree in Public Health (M.P.H.) from the University of California at Berkeley, I was interested in developing high throughput diagnostic technology for infectious agents that would replace expensive, state-of-the-art equipment out of reach to most public health laboratories. This was the beginning of my journey at Caltech, a journey that took me through a wide range of disciplines and a large number of laboratories. At Caltech, I really learned about the true meaning of collaboration as I struggled to build up my vision one piece at a time. Without the help of numerous professors and students, my work would have never been possible.

First, I would like to thank all of my advisors, who became like family over the past five years. I am forever in their debt for not only giving me access to resources within their laboratories, but also for patiently listening to my ideas and giving me moral support in times where it seemed like all paths led to failure. I would like to thank Dr. Richard Roberts for all of his valuable combinatorial chemistry advice and the generous use of lab space and supplies during my early polymer development work, and Dr. Frances Arnold for introducing me to the world of complex systems. I am deeply grateful to Dr. Stephen Quake, who stood by my side countless times, patiently giving me advice on a large variety of subjects, ranging from microfluidics to optics and electronics.

Second, I would like to thank a large number of professors outside of my field that directly or indirectly had a large impact on my research. I would like to thank Dr. Robert Grubbs for his polymer expertise and resource, and Dr. John Baldeschweiler for his helpful discussions on emulsion technology. A special thanks goes out to Dr. George

Georgiou for allowing me to work at his laboratory at the University of Texas at Austin on the flow cytometry study of bacterial enzyme systems.

Finally, I would like to thank all of the graduate and postdoctoral students that worked alongside me for their help in numerous situations where I just didn't have the technical expertise to go the distance alone. I would like to thank Dr. Mark Unger and Dr. Hou-pu Chou for their discussions and help in the area of microfabrication. To Sebastian Maerke, I am grateful for the days and nights he worked with me on setting up the valve and optomechanical systems. Finally, thanks to Dr. Markus Enzelberger for his work on the enzymatic screening systems in droplets. To all of you and countless others, I could not have done it alone.

Todd Thorsen

Pasadena, California

April, 2002

Abstract

In this thesis, I present a strategy for the design and development of microfluidic devices for high-throughput screening applications, such as mutant enzyme libraries expressed in prokaryotic hosts, where a few point mutations at the DNA level translates to hundreds of thousands of enzyme variants. The work falls into three main sections. Section I addresses fundamental research in polymer chemistry, where I explore the suitability of several polymers for microfluidic applications, examining properties such as molding, fluorescence, solvent compatibility, and adhesion/sealing to glass substrates. Section II describes my development of a two-phase microfluidic device, in which I report on crossflow-based dynamic formation of picoliter-sized water droplets in a continuously flowing oil-surfactant stream. A predictive model describing the fluid dynamics of droplet formation in this model is presented as well as its applications in screening bacterial populations. Section III reports the development of multilayer soft lithography technology using silicone rubber to build addressable high-density microfluidic arrays with thousands of integrated mechanical valves. This technology, which introduces the concept of fluidic large scale integration, is presented as a high-throughput parallel method to analyze bacterial enzyme expression at the single cell level. The detection of enzymatic activity in these high-density microarrays is described, comparing a self-constructed solid-state laser apparatus with a modified scanner (Axon Industries) used for looking at DNA arrays.

Contents

List of Figures

Chapter 2

Chapter 3

Chapter 5

Chapter 6

List of Tables

Chapter 1 – Overview

1.1 Introduction

Technological advances in chemical engineering and molecular biology have opened up a whole new world in which we can generate millions of unique compounds through combinatorial techniques. The diversity of these systems drives the need for efficient high-throughput screening (HTS) technology. However, characterization of these systems is far from a trivial process. Several platforms have emerged in the last few years to array or compartmentalize chemical libraries, including high-density 3456 well microtiter plates[1], bead-based optical fiber arrays[2], and high-density bead-based combinatorial libraries[3]. Unfortunately, the sophistication of the assay techniques has led to increasingly complex and expensive support instrumentation, with the bulk of industrial research going into miniaturizing microplates, building better robots to handle microplates, engineering better fluid dispensers, and building detection units capable of reading the "ultraminiaturized" plates[4].

The emergence of "lab-on-a-chip" microfluidic systems offers an exciting new platform for HTS technologies[5]. Unlike high-density microplate systems, often referred to as μHTS because of their ability to screen compounds in microliter-sized sample volumes, microfluidic networks, consisting of micromachined[6] or molded[7,8] channels with micron dimensions, have the capability to reduce individual assay volumes to picoliters. In addition to reduced reagent consumption, other benefits of microfluidic systems include rapid device prototyping, disposability, and the ability to create highly integrated addressable channel networks with multifunctional possibilities. Far from

being a mature technology, there is still a lot of work to be done to optimize microfluidic devices for HTS applications. State-of-the-art commercial microfluidic devices are principally made by the micromachining of silicon[9] and glass, and rely on electroosmotic flow[10,11] to drive liquid through the channels, requiring high salt concentrations and a voltage source. This process generates gas bubbles, creating ionic conditions that are far from optimal for assays like enzymatic activity or protein-protein binding interactions. Other problems with hard polymer microfluidic devices include the need to build up layers to efficiently seal the channel networks, making layer-layer adhesion a serious concern during the fabrication process, and the lack of a good compartmentalization technology for the large scale analysis of chemical or biological libraries.

The goal of this thesis is not to offer the solutions for specific screening problems, but rather to offer a general platform for addressing them. I describe the development of microfluidic devices for HTS applications having highly flexible parameters; a microencapsulation device suitable for aqueous solutions as well as organic solvents and a series of microfluidic devices with integrated elastomeric valves that function as high-density addressable arrays with picoliter volumes. Both of these systems create individual microenvironments with high informational content where thousands of single cells or small molecules such as DNA or proteins can be individually compartmentalized and examined. Model biochemical systems are presented to illustrate their potential as screening and selection tools in combinatorial assays such as recombinant enzyme libraries generated by random mutagenesis.

Having worked in industry for several years, I have been indoctrinated with the principle of quality control. The design process for an experiment is as critical as its

development. To this end, I present the research in this thesis from its "foundations," starting with the essential material components of the microfluidic devices, the polymers, transitioning to the design and development of each type of device, and finally to its applications. An organizational layout of each chapter follows for easy reference.

1.2 Organization

Chapter 2. Polymers and Microfluidics: Chemical and Mechanical Properties

Several polymeric materials are explored as materials for microfluidic devices. Properties such as swelling in organic solvent, elasticity, and adhesion are explored.

Chapter 3. Microfluidic Crossflow: Dynamic Droplet Formation

The technique of generating droplets in a two-phase microfluidic system is outlined. Initial discussion focuses on design and fabrication techniques, followed by theoretical work in which a predictive model is proposed to describe the droplet formation.

Chapter 4. Crossflow: Biochemical Screening Applications

A modified design of the original microfluidic crossflow device is presented for HTS applications using a model enzyme in a bacterial expression system. Physical parameters such as flow balance and surfactant effects on the system are addressed.

Chapter 5. Complex Addressable Microfluidic Arrays

This chapter covers the design and fabrication of complex microfluidic devices using multilayer soft lithography techniques. Using elastomeric polymers, the concept of

mulitplexors is described, creating addressable fluidic networks. Building on this technology, microfluidic large-scale integration (μLSI) is discussed, enabling hundreds of fluid channels to be controlled with few external components. Finally, the design, fabrication, and mechanics of several elastomeric prototypes for HTS are introduced.

Chapter 6. Complex Microfluidic Arrays: Biochemical Assays

Applications for the complex addressable microfluidic array devices are discussed, including *in vitro* protein synthesis and bacterial enzyme expression systems. Emphasis is placed on both screening strategies and the development of detection systems to quantitate enzyme expression at the single-cell level.

Chapter 2 - Polymers and Microfluidics: Chemical and Mechanical Properties

2.1 Introduction

Polymers are the most promising materials for microfluidic technologies since they can be used in mass replication technologies such as hot embossing, injection molding, laser micromachining, and casting[12]. The choice of polymer for a microfluidic device depends on its specific application. Polymers exhibit a wide range of mechanical properties, i.e., elasticity, hardness and brittleness, temperature stability, chemical resistance, and optical characteristics. Given the wide spectrum of available polymers, there is an acceptable material for nearly every application.

Polymer, coming from the greek *polumers*, meaning having many parts, is a macromolecular substance produced by the linking of repeating chemical units. The polymerization of the individual subunits, the monomers, can be started by a chemical substance, an "initiator" or by a change in physical parameters (i.e. light, temperature or pressure). In most polymers, the chain length is quite long and the polymer is considered a bulk material. As the absolute chain length for a specific polymer is highly variable, the melting point is not absolute, but rather defined within a temperature range in which the viscosity of the polymer undergoes a transition from a solid to a highly amorphous mass. At higher temperatures, another phase change occurs where the bonds within the

polymer chains become unstable, and thermal cracking begins to occur, leading to mechanical failure[13].

An important characteristic of a polymer is its glass transition temperature, T_g. When a polymer is cooled below this temperature, it is solid. Some polymers are used below their glass transition temperatures, like polystyrene and poly(methyl methacrylate) with T_gs well above 100°C, where they are hard and brittle. Other classes of polymers, such as elastomers, are used above their T_gs in a rubbery state, exhibiting properties such as softness and flexibility[14]. For fabrication processes, where the polymer is cast or injection molded, T_g is a very important parameter. As the temperature is increased over T_g, it is in a viscoelastic state and can be easily molded[12]. Removing the polymer from the mold prior to cooling below the T_g can be extremely detrimental, affecting the geometric stability of the molded pattern. Softeners can be used to lower the glass transition temperature and facilitate molding at lower temperatures. However, they chemically weaken the polymer matrix by intercolating between the polymer strands or by acting as chain termination elements.

Plastics can be classified into three categories based on their molding behavior, which is based on the manner that the monomers interconnect within the polymer chains. (i) *Thermoplastic polymers*. These polymers primarily consist of entangled chains of linear polymers. As the strands are typically long and unbranched, cross-linking between strands rarely occurs. They are relatively soft and can be easily deformed. At temperatures above the glass transition, they are easy to mold and will retain the molded shape when cooled below T_g[15]. Examples include polyethylene, polystyrene and nylon. (ii) *Elastomeric polymers*. Elastomers consist of weakly cross-linked polymer chains. The

backbones of these polymers are sterically less hindered than the thermoplastic polymers, allowing greater flexibility around the backbone. For example, the silicone polymers, of which poly(dimethylsiloxane) is an example, have very low T_g values (in this case -123°C) because the Si-O-Si linkage is very flexible and deformable. In response to an external force, elastomeric materials are readily stretched, but return to their original state (higher entropy) when the force is removed. (iii) *Duroplastic polymers*. These polymers are characterized by a high degree of cross-linking. It is necessary to cast these materials into their final shape using monomer and catalyst. The resulting product is typically hard and more brittle than thermoplastics. Examples include dicyclopentadiene and calcium fluorine polymers.

2.2 Specific Polymer Properties

Prior to designing actual functional microfluidic devices, I examined the physical and chemical properties of several polymers and polymer blends to find a material that would be suitable for my applications. As my original concept for a microfluidic screening device involved an encapsulation technology based on reverse micelles, a water in oil (w-o) emulsion system and a fluorescence detection strategy (see Chapter 3), I needed a polymer exhibiting excellent alkane resistance. Other important features included good optical clarity and low background fluorescence. While elasticity was not a strict material requirement in the production of early device prototypes, it was generally considered to be a useful property for making devices that are easy to remove from molds and seal to solid support structures such as glass. The lab was beginning to experiment with polydimethylsiloxane (PDMS) for the fabrication of simple T-junction based

devices for sorting DNA and cells using electrophoretic techniques[10], so this provided a natural starting material for my early studies. As PDMS proved to have inadequate chemical resistance against most oils, exhibiting swelling and degradation, my work broadened to investigate other groups of polymers, including dienes, urethanes and block co-polymers. A summary of this research follows.

2.2.1 Silicone-based Polymers

Silicone is a generic term for an entirely synthetic polymer containing a repeating Si-O backbone. The organic groups attached as side chains via silicon-carbon bonds define the class of the silicone[16]. Depending on the chain length and the nature of the organic groups, silicones can exist as emulsions, lubricants, fluids, resins, or elastomers. The most common and widely used elastomer is PDMS, having the basic repeating unit, $[(CH_3)_2SiO]$ (Figure 2.1).

Figure 2.1: Structure of repeating PDMS subunits.

Polydimethylsiloxane (PDMS)

Structure and Mechanical properties

Silicone-based polymers such as PDMS have become a popular material for replica molding and stamp making using soft lithography techniques[17]. Classified as an elastomer, PDMS has a Young's modulus (Y) value of ~1 MPa, making it relatively stiff

yet much more flexible than traditional micromachined materials like silicon (Y = ~1 GPa). The Young's modulus of PDMS depends on the extent of cross-linking between linear silicone chains. The cross-linking reaction is initiated by organic peroxides (Figure 2.2) or rare metal catalysts such as platinum (Figure 2.3). Silicones cross-linked by organic peroxides are typically one-part systems. The pre-catalyzed mixture consists of linear silicone chains and the peroxide catalyst. Curing is accomplished by heating the

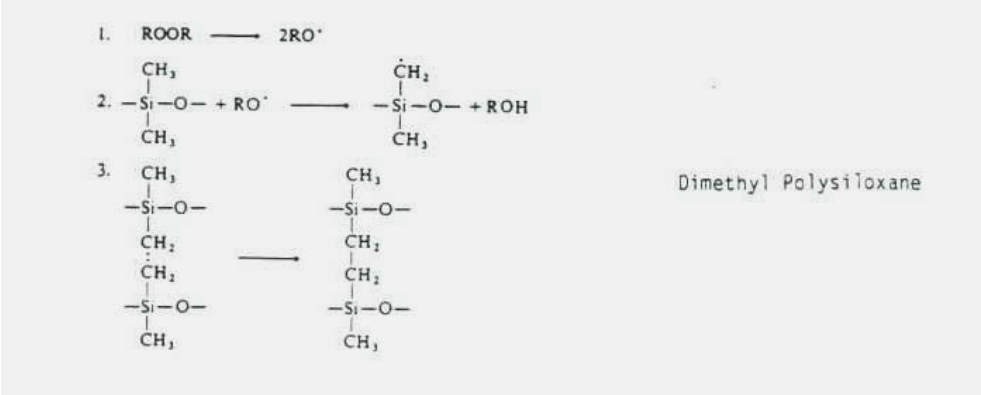

Figure 2.2: Peroxide-based mechanism for PDMS cross-linking

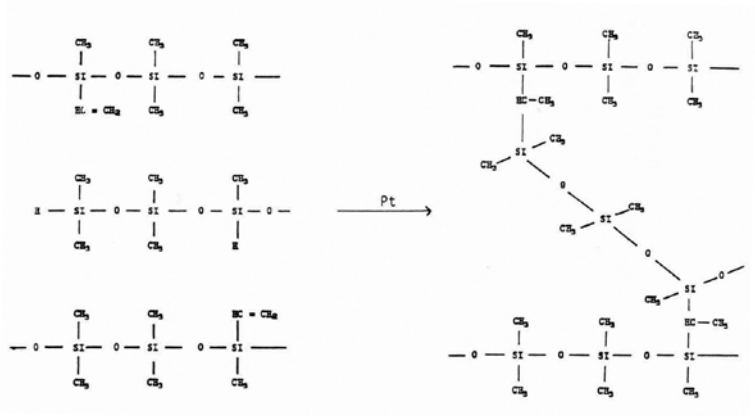

Figure 2.3: Platinum-based mechanism for PDMS cross-linking

mixture to break down the peroxides into free radicals, which initiate cross-linking between the side chain groups. The cure time depends on the activation temperature of the peroxide catalyst and the thickness of the part. The second method for curing silicone rubber utilizes a silicone hydride (SiH) cross-linking agent in conjunction with methylvinyl silicone polymer. In the presence of a precious metal catalyst such as platinum, a true addition reaction occurs, resulting in a uniformly vulcanized rubber without curative by-products[18]. As this reaction occurs quite readily at room temperature, the silicone precursor is sold as a two-part system, with one part containing the Pt crosslinking agent combined with silicone hydride substituted monomers and the other consisting predominantly of methylvinyl-based silicones, that is mixed just prior to casting. Crosslinking efficiency is affected by the spacing between the hydride groups and as well as the vinyl level of the precursors.

Chemical Resistance

PDMS is intrinsically hydrophobic, with the advancing contact angle of water at ~110°C. Its elastomeric structure makes it susceptible to swelling not only to alkanes, but also to halides, and strong acids and bases. Relative bulk swelling of PDMS was carried out in several solvents by immersing approximately 1 gram samples of the polymerized silicone (General Electric RTV 615 (10:1 part A:B)) in solvent and comparing their weight before and after (15 min) exposure to solvent (Table 2.1). However, these chemical resistance values were obtained using bulk polymer and provide only a rough estimate of the chemical compatibility of a particular solvent on the microfluidic scale.

To measure the solvent effects on the microscale, I fabricated simple prototype devices consisting of PDMS poured over a silicon master mold (Figure 2.4).

Bulk Silicone Solvent Resistance (General Electric RTV 615)

Solvent	~% Weight Increase (Post Exposure)	Visible Swelling
dH_2O	0.0	none
3 M HCl	2.0	low
1 M NaOH	0.5	low
EtOH (conc.)	3.2	moderate
Acetone	8.0	moderate
Toluene	85.0	high (degradation)
Mineral oil	5.4	moderate
Decane	45.0	high
Silicone oil	25.0	high

Table 2.1: Solvent resistance properties of bulk silicone (RTV 615)

To fabricate the silicon master mold, a silicon wafer was patterned and chemically wet-etched. A virgin <100> silicon wafer with a thin oxide layer was spin-coated with a thin layer of photoresist (SJR 1813, Shipley), soft baked at 85°C for 30 minutes, and subsequently patterned using a UV contact mask aligner with parallel lines and "T" channels with a width of 100 μm. The pattern was then developed with 20% v/v CD30 developer (Shipley) in water for 10 seconds. At this stage, the wafer has a positive photoresist pattern of the channels on the surface. The wafer was then wet-etched with 10% hydrofluoric acid to remove the oxide layer not covered by resist, followed by an

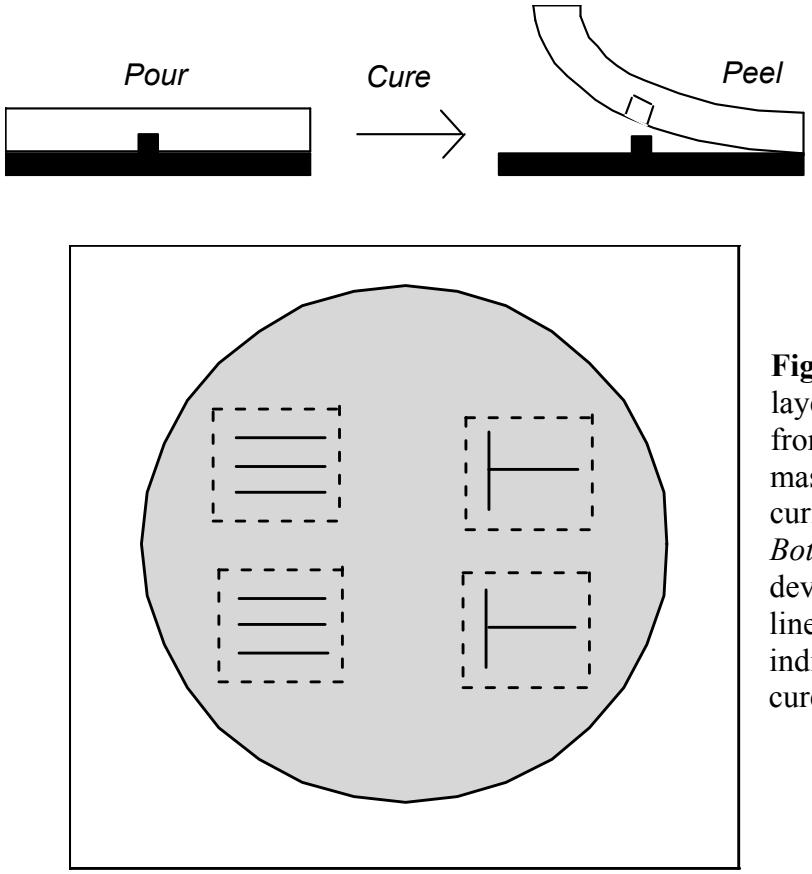

Figure 2.4: Fabrication of one-layer PDMS devices fabricated from a wet-etched silicon wafer master mold. *Top*: Casting and curing process for PDMS. *Bottom*: Channel mold for four devices (bird's eye view). Dotted lines not part of mold, but rather indicate cut positions to remove cured devices from mold.

anisotropic etch with KOH (50 g solid KOH in deionized water) at 50°C for 30 minutes at an etch rate of 0.2 μm/min. The final mold consists of channels ~100 μm in diameter and 6 μm deep. PDMS devices were then made using the silicon mold. To cast the devices, 10:1 part A/B RTV 615 was poured over the mold in a petri dish to a depth of 1 cm over the mold and cured at 80°C for 30 minutes. The 1" square devices (shown as four patterns on the wafer bound by dashed borders- two consisting of three parallel lines and two T junction patterns) were then cut from the mold. Holes were then punched with a 20G (I.D.= 585 μm) beveled steel punch at the channel ends and the devices were sealed hermetically to No.1 glass coverslips (VWR) at either room temperature (23°C) or in the oven (80°C) for 4 hours.

Flow tests were conducted with the devices using a syringe filled with the test solvent connected to a regulated pressure source (Figure 2.5). The syringe was connected to the PDMS chip via tygon tubing terminated with a 1.0 cm length of blunt end 23G hypodermic tubing (O.D.= 635 μm), which tightly fits into the punched fluid input port. Fluid was introduced into the chip by adjusting the pressure on the regulator. The input pressure range was varied from 0.5 to 15.0 psi using PDMS chips sealed at either room temperature or baked at 80°C. As the design goal was to engineer microfluidic devices through which we could flow oil-water mixtures, solvent compatibility tests were conducted with deionized water and several oils ranging from C_7 (heptane) to C_{16} (hexadecane). Heavier pure linear chain oils are solids at room temperature. Specific measurements included pressure at which liquid swelled channel shut and delamination pressure (at which point the PDMS chip separated from the glass slide) (Table 2.2). For deionized water, no swelling was observed throughout the pressure range. The chip delaminated from the glass slide at pressures ranging from 3.0-6.0 psi for the room temperature sealed chips and 12.0-15.0 psi for the baked chips, indicative of the weak

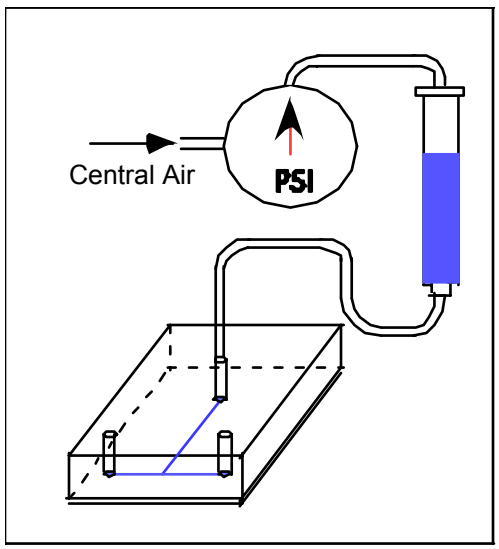

Figure 2. 5: Schematic for introducing solvent test fluids into the PDMS microfluidic devices. A regulator is used to precisely control the pneumatic pressure used to introduce the solvent into the chip.

non-covalent bond between the PDMS and glass. While the exact mechanism is unknown, the baking treatment probably increases the PDMS/glass bond by driving off surface water molecules, and increasing the PDMS /glass contact. For all oils, the microfluidic channels exhibited swelling and subsequent channel closure at low pressure (<5 psi). Delamination due to chip distortion and swelling occurred at very low pressure for all oils except mineral oil, which was only marginally higher. However, the fact that visible swelling was observed with mineral oil still made it incompatible with PDMS (RTV 615).

Microfluidic Solvent Resistance (General Electric RTV 615)

Solvent	Channel Swelling?	Delam. psi (R.T.)	Delam. psi (80°C)
dH_2O	No	3.0 - 6.0	12.0 - 15.0
heptane	Yes	0.5	0.5
octane	Yes	0.5	0.5
nonane	Yes	0.5	0.5
decane	Yes	0.5	0.5
dodecane	Yes	0.5 - 1.0	0.5 - 1.0
tetradecane	Yes	0.5 - 2.0	0.5 - 2.0
hexadecane	Yes	0.5 - 2.0	0.5 - 2.0
mineral oil	Yes	1.0 - 3.0	3.0 - 5.0

Table 2.2: Microfluidic solvent resistance (RTV 615). Summary of solvent compatibility tests for RTV 615 silicone rubber with several organic solvents. Microlfuidic channels swelling effects are shown as well as delamination pressures for chips sealed to a cover glass at room temperature and 80°C.

Multilayer PDMS Devices

It is useful to fabricate totally sealed devices, in which the cast microfluidic device is not hermetically sealed to a coverslip, but rather to a cured thin layer of polymer spin-coated on the coverslip at high rpm (5000-6000). As PDMS (RTV 615) is normally used at a ratio of 10:1 part A:B, bonding is simply accomplished by modifying the ratio of these components in two separate layers[19]. Part A contains the platinum catalyst and the PDMS bearing the vinyl groups while part B contains a crosslinker with silicon hydride (Si-H) groups. For a two-layer device, the thick top layer used to mold the microfluidic channels is made of 3:1 A:B, giving it excess vinyl groups, while the thin bottom layer spin coated on the glass coverslip is made from 30:1 A:B. Both layers are cured for 90 minutes at 80°C. The top layer is then processed (cut to size, input holes punched) and subsequently sealed to the bottom thin layer. After an additional 90 minutes at 80°C, the two layers are covalently sealed together and can not be separated. This technique is also fundamental to the fabrication of integrated valves, as discussed in Chapter

Chemical testing in the multilayer PDMS devices was carried out using the same pressurized syringe apparatus. As the channels were no longer in direct contact with coverslip glass, delamination was not feasible. The alkanes still swelled the microfluidic channels shut at low pressure (<5 psi) for all alkanes except for mineral oil. With mineral oil, the device was filled at 10-15 psi. However, the channels eventually swelled over a few minutes, increasing the resistance to flow and rendering the devices unusable.

Chemically Modified PDMS:

After conducting chemical resistance studies on PDMS (GE RTV 615) and finding it unsuitable for oil-based compounds, some research was put into modifying the polymer

to make it less susceptible to oil absorption without compromising its mechanical properties. Studies included making surface chemistry modifications on the channel walls, blending PDMS co-polymers with fluorinated silicone derivatives, and curing PDMS in the presence of surfactants and perfluorinated additives.

Surface chemistry modification of cured PDMS

The surface of PDMS can be readily converted from hydrophobic to hydrophilic by brief exposure to oxygen plasma. A well-documented process[20-21], the Si-H groups on the surface of cured PDMS are converted to Si-OH. The advancing contact wetting angle for water, previously ~110° prior to treatment, becomes ~10°. To study the effect of oxygen plasma treatment on oil resistance, sample PDMS microfluidic devices with parallel channels were fabricated as previously described and treated with oxygen plasma (0.8 torr oxygen plasma, load coil power ~100W, 15 sec exposure). Oxygen plasma treated devices were placed on glass coverslips and baked for 4 hours at 80°C. Repeating the testing with pressurized oil solutions produced results comparable to untreated PDMS devices. While the channel surface was hydrophilic, resulting in the oils rounding up instead of wetting the channel walls upon injection into the devices, swelling was still clearly observable, stopping the flow and delaminating the PDMS from the glass surface.

Fluorinated PDMS Co-Polymers

As the surface treatment of PDMS failed to serve as an adequate barrier against the oils, fluorinated derivatives of PDMS were investigated as a potential solution to the problem. Perfluorinated compounds are unique in that they are typically immiscible in both organic solvents and aqueous solutions. The first fluorinated co-polymer we made was a mixture of 50% w/w vinyl-terminated perfluorosiloxane (Gelest) and 50% PDMS

(GE 615 10:1 A/B). The vinyl functional group on the fluorinated derivative allows it to cross-link with the PDMS under standard curing conditions. The two compounds were mixed and degassed under vacuum for 30 minutes to remove trapped gas bubbles prior to curing. The degassed mixture was poured over the parallel and T channel mold and cured for 2 hours at 80°C prior to mold release. The final cured polymer was slightly opaque and did not retain the mold pattern. Lots of air bubbles were evident at the mold surface. Additional blends were made with 10 and 25% w/w perfluorosiloxane/PDMS. For these formulations, pattern retention was improved and the gas bubbles were absent, but not as good as devices made entirely of PDMS. The fluoro- groups in the polymerized co-polymer make the devices slippery, reducing the adhesion to the glass coverslips. Swelling in heptane and decane was dramatically lower, but distortion was still evident over time and the devices delaminated from the coverslips within 5 minutes even when the channels were passively filled with solvent by gravitational flow.

Doped PDMS Devices

Doped PDMS devices were made by mixing PDMS with hydrophilic and perfluorinated compounds prior to the mixing process. For the hydrophilic hybrid device, polyethylene glycol 600 acrylate was chosen as the hydrophilic component due to the abundance of OH groups in the compound, and its vinyl group, which could potentially crosslink with PDMS during the curing process. 1, 5, and 10% w/w PEG600/PDMS (10:1 A/B GE615) was blended together. The mixtures became cloudy during the blending process. The blends were then degassed under vacuum and cured at 80°C for 2 hours. The final products were not elastomeric, having brittle, waxy consistencies that made them non-functional. The perfluorinated doped devices were made with 0.5% w/w

Fluoroguard (Dupont), a proprietary additive based on a fluorinated synthetic oil. Fluoroguard was optically clear, even when mixed with PDMS. The two compounds were mixed, degassed, poured over the silicon mold, and cured at 80°C for two hours. The final product was slightly hazy and exhibited some background green fluorescence when excited at 488 nm. Adhesion to glass coverslips was comparable to pure PDMS devices, but swelling and delamination was still problematic for all oils.

Other Silicone Polymers

In addition to General Electric 615, another formulation of PDMS was investigated as a material for fabricating microfluidic devices compatible with oil and water. The material, Dow Corning Sylgard 184, is a two-part cure PDMS that is optically clear and has a Young's modulus (2.5 MPa) comparable to that of RTV 615 (750kPa). Sylgard 184 is slightly stiffer than RTV 615, presumably due to a higher degree of crosslinking during the curing process and a different monomer formulation. More importantly, Sylgard 184 exhibits moderate chemical resistance to long-chain alkanes such as mineral oil. However, it still exhibits significant swelling in the presence on n-alkanes. In multilayer Sylgard devices, mineral oil was successfully flowed through 60μm x 10μm channels at driving pressures of 15 - 25 psi. At lower pressures, resistance due to moderate swelling inhibited flow. As initial experimentation with Sylgard 184 took place over a year after the primary polymer chemical compatibility studies were conducted, extensive experimentation with other polymers continued in the meantime. Sylgard 184 was eventually used for the fabrication of the later crossflow device prototypes discussed in Chapters 3 and 4.

2.2.2 Diene-based Polymers

Diene-based polymers like dicyclopentadiene (DCPD) solve the chemical resistance problem encountered with PDMS. As a low cost, easily obtainable by-product of the petroleum cracking process, DCPD has excellent chemical resistance against alkanes as well as inorganic acids and bases. The polymer ranges in color from optically clear to pale yellow after polymerization, depending on the catalyst, and exhibits low background fluorescence. However, DCPD is not inherently elastomeric, exhibiting a high degree of crosslinking upon polymerization that classifies it as a duroplastic. Its mechanical toughness and chemical resistance has made it a popular polymer for use in aerospace, marine, ballistic, and electronic applications.

Dicyclopentadiene (DCPD)

Structural and Mechanical properties

DCPD has excellent molding capabilities[22], and is primarily used for injection molding of items such as hazardous chemical storage tanks, boat shells, and printed circuit boards. The neat polymer is mechanically tough, with a Young's modulus value of 1.5-3.0 GPa, depending on the catalyst employed for the crosslinking. The polymerization reaction is initiated by organometallic catalysts like the Grubb's reagent (Figure 2. 6), which opens the vinyl bonds of DCPD using a mechanism in which a covalent intermediate is formed between substrate and catalyst (Figure 2.7). The reaction is commonly referred to as ring opening metathesis polymerization, or ROMP.

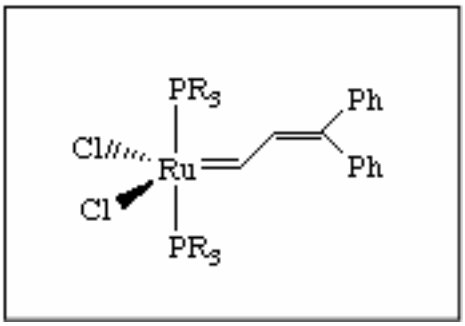

Figure 2.6: Ruthenium-based Grubb's catalyst for ROMP reactions

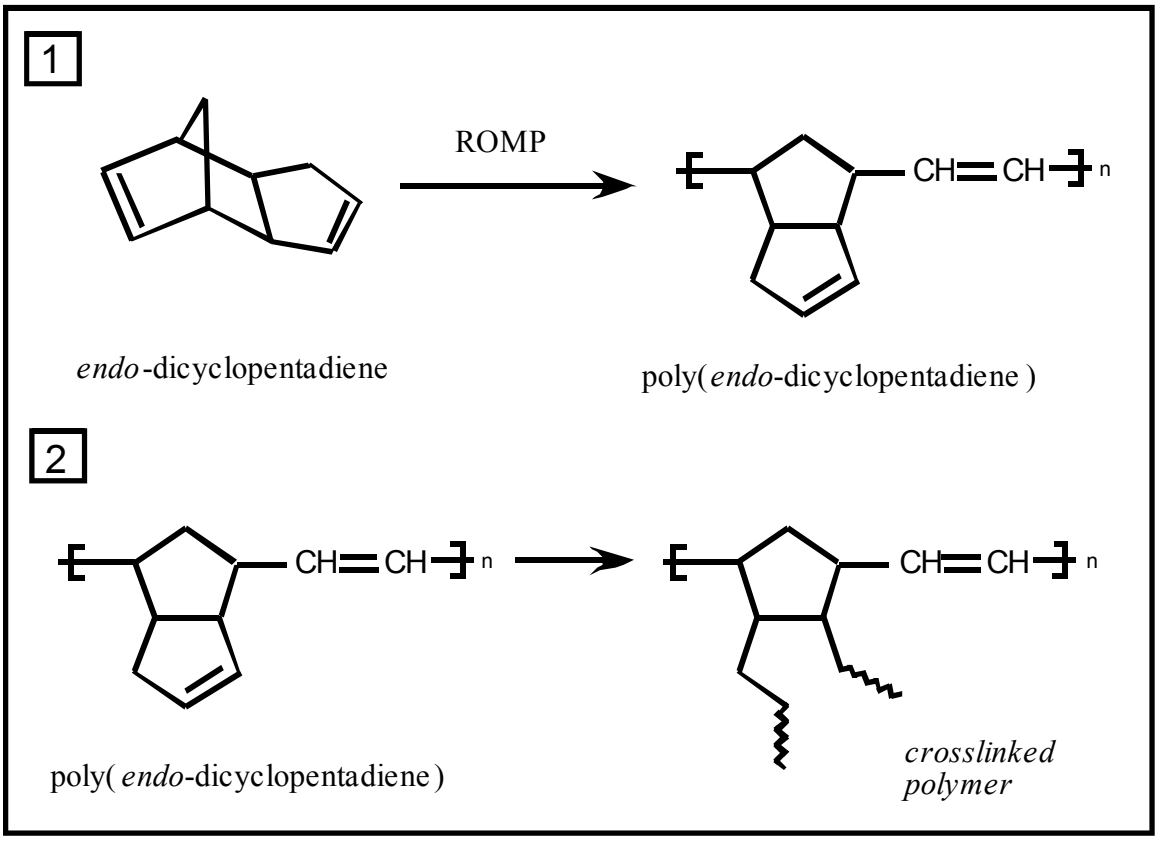

Figure 2.7: Dicyclopentadiene polymerization mechanism. Ruthenium catalyst opens the double bond in step 1. Cross-linking in step 2 occurs by traditional vinyl polymerization mechanism.

Chemical Resistance: Bulk and Microfluidic

For bulk solvent testing, DCPD (Sigma-Aldrich 99.5 % pure) was polymerized into disks in small glass petri dishes in the presence of catalyst at a monomer/catalyst ratio of 1:12,000 (mol/mol). Just prior to the reaction, the catalyst was resuspended in a small volume (~250μl) of methylene chloride and added to the DCPD monomer. The reaction mixture was cured at 200°C for 5 minutes, consuming the catalyst while boiling off excess monomer. The final product was optically clear, extremely hard, and light amber in color. As the disks were hard to break into smaller pieces, solvent testing was carried out on whole disks of polymerized DCPD by pipetting small aliquots of solvent on the disk surfaces and looking for swelling. No swelling was observed for all n-alkanes tested, ranging from heptane to hexadecane, 10% solutions of concentrated HCl or NaOH, or alcohol solutions. Some physical swelling and darkening of the polymer surface was observed for pure toluene. Overall, the chemical resistance was in agreement with the literature.

Microfluidic solvent resistance measurements were conducted using poly-DCPD devices cast from the same type of silicon molds used for the PDMS experiments. Significant problems were encountered during device fabrication. Using 1:12,000 monomer/catalyst for the molding process on the silicon wafer, the rapid polymerization at 200°C put stress on the silicon wafer, causing it to frequently crack. This problem was remedied by lowering the catalyst/monomer ratio of the mixture from 1:24,000 to 1:96,000. The final cured products showed good mold replication fidelity and were much softer than the 1:12,000 mixture. The softer products exhibited both high plasticity and elasticity, being maleable and returning to their original shape after deformation.

Adhesion to glass of the finished microfluidic devices was inconsistent. The softer poly-DCPD blend devices with the lower catalyst content showed initial excellent adhesion to a No. 1 coverslip. However, the softer blends contained a high percentage of uncured monomer, which boiled off at room temperature over time, causing the devices to curl and delaminate from the coverslips. To test the devices for solvent resistance, a clamping apparatus was designed that kept the microfluidic chips flat as pressurized solvent was introduced (Figure 2.8). The devices were sealed against a No. 1 coverslip and clamped between a piece of plexiglass and teflon with threaded holes for the syringe connection hardware. Nitrile O-rings were used to seal the interface between the poly-DCPD device input holes and the teflon plate when the clamping apparatus was tightened. Visualization of the flow through the plexiglass plate under a 10x objective of a light microscope (Olympus IX50) showed excellent chemical resistance (no visible swelling) for water and all n-alkane solvents tested (all linear alkanes from heptane to hexadecane) at external syringe pressures up to 15 psi. However, since physical clamping was necessary for the flow tests, delamination pressure studies could not be conducted.

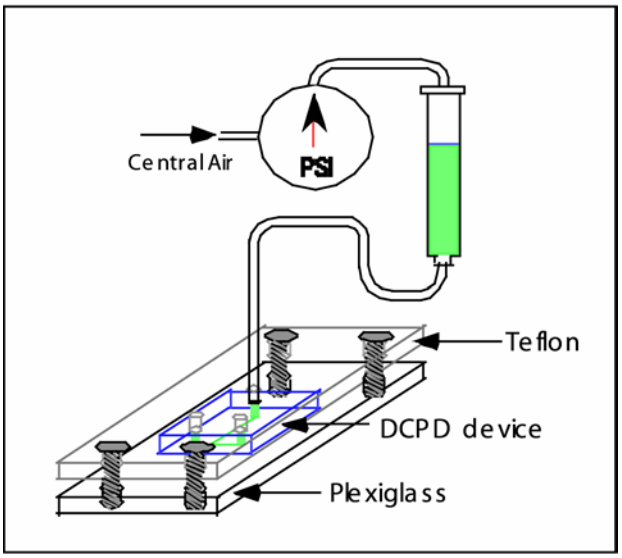

Figure 2.8: Clamping apparatus for solvent testing in polyDCDP microfluidic device.

Multilayer polyDCPD Devices

Attempts to fabricate multilayer polyDCPD devices were generally unsuccessful. Unlike PDMS, which contains a linear vinyl-terminated component and a crosslinking component, DCPD is its own crosslinker, which makes it difficult to create layers with different compositions for bonding. Some two-layer polyDCPD devices were constructed by adding extremely low catalyst concentrations to the monomer (<1:100,000 (w/w)), but layers for these devices either failed to cure efficiently, creating viscous partially cured mixtures, or, upon bonding, produced filled in or distorted channels due to uncured surface residue.

DCPD Co-Polymers

While microfluidic devices fabricated from pure DCPD exhibited low swelling in the presence of organic solvents, the necessity of using a clamping apparatus combined with a low resolution objective to image through the Plexiglass make the devices inefficient for sensitive screening applications. To address this issue, we produced a group of DCPD co-polymers that behaved less like duroplastics and more like elastomers.

DCPD-Cyclooctadiene (COD)

1,5-cyclooctadiene (COD) (Aldrich Chemicals) can be used in a co-polymerization reaction with DCPD to create a co-polymer that is softer and more flexible than polyDCPD. The ROMP reaction breaks open the COD ring to produce a reactive vinyl group that crosslinks with DCPD in reaction 2 of the traditional polyDCPD mechanism, breaking up the rigid, densely crosslinked network of polyDCPD.

Initial prototype devices were fabricated from 75% DCDP and 25% COD with a ruthenium catalyst ratio of 1:6000 (mol/mol based on DCPD). After mixing the catalyst

with the monomers at room temperature (~23°C), cure time was 85°C for 30 minutes. Complete experimental results with different co-polymer ratios are shown in Table 2.3.

Dicyclopentadiene/ 1,5-Cyclococtadiene Co-Polymers

% DCPD	% 1,5-COD	Ru Catalyst Ratio	Product Physical Properties
80%	20%	1:6000	tough, leather-like consistency no seal to coverslip high DCPD odor
50%	50%	1:6000	spongy, elastomeric consistency seals to coverslip well some DCPD odor
40%	60%	1:6000	elastomeric consistency seals to coverslip well low odor
25%	75%	1:6000	very elastomeric/plastic, soft excellent coverslip adhesion low odor *this blend had trouble curing *fresh Ru catalyst essential

Table 2.3: Dicyclopentadiene/ 1,5-cyclooctadiene co-polymer study. Different ratios of DCPD and COD create co-polymers with different physical and mechanical properties.

DCPD/COD co-polymers can be tuned to have excellent physical properties, creating soft, elastomeric polymer blends. Higher proportions of 1,5-COD produce more flexible devices, but are harder to cure. The polymerization kinetics are much slower for the co-

polymer (vs. pure DCPD), resulting in several failed polymerizations due to boil off of the methylene chloride and precipitation of the ruthenium catalyst in the mixture prior to polymerization. The co-polymerizations also leave trace amounts of uncured monomer trapped in the devices, whose potent smell is an undesirable product. However, the co-polymers with a high fraction of 1,5-COD show excellent coverslip adhesion (tested up to 30 days without delamination).

Chemical Resistance: Bulk and Microfluidic

Chemical resistance of the DCPD/COD co-polymers was comparable to polyDCPD devices. No swelling was observed for water and all alkanes (C_7 - C_{16}) in bulk tests in which solvent was pipetted on the surfaces of the co-polymers. Microfluidic tests with pressurized solvent were still difficult to conduct because we had not developed a good methodology to punch small inlet holes in the relatively tough devices. Devices cast from the silicon molds still needed to have inlet holes punched with a large diameter (~5mm) beveled steel punch, making the clamping apparatus still necessary for fluid introduction. Microfluidic solvent tests were also comparable to the results observed with polyDCPD devices. Later technological developments (see section 2.2.3- Polyurethane-based Polymers), which used a small drill bit to make ~600 μm diameter inlet holes in tough polyurethane devices, should also work for the DCPD/COD devices, eliminating the need for a clamping apparatus to introduce fluid into the DCPD/COD microchannels.

2.2.3 Polyurethane-based Polymers

Polyurethanes make up a broad class of synthetic polymers and are used in a wide variety of products such as wood sealers, synthetic fibers (Spandex), and foams. The backbone of polyurethanes consists of a urethane linkage (Figure 2.9) formed by the

addition polymerization of a diisocyanate (whose molecules contain two –NCO groups) and a dialcohol monomer (two –OH groups). The diisocyanate and dialcohol monomers in the reaction can be long, short, aliphatic or aromatic, producing polyurethanes with a wide variety of physical and chemical properties.

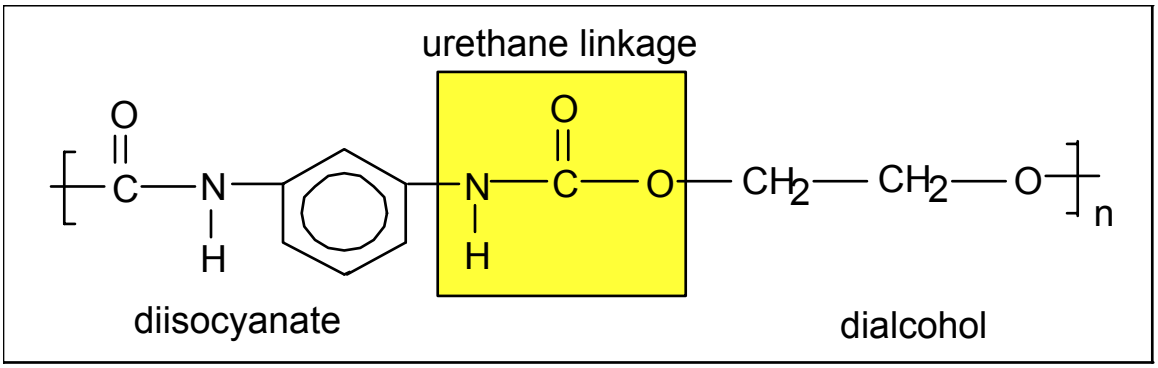

Figure 2.9: Urethane linkage diagram formed by the addition polymerization of a diisocyanate and a dialcohol group.

Urethane Diacrylate

Urethane acrylate oligomers are high molecular weight, reactive materials that can be polymerized using several free radical mechanisms, including electron beam (EB), ultraviolet radiation (UV), peroxide decomposition or Michael Addition reaction chemistry[23]. Urethane acrylate monomers are synthesized by combining a diisocyanate and a polyester or polyether polyol to yield a diisocynate terminated urethene. A subsequent reaction with a hydroxy terminated acrylate produces the oligomers. The acrylation step provides the reactive (C=C) groups on the oligomers (Figure 2.10).

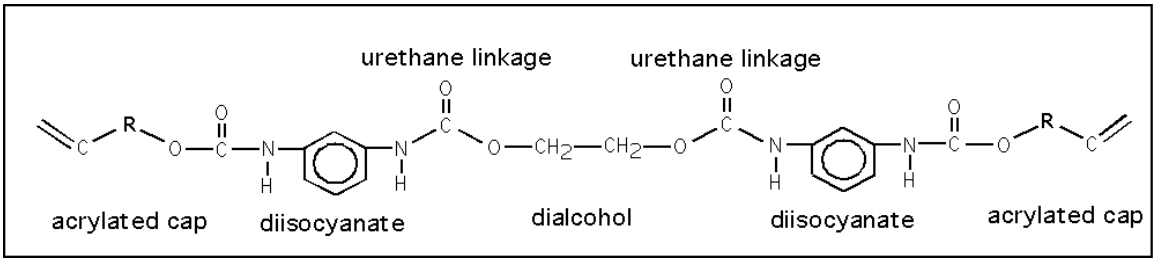

Figure 2.10: Urethane diacrylate oligomer. Reactive terminal vinyl groups are activated during polymerization.

Structural and Mechanical properties

As a chemically diverse group of polymers, polyurethanes synthesized from acrylated monomers vary from soft, rubbery elastomers to hard systems that resemble ceramics. Polyurethanes that are extensively cross-linked tend to be rigid and extremely tough, with Young's modulus values in the GPa range like silicon and pure polyDCPD. These hard, dense systems have very good chemical and moisture resistance. In contrast, elastomeric polyurethanes have a low degree of crosslinking. These polymers have good impact strength and flexibility, resembling silicones. However, the linear nature of the chemical bonds as an elastomer makes it more susceptible to the uptake of water and other hydrophilic compounds.

For our prototype microfluidic devices, we chose an aliphatic, UV-curable urethane from UCB Chemicals (Ebecryl 270). The aliphatic nature of urethane is based on the diisocyanate group present in the oligomer. While most common diisocyanates in polyurethanes are aromatic, these compounds are sensitive to UV and begin to chalk and darken when exposed to sunlight. In contrast, aliphatic diisocyanates come in optically clear or pigmented variations and are not as sensitive to UV light, properties which make them a good choice for microfluidic applications where optical detection strategies are used. The polymerized Ebecryl 270 is harder than silicone (Young's modulus ~100 kPa),

yet still behaves as an elastomer and seals exceptionally well to glass coverslips. Microfluidic pressure tests using devices fabricated from the silicon T-channel mold (100 μm wide x 6 μm deep channels) passively sealed to glass withstood pressures up to 20 psi (dH_2O) without delamination.

A UV-cure catalyst was selected for Ebecryl 270 (Irgacure 500 - Ciba Specialty Chemicals). The UV-curing process provides a rapid (<10 minutes for a 5 mm thick polymer layer), tightly controlled environment for polymerizing urethane oligomers. However, a good knowledge of the chemistry of the process is essential to understand problems such as curing failure for thin films and initial photoyellowing immediately after UV exposure.

During UV curing in air, the presence of oxygen has a detrimental effect on the cure response of free radical systems, especially for thin film coatings[23]. Molecular oxygen reacts with the free radicals generated during the curing process, forming peroxy radicals. The reactivity of the peroxy radicals is insufficient to drive the free radical polymerization process to completion, resulting in chain termination and an under-cured product. This phenomenon was observed in our initial polymerization setup, which consisted of an UV light chamber (Electolite Corporation - Model ELC 500) with 4 x 9 W bulbs (365 nm). Curing in the presence of oxygen (Ebecryl 270 with 1% Irgacure catalyst (Ciba-Geigy)) resulted in a sticky, uncured film on top surface of the polymerized urethane regardless of the exposure time (1.0-30.0 minutes) or polymer thickness (10 μm-5 mm). To solve this problem, we added a nitrogen line to the curing chamber to purge the chamber of oxygen during the curing process. Curing for 10 minutes in the presence of nitrogen resulted in evenly cured films (10 μm-5 mm).

Initial photoyellowing of UV-cured polyurethanes occurs immediately after exposure to the curing radiation. However, this initial yellowing of the polymer is partially reversible and will bleach out during the first couple of hours after exposure. The active component of the catalyst, Irgacure 500, is an α-hydroxy alkyl acetophenone (1-hydroxycyclohexyl phenyl ketone), which can form colored yellow benzil products and other semi-quinoid structures after the radical state is generated by UV light (Figure 2.11)[25]. In tests with Ebecryl 270 and 1% Irgacure 500, the cured polyurethane was translucent and bright yellow in color after a 10-minute exposure in the UV light chamber. However, after the cured polymer pieces sat at room temperature for 24 hours under fluorescent lighting, no visible coloration was evident, in support of a mechanism that the colored compounds either bleach out or undergo further reactions to yield colorless products.

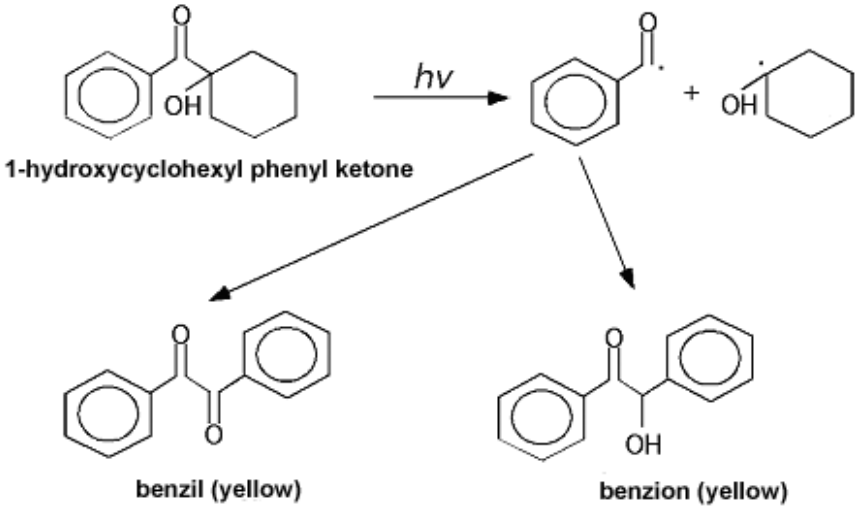

Figure 2.11: Photodegradation of 1-hydroxycyclohexyl phenyl ketone

Chemical Resistance: Bulk and Microfluidic

Bulk tests with cured Ebecryl 270 were conducted by pipetting droplets (~30 μl) on the surface of 5 mm thick polymer sections to look for physical swelling. No swelling was observed with deionized water, alkanes (C_7-C_{16}), mineral oil, and alcohols (isopropanol, ethanol), suggesting that the polymer would be appropriate for emulsion-based experiments. Microfluidic tests were conducted with T-channels devices cast from the silicon mold. Ebecryl 270 with 1% Irgacure 500 was poured to a depth of 5mm over the silicon mold. After curing in the ELC-500 for 10 minutes, the cured polyurethane was peeled away from the mold and the input holes were drilled at the channel ends with a #78 drill bit at 1000 rpm (600 μm diameter). The individual devices were then cut from the mold with a razor blade and the polymer was washed with isopropanol to remove residue from the drilling process. The finished devices were then hermetically sealed to No. 1 coverslips. Pressure tests were then conducted using the same apparatus used to test the silicone devices. The noncovalent glass/polyurethane bond was much stronger than the PDMS/glass bond, delaminating at water input pressures of 12-20 psi. No swelling was observed for all alkanes (C_7-C_{16}), and their delamination pressures were comparable to water.

Multilayer Polyurethane Devices

Multilayer polyurethane devices are easy to fabricate. We created monolithic multilayer Ebecryl 270 devices by simply washing the surfaces of two cured pieces with isopropyl alcohol to remove any oxidation products, sealing the pieces together with light pressure, and curing in the UV oven for an additional 10 minutes to crosslink the pieces at the interface. Unlike PDMS, the composition of the two pieces does not have to differ

in catalyst composition or monomer content. Activated acrylate groups at the interface efficiently initiate the crosslinking process. Using this technology, we created Ebecryl 270 microfluidic devices consisting of a thick layer (~5mm) with molded channels bonded to a No.1 coverslip spin coated with a thin layer (~20μm) of Ebecryl 270. The two-layer device withstood pressures of 50 p.s.i. (deionized water) without delamination.

2.3 Conclusions

The key to developing functional microfluidic devices for a specific application starts with the fabrication material. Elastomers like PDMS are a good choice for biological applications using water-based buffers. PDMS is easy to mold, cut and process into functional microfluidic devices. Its elasticity makes it ideal for fabricating multilayer microfluidic devices with integrated pumps and valves (Chapter 5). PDMS is a poor material choice for applications that use oils, alcohols, aromatics, strong acids or bases, exhibiting strong swelling in these solvents. Diene-based materials like DCPD exhibit much better solvent resistance, but are physically much harder, making it difficult to cut individual devices to size and seal them to glass substrates. Elastomeric polyurethanes, intrinsically hydrophilic, show excellent resistance to oils and can be fabricated as single layer microfluidic devices that seal strongly to glass coverslips or as multilayer monolithic devices. However, elastomeric polyurethanes like Ebecryl 270 should not be regarded as ideal polymers for all microfluidic applications. As hydrophilic polymers, they absorb water, ~5 - 25% by weight, depending on their formulation, making PDMS a better choice for aqueous microfluidic applications. As the academic and commercial

interest in microfluidic devices grows, we should see large advancements in research dedicated to their basic building blocks, the polymers.

Chapter 3: Microfluidic Crossflow Dynamic Droplet Formation Technology

3.1 Introduction

High-throughput screening (HTS) is an established technology in the pharmaceutical industry[26]. Over the past decade, there has been a logarithmic increase in the industry's ability to screen large combinatorial libraries of compounds against target molecules[27]. The technology to achieve this has come in the form of robotics, high-density microplates, small-volume (microliter) liquid handling, and sophisticated detection schemes. Significant industrial effort has gone into the design of HTS workstations capable of screening tens of thousands of compounds in a 24-hour period. However, these workstations come with a large price tag, often costing several hundred thousand to millions of dollars.

The goal to develop assay systems that are smaller, faster, and cheaper has been realized in the field of microfluidics. Using materials such as glass, silicon, and hard plastics such as polycarbonate, microfluidic devices have been used to demonstrate a diverse array of biological applications, including biomolecular separations[28], enzymatic assays[29], polymerase chain reaction (PCR) [30], and immunohybridization reactions[31]. Capable of analyzing subnanoliter liquid volumes, these devices typically use electroosmotic flow to manipulate liquid within the chips. Under electroosmotic flow, positive ions migrate toward the negative electrode, creating a net directional flow that

carries the other solvent molecules in the same direction. While electroosmotic flow has proved to be useful for specialized reaction conditions, it is generally inappropriate for HTS technologies. Electroosmotic flow requires a specific ionic strength that may not be compatible with platforms based on measuring catalytic activity or ligand-ligand binding affinity. Additionally, the electroosmotic fluidic circuits are not generally scalable. As channel size dimensions decrease, it becomes extremely difficult to stop flow or balance pressure differences.

In thinking about a generic design for microfluidic HTS devices, two different processing schemes become evident: serial and parallel. Using a serial strategy, each compound of interest is screened sequentially using a common microfluidic channel with a single detection element. Mechanically, throughput depends on factors such as flow speed, sample concentration, and the acquisition time of the detector. In contrast, parallel screening functions like an ultrahigh-density microtiter plate, in which thousands of compounds are arrayed into individual picoliter-scale compartments, with a detector element that probes the entire matrix. Throughput is principally limited by the number of compartments in the array.

We designed and developed microfluidic chips employing serial and parallel screening strategies. Unlike state-of-the-art microfluidic devices relying on electroosmotic flow, fluidic trafficking in our chips was achieved using integrated elastomeric valves that are scalable and whose function is independent of solvent composition. The mechanics and theory behind the serial approach, using emulsions as reaction vesicles, will be addressed in this chapter and the subsequent one, while fundamental work on the high-density parallel array chips begins in Chapter 5.

3.2 Microencapsulation

While affinity-based selection strategies have been effectively used to analyze protein-protein binding interactions using large combinatorial protein libraries consisting of billions of variants[32,33], screening such libraries for other properties such as catalytic activity has remained a challenge. Large mutant enzyme libraries are typically expressed in organisms like yeast or *E. coli*. The screening of a large cell population of the basis of biocatalytic activity primarily involves the physical separation of the cells that allows the assay of a single colony or cell[34]. Although libraries consisting of random single DNA point mutations (6×10^3 variants for a 300-residue enzyme) are feasibly screened through plate assays and spectroscopic techniques, the number of variants increases exponentially for each additional mutation, outpacing techniques which require the physical isolation of individual mutants. The critical step in the screening process is signal development that comes from exposing the expression host to the selected substrate. Elaborate HTS strategies have been devised to look at enzyme libraries, such as fluorescence-activated cell sorting (FACS) of an enzyme library tethered to the cell surface via an outer membrane protein (OmpA) linker[35]. A FRET substrate is cleaved and the product non-covalently attaches to the cell surface of the active mutants, allowing them to be sorted on the basis of fluorescent activity. However, this technique is not generally applicable to most enzyme systems, as most substrates either do not enter the cell or generate soluble products that rapidly diffuse away from the cell. In such systems, compartmentalization is needed to keep the signal associated with the cell(s) that generate it. Compartment-alization can be achieved using either a parallel approach, in which the cells are arrayed

individual chambers using elastomeric micrarrays (Chapter 5), or a serial approach, in which cells and substrate are encapsulated in vesicles like liposomes or reverse micelles and sequentially analyzed like cells in a FACS machine.

Encapsulation of biological agents is not a new concept for the pharmaceutical industry. For the past two decades, research has been carried out using liposomes as carriers for a wide variety of drugs including anti-tumor and anti-fungal compounds as well as genetic drugs such as antisense nucleotides and plasmids for gene therapy[36]. However, liposomes are difficult to prepare, requiring organic solvents to hydrate the dried lipid mixture and techniques such as sonication or french press to size the final liposomes. Problems with the final product include size heterogeneity and poor aqueous encapsulation rates, often as low as 20%[37]. An alternative to liposomes as encapsulation vesicles is emulsions, consisting of water, oil and a surfactant. Depending on the relative concentration of each component, emulsions can exist as micelles consisting of surfactant stabilized oil droplets in an aqueous solution or as reverse micelles in which water droplets are present in a bulk oil solution. While reverse micelles have the advantage over liposomes of encapsulating 100% of the aqueous phase, synthesis of homogenous emulsions has been considered a black art[38]. Recognizing their potential as miniature bioreactors, we carried out fundamental research that took us from basic emulsion formulation to the development of microfluidic devices capable of producing highly homogenous emulsions. The description and discussion of this work are the focus of this section.

3.2.1 Bulk Emulsions

Fundamentals

Emulsions are metastable colloids consisting of two immiscible fluids, one dispersed in the other, in the presence of a surfactant[39]. The relative ratio of the three fractions determines the overall morphology of the surfactant phase, which can range from oil-in-water (o/w) micelles to water-in-oil (w/o) reverse micelles with a wide range of intermediate structures such as lamellae and cylinders (Figure 3.1). For water-in-oil

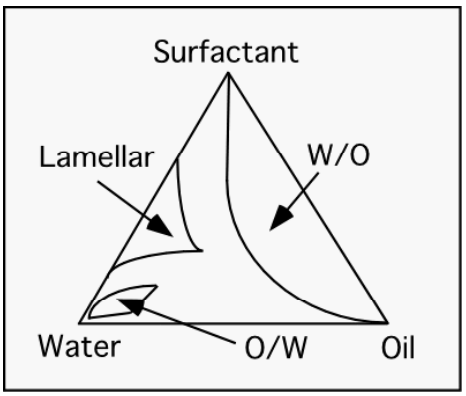

Figure 3.1: Phase diagram illustrating the relationship between the relative fractions of water/oil/surfactant and the emulsion morphology.

emulsions, the size of the reverse micelle is based on several parameters including the type of oil and surfactant used, and temperature. Short-chain oils penetrate the surfactant layer, increasing the spontaneous curvature of the reverse micelles and decreasing the encapsulated aqueous phase. The limit of penetration corresponds to the length of the surfactant molecule[29]. Similarly, short chain surfactant molecules form small reverse micelles with a high spontaneous curvature. Higher temperatures lead to the formation of larger reverse micelles when non-ionic surfactants are used. This is due to a decrease in the size of the polar head groups as they lose ordered water molecules[30].

The degradation and destruction of emulsions occur through two mechanisms. The first, referred to as Ostwald ripening, occurs when the discontinuous phase is

sufficiently soluble in the continuous phase, gradually coarsening the emulsion over time. The second mechanism, coalescence, occurs when the surfactant is depleted at the interface between two droplets in the discontinuous phase, causing the droplets to merge. This process is accelerated by heterogeneity in the emulsion mixture. The metastability of an emulsion is correlated with surfactant concentration at the droplet interface. Appropriately formulated, emulsions can be stable for years.

Bulk Preparation - Propeller Method

The first w/o emulsion formulation experiments in the laboratory were carried out in bulk using the propeller method of Tawfik and Griffiths[38]. The rationale behind their technique was to develop a set of manufacture conditions to encapsulate combinatorial libraries of self-encoding RNA-enzyme fusions along with substrates that could generate fluorescent products. The substrates and protein fusion mixtures would be chilled to 4°C, combined, and emulsified under ice cold conditions to slow down substrate catalysis prior to encapsulation. Sorting of the enzyme containing droplets would occur by flowing the emulsion through a microchip and sorting the droplets on the basis of fluorescent intensity. For the emulsion optimization, the principal challenges were to create a formulation of an oil/surfactant mixture that was not too viscous at the preparation temperature (4°C) and to optimize the stirring conditions such that a reverse micelle preparation was fairly homogeneous. Initial w/o emulsions were created using freshly prepared 1 ug/ml fluorescein in 10 mM Tris-HCl pH 7.5 as the aqueous phase, a 9:1 ratio of Span80/Tween80 as the surfactant, and one of several alkanes as the oil phase (heptane, decane, dodecane, or light mineral oil). The oil/surfactant mixture (95% oil/ 5% surfactant) was mixed by vortexing prior to the addition of the aqueous phase. 5 x 10 µl

aliquots of aqueous phase were added to 1 ml of oil/surfactant stirred at 1200 rpm with a micro magnetic stir bar over a period of 2 minutes at 4°C. The mixture was then stirred for an additional 1 minute before being transferred to ice. Both the mineral oil and heptane-based emulsions remained as a suspension after 15 minutes, while reverse micelles in decane settled out and the dodecane emulsion solidified. The reverse micelles were examined under a 40x oil immersion lens using a light microscope equipped with a mercury lamp and green bandpass filter. Sizing of the micelles was based on a visual comparison with 1μm diameter green latex beads mixed with the sample. All of the preparations contained a heterogeneous size distribution of micelles, with the largest size distribution seen in the mineral oil based preparation. The average size (diameter) for the reverse micelles in the preparations ranged from ~0.5 μm for the hexane-based preparation to ~5-10 μm for the mineral oil based preparation, with reverse micelles in the decane-based preparation averaging ~2-3 μm. The size distribution was broad for all three preparations, spanning an order of magnitude. Several large aggregates were observed in the decane and mineral oil-based preparations (Figure 3.2).

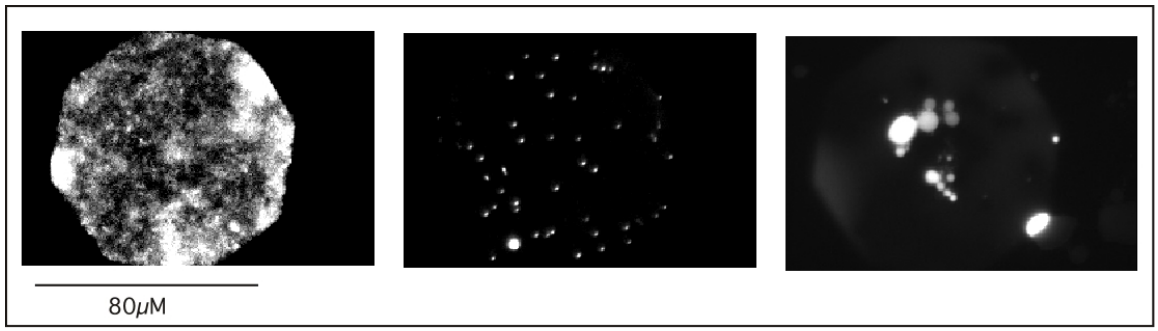

Figure 3.2: Light microscope images (40x, NA 1.2) of reverse micelles in (a) heptane, (b) decane, and (c) light mineral oil (from left to right). Reverse micelles contain1 μm fluorescein in Tris/HCl, pH 7.5. The reverse micelles in heptane are too small (<0.5 μm) to be resolved by the light microscope, and thus take on a cloudy appearance.

The principal problems with the initial emulsion preparations were turbid flow and slow propeller speed. Attempts to stir the emulsions at a faster rpm in the vials resulted in destabilization of the magnetic stir bar and non-laminar flow. To minimize turbulence and increase the stirring speed, a flat-bottom 24-well crystallography plate was used. Stable stirring speeds of up to 3000 rpm were observed at room temperature and 2500 rpm at 4°C for both heptane and decane-based emulsions. Further studies with mineral oil were discontinued due to its high viscosity. High stirring speeds (2500 rpm, 4°C) produced a fairly homogenous preparations of reverse micelles in heptane with a very small diameter (100 nm) and decane-based reverse micelles with a mean diameter of 1-2 μm. Stirring for longer periods of time after the aqueous addition (up to 10 minutes) reduced the size distribution of the prepared reverse micelles. However, long term stability of the prepared emulsions was still problematic. Coalescence of the heptane and decane mixtures was observed within 6-12 hours, creating aggregates of small (1-2 μm) and very large (>50 μm diameter) droplets.

Bulk Preparation - Crossflow Membrane Emulsification

Data acquired from the propeller studies suggested that emulsion stability could be improved and that would decrease droplet heterogeneity. Studies in the early 1990s from Japan suggested that this could be achieved through a process referred to as crossflow membrane emulsification[42,43]. The concept of membrane emulsification is simple and involves injecting the disperse phase through a porous substrate in such a way that the droplets formed at the ends of the pores at the membrane surface are sheared off by the continuous phase flowing normal to the membrane surface[44] (Figure 3.3). This procedure was initially carried out using microporous glass (MPG) with a tightly defined

pore size (0.5-5.25 μm) and a discontinuous oil phase sheared into a bulk water phase[42]. The formed droplets were ~3.25x larger than the pore sizes with a relative standard deviation of 10%. The problem with using glass membranes is that they are long (150 cm), cylindrical membranes used for industrial-scale production of emulsions (several liters) and are not practical for HTS applications where microliters of reagents are

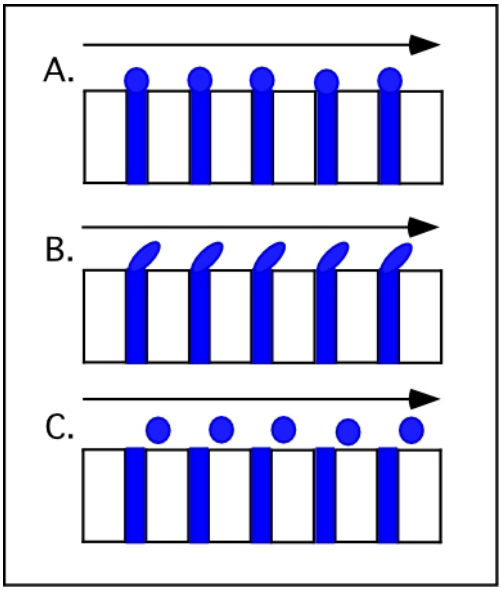

Figure 3.3: Basic stages of crossflow membrane emulsification. A) Extrusion of discontinuous phase through the pores. B) Shear of droplets at the membrane interface by the continuous phase. C) Release of monodisperse droplets into the continuous phase.

typically available. However, a good approximation of the process can be made using a single glass capillary drawn out to a narrow (1 - 10μm) diameter. Peng and Williams carried out such an experiment, generating monodisperse o/w droplets with diameters ranging from 0.5 to 1.5 μm [44].

Bulk crossflow experiments were carried out in the laboratory using a syringe-capillary hybrid device, which was used to inject the discontinuous water phase into the oil/surfactant solution (decane, 4.5% Span 80, 0.5% Tween 20). To fabricate the syringe device, a 5 μl capillary tube (Drummond Scientific) was heated over a low gas flame and

a 26 3/8 G needle was forced into the capillary, expanding it. The needle capillary junction was then sealed with epoxy. The capillary attached to the needle was drawn out over a low gas flame to narrow its diameter. Crude estimates of final inner diameters of capillaries drawn by this method, made by visualization under a light microscope, ranged from 1-10 μm. The syringe-capillary apparatus was filled with water, clamped in a ring stand, and a mass was put on the drawn plunger to generate a constant flow into the stirring continuous phase (Figure 3.4). Flow rate was estimated by collecting droplets

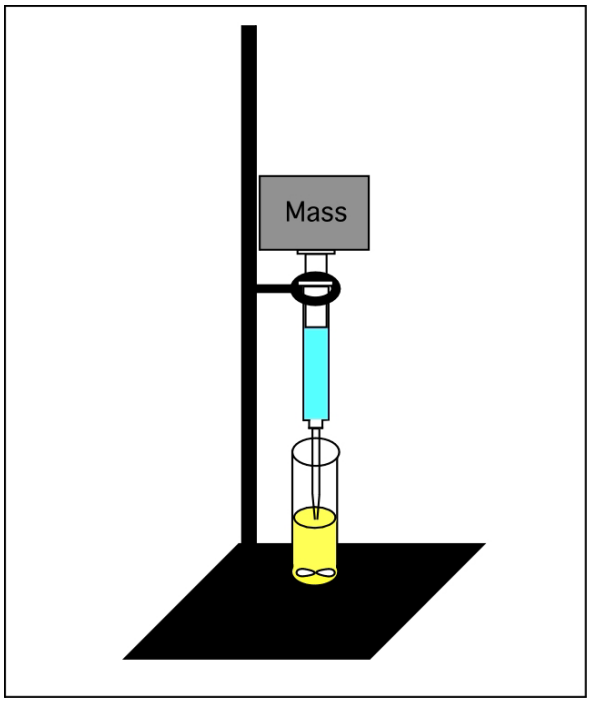

Figure 3.4: Experimental setup for capillary-based crossflow (w/o) emulsification experiment. A constant mass over the syringe provides a constant flow rate as water is introduced into the stirring continuous phase.

of water from the capillary tip prior to the emulsification process and weighing them on a precision balance (Mettler Model AG104). For a 180 g mass, flow rate from a capillary tip (i.d. ~5 μm) was ~1 μl/minute. The microcapillary crossflow emulsification experiment was conducted by immersing the capillary tip in a crystallization chamber containing 2 ml of the stirring continuous phase (decane/4.5% span 80/0.5% Tween 20, 4°C, 1250 rpm) and injecting a total volume to10μl of water over a period of 10 minutes.

The final emulsion was still highly polydisperse (0.5 to 10 μm diameter droplets, ave. ~ 3 μm). Problems encountered during the experiment that contributed to the polydispersity included evaporation of the decane in the continuous phase (~25% of the total volume over 10 minutes at 4°C) and the roughness of the capillary tip surface. Additional experiments were conducted, including changing the stir speed of the continuous phase (500 - 2000 rpm), rounding the tips of the drawn capillaries over gas flame, and using parafilm to seal the continuous phase chamber during emulsification to prevent evaporation. None of these modifications produced suitable monodisperse, stable emulsions. Clearly, it was necessary to have much tighter control parameters to generate monodisperse emulsions. A method was needed that provided excellent control over pore size, contact angle, and flow rate at the shear interface. The answer was found in microfluidics.

3.2.2 Microfluidic Crossflow

Fundamentals

Sometimes, the most beautiful experiments are the simplest ones. Microfluidic crossflow devices spontaneously make vesicles by using two perpendicular intersecting microchannels to shear the discontinuous phase into the continuous/ surfactant phase. The resulting monodisperse, stable droplets are generated at a frequency controlled by the input pressures of the two phases.

The initial designs for crossflow microfluidic devices started with the concept of extruding water into the oil phase. Reported data from the crossflow experiments carried out using microporous glass[42,43] and single glass capillaries[44] suggested that the two critical parameters were the dimensions of channel (or pore) through which the

discontinuous phase is introduced into the continuous phase and the contact angle of the shear force. Transferring this technology to the microfluidic realm required extensive design revisions, a good fabrication methodology, and optimization of the on-chip emulsion chemistry. The documentation of this work, leading to the invention of the microfluidic crossflow chip, will be presented in an "evolutionary" format, beginning with the early prototypes.

Microfluidic Droplet Formation: Simple "T" channel Architecture

The first microfluidic crossflow device was designed with 50 - 100 µm wide channels, a perpendicular junction, where the two phases are mixed, a serpentine channel to incubate the contents of the vesicles, and a "T" junction for sorting the encapsulated combinatorial libraries (Figure 3. 5). At the time, sorting technology in the laboratory consisted of using electroosmotic flow to sort beads or DNA on the basis of

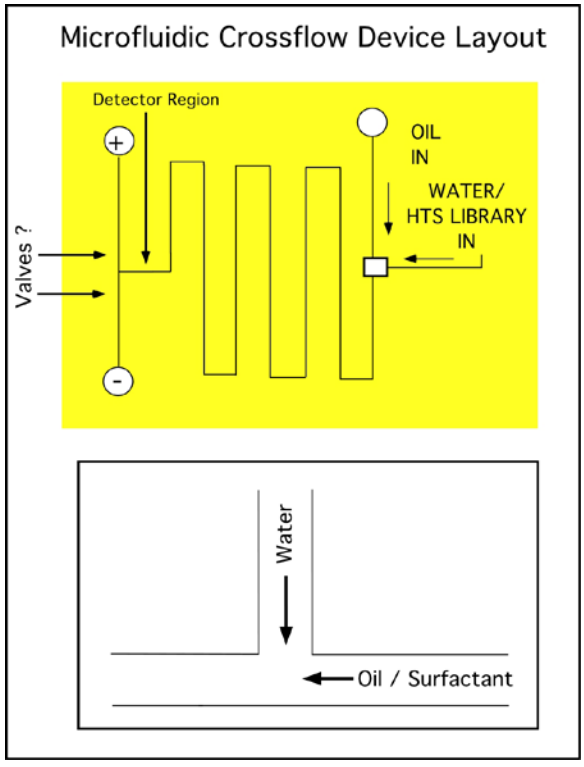

Figure 3.5: First microfluidic crossflow chip design (top). Channel widths had a single fixed valve on different prototype masks ranging from ~50 - 100 µm. Close-up of perpendicular shear junction shown at bottom.

fluorescent intensity, which could not be applied to non-conductive (w/o) emulsions. We envisioned monolithic valves fabricated on the microfluidic device that could be used for droplet sorting, but my work in this area was still in its early stages.

Initial crossflow devices were fabricated from polyurethane (Ebecryl 270), which exhibited good resistance to alkanes used in the experiments. The masks were designed using Adobe Photoshop and printed as transparencies on Linotronic film at a resolution of 3386 dpi. Film-based masks represent a cheap alternative (~$20) to chrome mask designs, which cost anywhere from five hundred to thousands of dollars, depending on the pattern size and resolution. While chrome masks can be made with sub-micron features, this type of resolution is unnecessary for most microfluidic applications. Each square pixel on the Linotronic mask is ~7.5μm on side, but the roughness of single pixels on the film limit their utility as masks to 3 x 3 pixel (22.5 μm^2) features.

Unlike the wet-etched silicon molds used to fabricate the polymer chemical resistance test devices, the crossflow devices were cast from a thick photoresist (Shipley SJR5740) that functions as the mold for the channels. SJR5740 was spin-coated on a silicone wafer pre-treated with hexamethyldisilazane vapor (HMDS) as an adhesion promoter at 3000 rpm for 60 seconds. The coated wafer was then soft-baked to remove excess solvent (85°C / 60 minutes). The wafer was then patterned using the mask aligner and developed (Microposit 2401 developer, 1:5 in dH_2O). At this point in the procedure, a positive mold of the crossflow pattern composed of photoresist is visible on the wafer surface. The mold is then hard baked at 120°C for 20 minutes on a hotplate to round the channels and promote their adhesion to the wafer. If the channels are not rounded, moderately hard elastomers like polyurethane can bond to the rough photoresist during

the crosslinking process, breaking it off the wafer during the mold release. There are other essential reasons to round the photoresist channels that will be discussed in later sections. Two layer devices were cast from Ebecryl 270 consisting of a thick molded layer (~5 mm) containing the channel structures and a thin layer of polyurethane spin-coated on a No. 1 glass coverslip (~20 µm) to seal the bottom of the channels as described in Chapter 2 (*Multilayer Polyurethane Devices*).

The first crossflow experiments consisted of simply shearing pressurized water into oil at a perpendicular microfluidic junction to produce slugs of water that traveled down the main channel to the output. While this procedure may seem counterintuitive after the extensive discussion on emulsion stabilization, surfactant (1% Span 80 in decane) was found to promote chaotic droplet break at the water/oil interface at the "T" junction. By lowering the surface tension between oil and water, surfactant forced the oil up into the water channel (Figure 3.6), disrupting the pressure balance of the system.

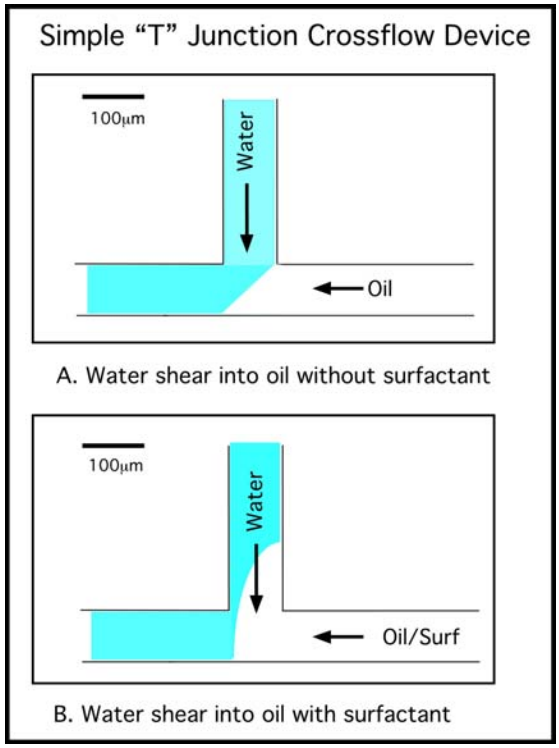

Figure 3.6: Effect of surfactant on droplet formation in a simple "T" junction polyurethane device. In the absence of surfactant (A), shear is even and regular. With surfactant in the oil phase, the oil water/interface is distorted and uneven droplet breakoff occurs.

The initial crossflow experiments with the "T" channel device utilized water and decane introduced into the respective input channels at constant pressures. To set up the experiments, oil and water were loaded into separate disposable 1cc syringes and connected to the drilled input ports with Tygon tubing fitted at the end with blunt end stainless steel adapters (23 gauge luer stub adapter - Becton Dickinson). The syringes were then pressurized with separate regulated air sources to introduce oil and water into the respective channels. At the crossflow junction, long water droplets were periodically produced (0.5 - 2.0 mm in length) as the water was sheared off into the oil (Figure 3.7), with the length dependent on the absolute water and oil pressures.

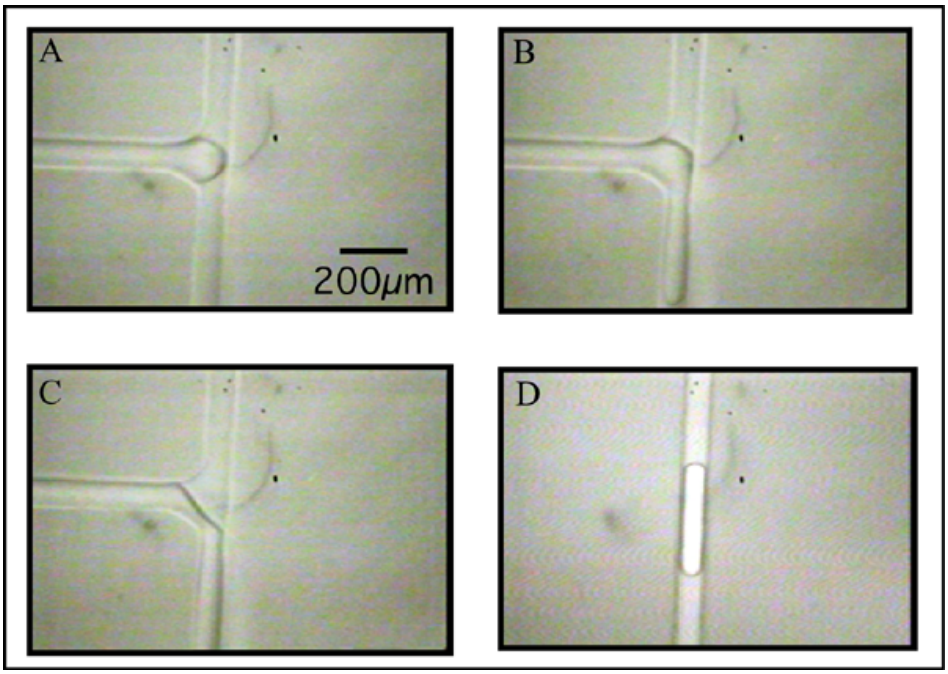

Figure 3.7: Surfactant-free microfluidic crossflow in square T- channel Ebecryl 270 microfluidic device using decane and water. A) Pressurized water entering the T-junction. B) Water enters the oil stream and is forced toward the outlet. C) The water droplet is sheared off by the oil stream. D) After break-off, the water droplet flows down the microfluidic channel toward the outlet.

Experiments were conducted using variable water and oil pressures (0 - 25 psi (0 - 180 kPa)). Droplet length and period were dependent on both the difference between the oil and water pressures and the average water/oil pressure. At higher relative water pressures, droplet breakoff occurred at a higher frequency, producing long droplets. At higher relative oil pressures, the inverse was true, with smaller droplets produced at a lower frequency (Figure 3.8).

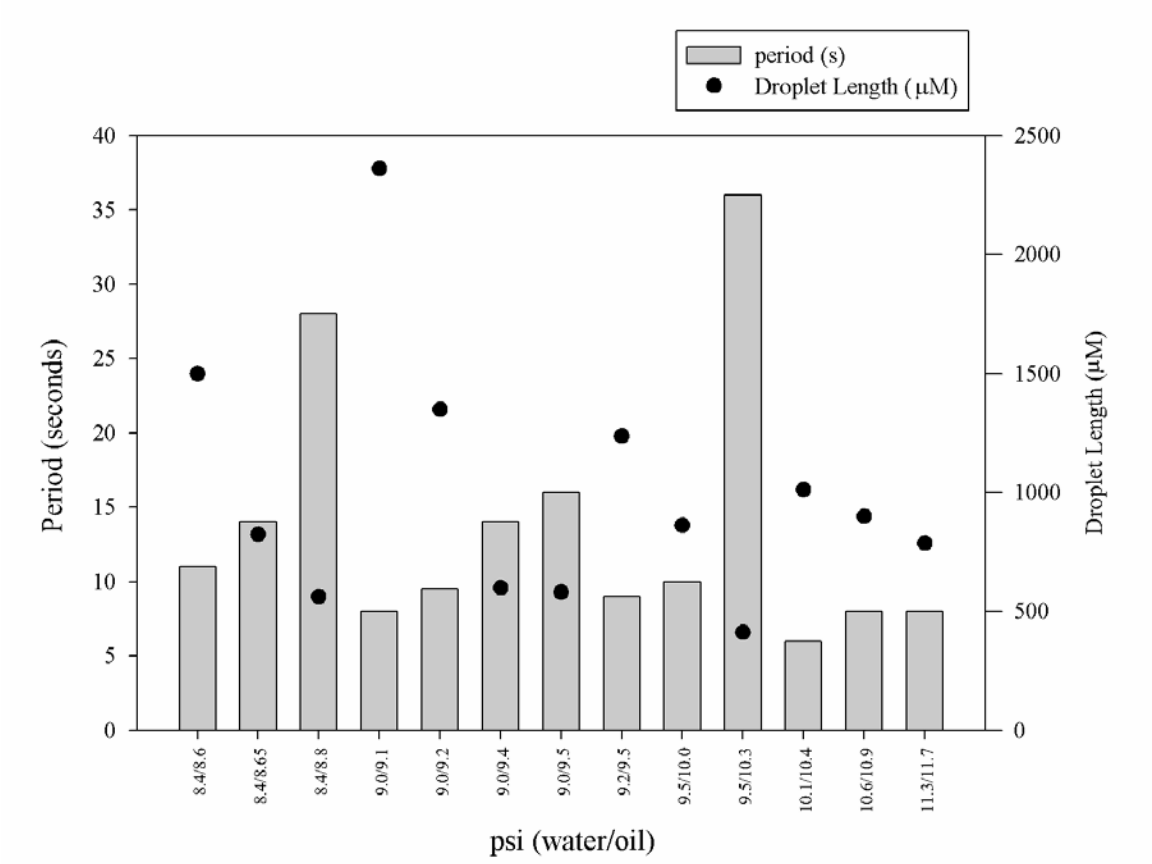

Figure 3.8: Relationship between water droplet size and breakoff frequency in a simple "T" junction polyurethane microfluidic device using pressurized decane and water.

In an effort to increase the frequency of droplet generation in the devices, pumping the water into the oil phase at the T-junction was explored. The main problem with the passive crossflow observed in the water/decane system was the duration between droplet formation (5 - 20 seconds). The proposed solution to this problem was to vary the input pressure to the water syringe using a solenoid valve and two regulated air pressure sources (Figure 3.9). By switching between the two air sources, water could be pulsed at the T-junction, shearing off a single droplet of water each cycle. The solenoid-based

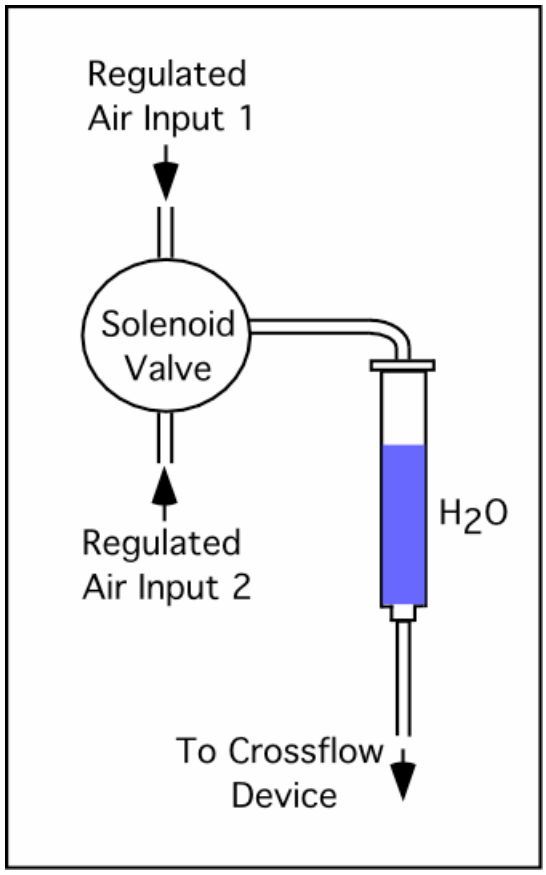

Figure 3.9: Layout for solenoid valve driven pump for pulsed droplet formation.

valve (Neptune Technologies - 15 psi max) also needed a driver to switch between the two input pressures. A circuit was designed that uses a function generator for this purpose (Figure 3.10). A square wave function was used to set the rate that the valve toggled

between the two input pressures as well as the duty cycle of the valve. However, under experimental conditions using water and decane in the polyurethane chip, pumping only

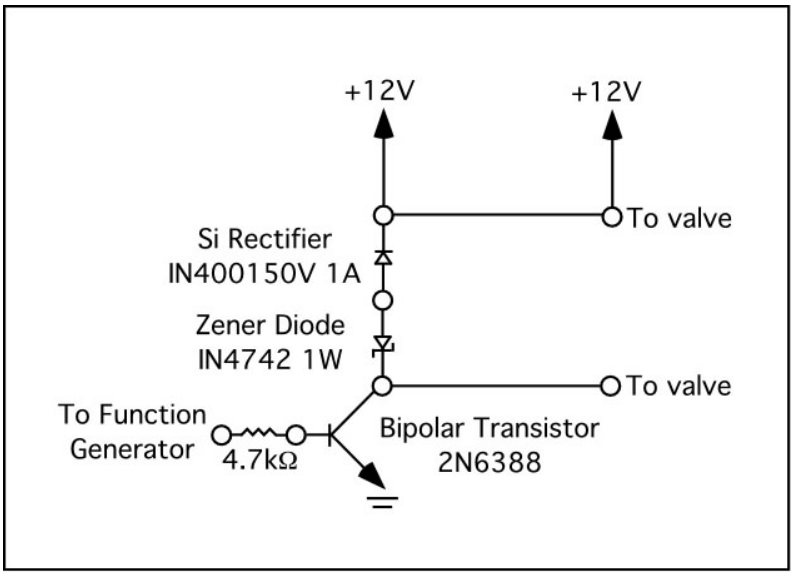

Figure 3.10: Soleniod driver schematic.

made the droplet break chaotic. As water was forced into the pressurized oil stream, water flowed toward the oil inlet, disrupting the oil flow and producing highly polydisperse droplet sizes (Figure 3.11).

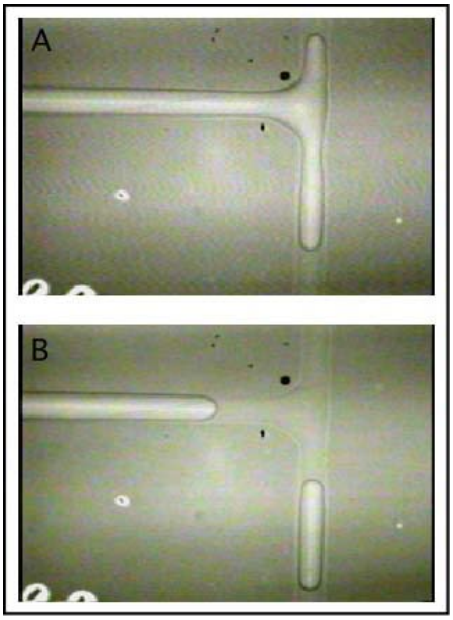

Figure 3.11: Solenoid-driven crossflow: A) High pressure toggle on solenoid valve forces water into the oil channel. B) Low pressure toggle causes water to retreat and remaining droplet flows toward outlet.

Microfluidic Droplet Formation: Restricted "T" channel Architecture

The solenoid-driven pumping of water into the T-junction of the microfluidic device clearly was not the answer to high-frequency droplet formation. Passive crossflow using constant pressures to drive the oil and water streams was still clearly desirable because it produced fairly homogeneous droplet sizes at regular intervals. A design modification was needed to increase the velocity at the point of crossflow. A new device was designed in which the width of the channels at the "T" junction was reduced by 50%. The new polyurethane devices had water and oil input channel dimensions of 60 µm (w) x 9 µm (h), with the "T" junction dimension of 30 µm (w) x 9 µm (h). The constriction increased the local velocity at the point of crossflow. The droplets generated by the device were smaller that those generated by the simple "T" channel device and were produced at a higher frequency (Figures 3.12 and 3.13).

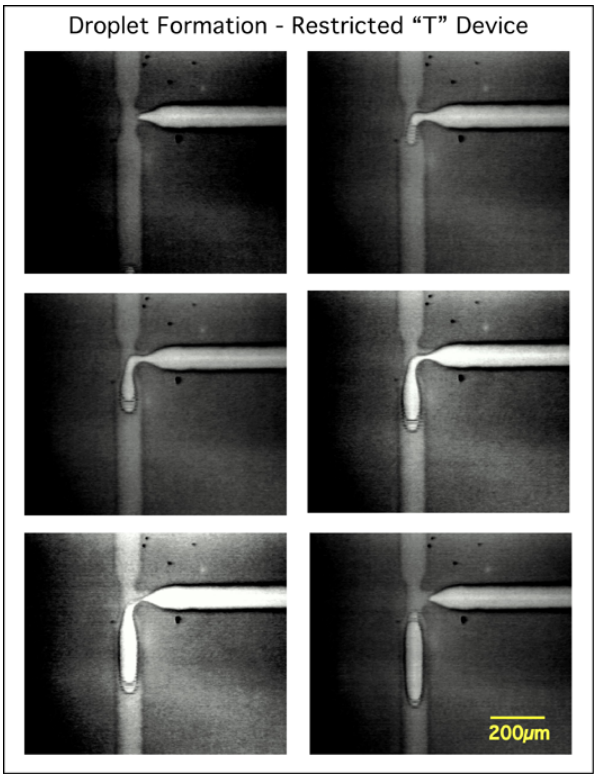

Figure 3.12: Crossflow using restricted "T" polyurethane microfluidic device to generate water droplets in decane.

Microfluidic Droplet Mixer: Dual "T" channel Architecture

As the crossflow architecture on the chip was being developed, some thought was put into designing a microfluidic mixer that could be used to combine multiple reagents at the crossflow junction. Video analysis of the water/decane interaction at the crossflow junction in the simple "T" channel devices revealed that the water, prior to flowing toward the outlet, plugs the junction, dropping the pressure of the liquid flowing toward the outlet. This was confirmed by the observation that the droplets flowing toward the outlet slow down briefly during each crossflow cycle. Realizing that this pressure drop could be exploited to introduce multiple water streams into the oil stream in a sequential pattern, a mask was designed with two "T" channels orthogonal to the oil stream through which two independent water streams could be introduced (Figure 3.13).

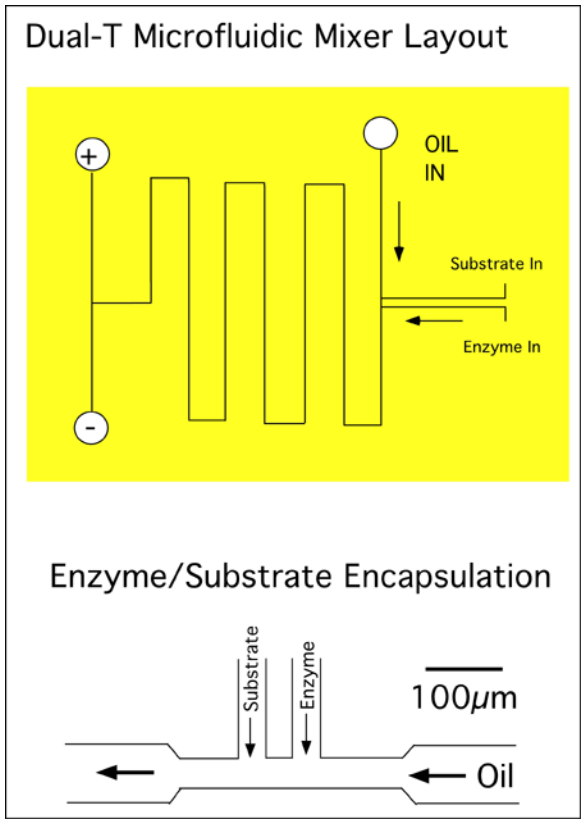

Figure 3.13: Dual-T microfluidic mixer layout. By independently controlling the two aqueous inputs, a single mixed droplet can be sequentially formed prior to shear. Channel width transitions from ~60 μm to ~30 μm at the crossflow junction.

To test the device, one water input channel was filled with 1 mM bromophenol blue dye in dH_2O and the other water channel was filled with 1 mM Orange G dye in dH_2O. Tetradecane was used for the oil phase. All of the water and oil inputs were pressurized to ~10 psi and minor pressure adjustments were made to equilibrate both of the water channels just to the point where they intersect with the oil stream. The microfluidic mixer functioned as follows: A) As the water stream closest to the oil input entered the T-junction, it blocked the oil flow to the outlet. B) During the brief moment when the upstream blocked the flow, the oil pressure against the second water stream decreased, causing it to flow into the T-junction. C) Both water streams mixed briefly and were sheared off by the oil flow (Figure 3.14). The mixing-shearing cycle was extremely stable, exhibiting good periodicity (~2 sec.), with droplet volumes of ~2 nL.

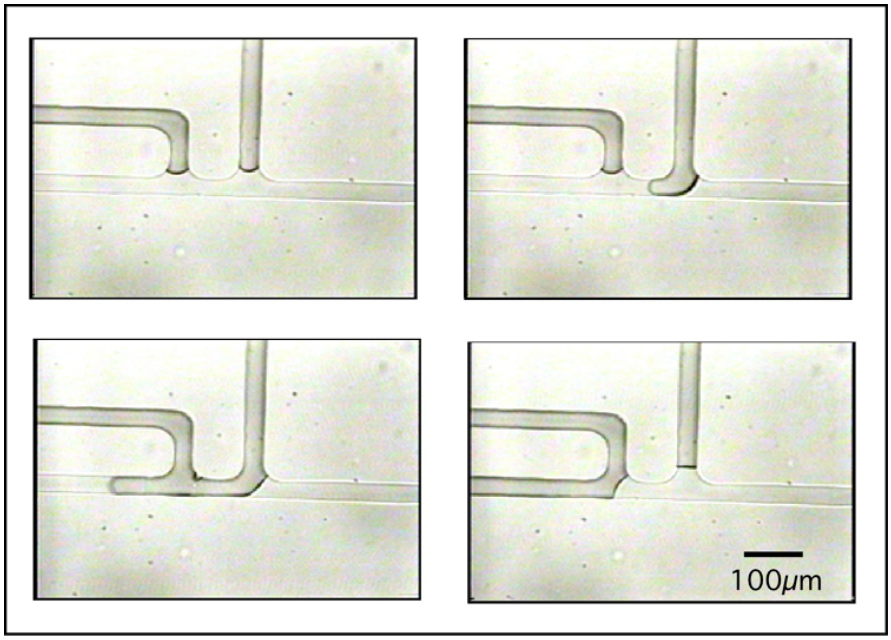

Figure 3.14: Dual-T microfluidic mixer. Water from the input channels enters the oil stream sequentially, mixing upon contact with each other, prior to being sheared into droplets.

High-Frequency Vesicle Generating Microfluidic Devices

The principal problem with the droplet-generating polyurethane crossflow devices is the shrinking that was observed as the droplets traveled down the channel to the output ports. This phenomenon was not surprising given the hydrophilic nature of polyurethane combined with the general porous structure of elastomeric polymers. A chemical barrier was clearly necessary to reduce the water uptake in the devices. The answer to this problem was, surprisingly, surfactant.

While surfactant (Span 80) disrupted the crossflow dynamics in the simple "T" channel architecture polyurethane devices, the formed droplets did not shrink as they flowed through the serpentine channel toward the outlet. The surfactant coated the channel, with its polar residues attracted to the channel wall, creating a moisture barrier within the chip. The "waterproofing" capability of the surfactant in the polyurethane chip was clearly important, but not really appreciated in the simple "T" devices, as its presence promoted chaotic droplet break at the T-junction.

In the restricted "T" channel architecture devices, surfactant causes a dramatically different effect. As the oil/surfactant mixture flows through the constriction at the T-channel, the velocity of the fluid increases, increasing the shear force at the oil/water interface. If the constricted channel is coated with surfactant, water entering the oil stream has no affinity for the channel, forming small vesicles instead of long droplets (Figure 3.15). As these vesicles slow down as they flow toward the outlet into the wider channel, they round up into spheres of water surrounded by a layer of surfactant within the oil/surfactant stream. These droplets are like the reverse micelles formed in a bulk

(w/o) emulsion. The diameter and periodicity of these droplets depend on the channel geometry and the relative water and oil/surfactant pressures. We have generated spherical droplets with diameters ranging from 1 μm to 9 μm. Larger droplets can be generated, but they flow through the channel as flattened disks due to the height of the channel (~9 μm). The formed droplets are monodisperse, extremely stable (>24 hours), and can be

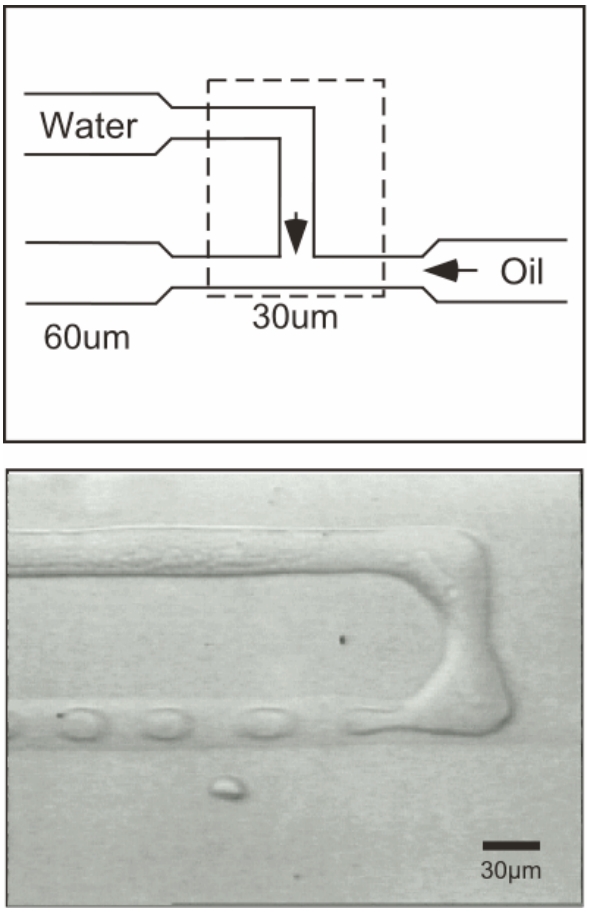

Figure 3.15: Microfabricated channel dimensions at the point of crossflow and photomicrograph of water introduced into the continuous oil-surfactant phase. Dashed lines denote area in photomicrograph.

generated at high frequencies (~50 Hz under our experimental conditions). Their potential application as miniature bioreactors will be discussed in Chapter 4. The beauty of the vesicle-generating crossflow device lies not only in its potential HTS applications, but also in the fascinating fluid mechanics that govern its functionality. By modifying the

input pressures and the channel geometry, complex patterns of droplets can be generated, ranging from a single continuous string of droplets to helices and ribbon motifs. The physics behind this behavior is the topic of the next section.

3.3 Microfluidic Crossflow: Theory and Fluid Mechanics

Complex pattern formation is ubiquitous in nature. Efforts to understand these effects have led to important insights into nonlinear dynamical systems and fundamental nonequilibrium physics[45]. Fluid systems have been fertile ground for pattern formation, with classic examples such as Rayleigh-Benard convection, Taylor-Couette flow in rotary systems, nonlinear surface waves, liquid crystals, and falling droplets[46]. Key ideas that have emerged from the study of pattern formation are the central roles of instability and nonlinearity, as well as the influence of perturbations and boundary conditions on the morphology of the patterns. The elements of instability and nonlinearity are generally not present in microfluidic devices because the length scales are small enough that inertial effects in the fluid can be neglected. As most microfluidic devices operate at low Reynolds number[47], the Navier-Stokes equation for fluid flow becomes linear and the flow is laminar. This result has many practical consequences for efforts to miniaturize biological assays and produce lab-on-a-chip systems[48.49]. In this section, we show how the interaction between two immiscible fluids can be used to introduce nonlinearity and instability in a microfluidic device. The resulting complex pattern formation is an unexpected and fascinating example of self-organization in a dynamic system far from equilibrium.

Emulsions are formed by shearing one liquid into a second immiscible one, often in the presence of surfactant, to create small droplets. The droplets can be remarkably stable, maintaining their shape and distribution for years[50]. Significant advances have been made in the past few years to produce emulsions that are monodisperse, with standard deviations in droplet size less than 5%[51,52,53,54]. Unlike the standard crossflow techniques for generating water-in-oil emulsions, in which the discontinuous phase is forced through narrow pores[52,54] or capillaries[52,55] into an open continuous phase, we accomplish droplet formation at the junction of two microfluidic channels containing water and an oil surfactant mixture. The water partially obstructs flow at the junction, but is not broken off at the channel interface as in traditional crossflow devices. Droplet formation is achieved by high shear forces generated at the leading edge of the water perpendicular to the oil flow, generating picoliter-scale droplets. Although the system remains at low Reynolds number, the flow is nonlinear because of interactions on the boundary between the two fluids. The two important effects are that the boundary is not static and that the motion of one fluid can entrain the other[56]. The resulting instability that drives droplet formation is a well known competition between surface tension and shear forces[57].

The emergence of static crystalline structure in emulsions has been documented previously[52,54]. In our experiments, the droplets self-assemble into a variety of coherent, moving patterns as they are formed. We examine the control parameters that lead to vesicle formation and organization in an emulsion in a microfluidic device, illustrating the relationship between droplet pattern formation, pressure and the geometric boundary conditions of the system. The droplet size and frequency can be precisely controlled by

modifying the relative pressure driving the water and oil streams, enabling the production of a wide range of vesicle shapes and patterns. Under conditions where the water pressure is lower than the oil pressure, monodisperse separated reverse vesicles are formed. As the relative water pressure is increased at fixed oil pressure, the droplets become ordered into a single continuous stream. At water pressures that exceed the oil pressure, complex, organized patterns begin to emerge in the stream, ranging from helical-like structures to coherent ribbon motifs.

The microfluidic devices utilized in our experiments are fabricated by pouring acrylated urethane (Ebecryl 270 – UCB Chemicals) on a silicon wafer mold containing positive-relief channels patterned in photoresist (SJR5740 – Shipley), which is then cured by exposure to UV light. The channels are fully enclosed by curing the patterned urethane on a coverslip coated with a thin layer of urethane and bonding the two layers together through an additional UV light exposure. The measured channel dimensions are approximately 60 μm wide by 9 μm high, tapering to 35 μm by 6.5 μm in the region where the water and oil/surfactant mixture meet at the crossflow intersection (Figure 3.16). The fluids are introduced into the urethane microfluidic devices through pressurized syringe reservoirs containing water and oil. Various oils were tested in the device, including decane, tetradecane, and hexadecane, combined with the surfactant Span 80 concentrations (v/v) of 0.5%, 1.0% and 2%. The device is equilibrated prior to crossflow by priming the outflow channel with oil/surfactant to eliminate water interaction with the hydrophilic urethane. The production of reverse vesicles is then initiated by modifying relative oil/surfactant and water pressures such that the water

enters the crossflow junction perpendicular to the oil stream, shearing off into discrete droplets.

The shape of the channels influences the size distribution and morphology of the droplet patterning and can be modified by heating the photoresist mold on the silicon wafer (80-110°C) to round the normally rectangular channels. The photoresist flows during the heating process, creating localized maxima and minima at the perpendicular intersection in the mold where the water is sheared into the oil/surfactant phase and the transitions from the restricted to the wide channels. Channels that have not been rounded produce only monodisperse reverse vesicles with regular periodicity that associate with the walls of the wide channel as they flow through the device (Figure 3.16).

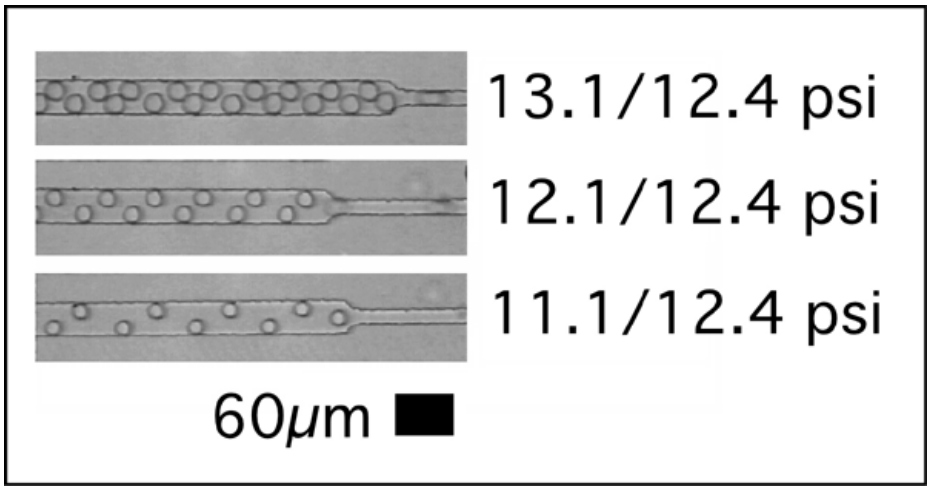

Figure 3.16: Reverse vesicles in square channels. Photomicrographs show the transition from the 30 μm wide channel to the 60 μm wide channel. Respective pressures for the water and oil/surfactant (hexadecane/ 2% Span 80) are noted in figure.

The relative water/oil-surfactant pressures determine the size and spacing between the reverse vesicles. The patterns in a rounded channel are more complex, ranging from

periodic droplets to “ribbons,” “pearl necklaces,” and helical intermediate structures. The self-organization of the reverse vesicles depends on the differential pressure between the water and oil-surfactant phases, with higher relative water pressures driving the formation of increasingly complex droplet arrays (Figure 3.17).

The diverse pattern formation found in the rounded channels can be classified as follows. When the oil pressure greatly exceeds the water pressure, the water stream is held in check by surface tension and only the oil flows. As the water pressure is increased past a critical point, single monodisperse separated droplets are formed at a frequency of 20-80 Hz. Small adjustments in the water pressure in this range change the radii of the formed droplets, with higher water pressures generating larger droplets. When the relative oil and water pressures are approximately balanced ($P_w \sim P_o$), droplets are formed in a pearl necklace-like configuration (Figure 3.17 D,E). They stack up against each other during the transition from the 30 μm channel to the wider 60μm channel due in part to the increased drag of the necklace (which is larger than the separated monodisperse droplets). At water pressures that slightly exceed the oil pressure ($P_w > P_o$), the packing density of the droplets in the 60 μm channel increases. The first complex structure that emerges with increasing oil pressure is a transition from the pearl-necklace shape into a zig-zag pattern of droplets (Figure 3.17 G). At moderately higher water pressures (~10% higher than the relative oil pressure), shear occurs at both the crossflow junction *and* the transition from the narrow to wide microchannel. Polydisperse and bi-disperse motifs appear as helices and patterned multilayer ribbon structures. The patterns remain coherent as the arrayed droplets flow down the entire length of the channel from the breakpoint to the outlet (~4 cm). At excessive water pressure, water co-

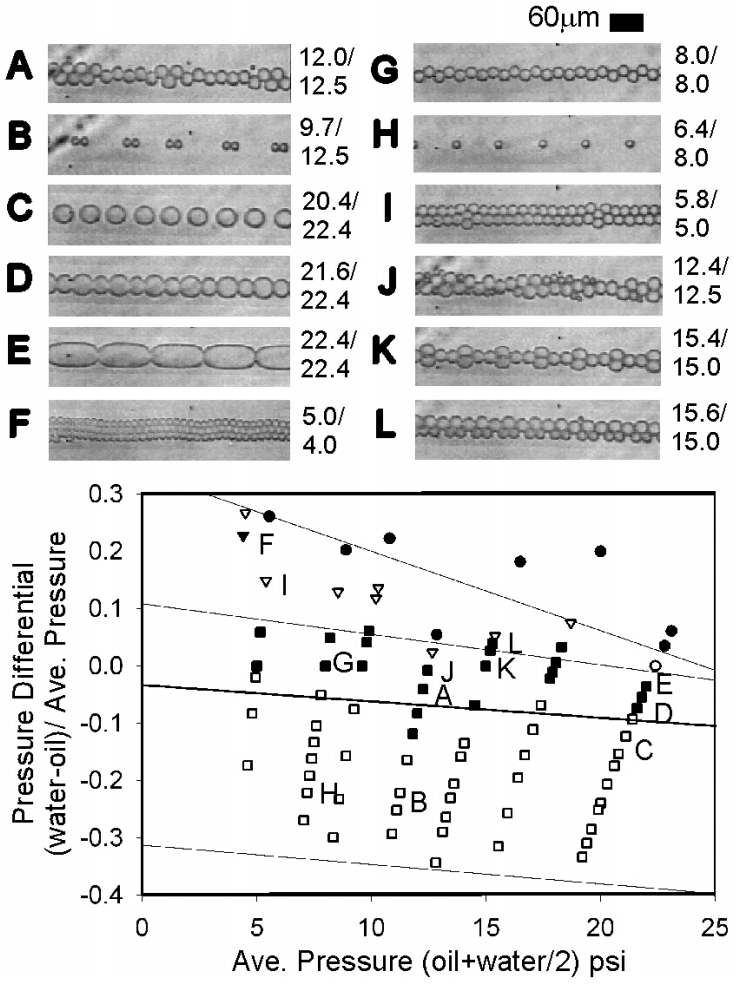

Figure 3.17: Droplet patterns in rounded channels at different water and oil/surfactant pressures (psi - noted in figure) and the corresponding phase diagram depicting the relationship between the oil and water pressure differences and droplet morphology. Solid lines are used to define approximate boundaries between the following droplet states (top to bottom): solid water stream, ribbon layer, pearl necklace, single droplets, and solid oil stream. Symbol definition: solid water stream (closed circle); elongated droplets (open circle); triple droplet layer (closed triangle); double droplet layer (open triangle); joined droplets (closed square); separated droplet (open square). Photomicrographs show 60 μm channel regions downstream of the point of crossflow.

flows with the oil as separate streams, as one would expect for laminar flow of two conjoined streams.

The simplest model for droplet formation is based on the shear forces generated between the water and oil-surfactant at the crossflow junction. The predicted size of a droplet under external shear force is approximated by the equating the Laplace pressure with the shear force[57]:

$$r \sim \frac{\sigma}{\eta \dot{\varepsilon}}, \qquad (1)$$

where r is the final droplet radius, σ is the interfacial tension between the water/oil/surfactant, η is the viscosity of the continuous phase, and $\dot{\varepsilon}$ is the shear rate.

In the microfluidic device, a shear gradient is established as water tries to expand into the pressurized continuous phase. The water stream never completely blocks the flow of the continuous phase, and the oil-surfactant flows through the restriction at velocities up to ~6.4 cm/s. Equation (1) gives a good approximation of the droplet sizes generated in the microfluidic device when the shear rate is estimated as $\dot{\varepsilon} \sim 2v / y_0$, where y_o is the channel radius at the center of flow estimated by triangular approximation and v is the velocity of the fluid through the gap. Predicted droplet sizes are within a factor of two of actual droplet size measured by video microscopy for monodisperse droplets generated at water and oil pressures ranging from 8.0 – 22.4 psi (Figure 3.18).

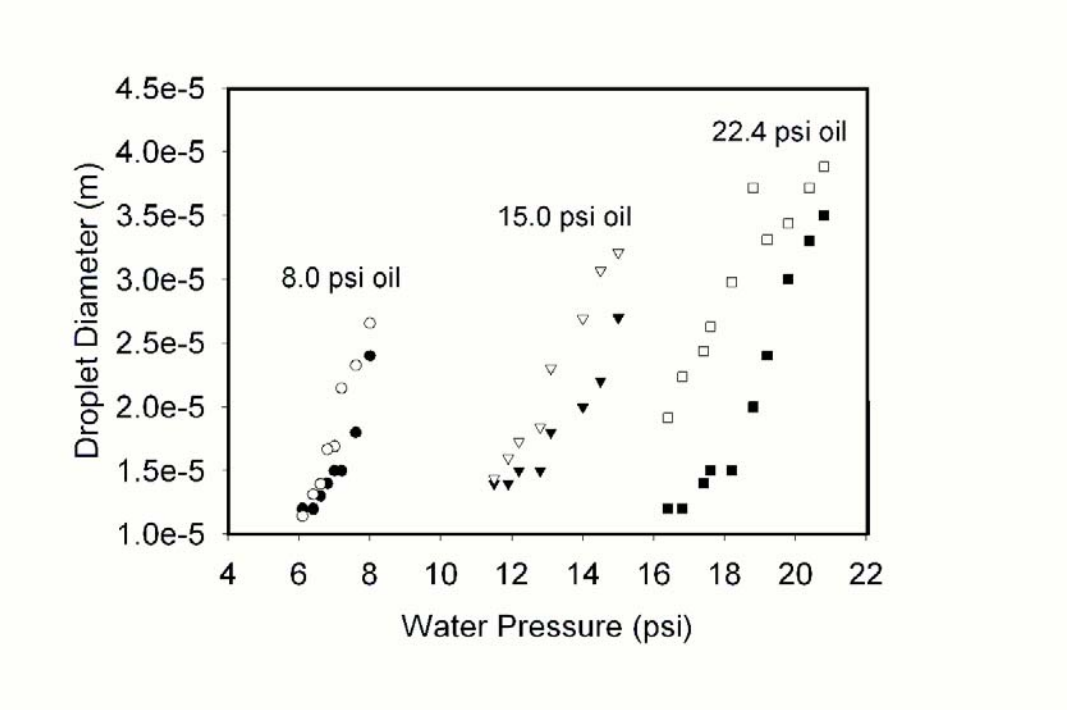

Figure 3.18: Predicted vs. actual drop size at different water and oil/surfactant pressures. The predicted sizes were calculated using equation 1. Open symbols, predicted size; closed symbols, experimental.

Pattern formation in the microchannels appears to be driven by the drag force of the droplets and contact friction with the floor and ceiling of the device. As the droplets transition from the narrow crossflow junction to the 60 μm channel, they slow down significantly relative to the oil phase. At higher droplet frequencies, they begin to collide, stacking up into organized patterns at the transition between the 30-60 μm channel. Complex structures form in rounded channels at high relative water pressures as colliding droplets are pushed from the center of the flow stream. The pattern formation results as a trade off between the interfacial tension of the droplets and the shape of the channels – droplets prefer to stay in the middle of the rounded channels in order not to pay an energy penalty for deformation in the crevices at the edge of the channels. Secondary shearing at the slowing junction also affects pattern formation-if the initial droplet is not

commensurate with the size selected by the junction, then size dispersity is introduced to the stream and asymmetric motifs appear (Figure 3.17 J, L).

We have mapped a crude phase diagram that shows the pattern morphology is predominantly dependent on only the dimensionless differential input pressure. However, some of the most interesting patterns are found only at certain absolute values of the input pressure (Figure 3.17). Somewhat surprisingly, these structures maintain a high degree of coherence, despite the fact that they are formed dynamically when the system is far from thermodynamic equilibrium. Furthermore, this system shows an unusual richness in the variety of phases it can display, especially considering that the boundary conditions (which also function as order parameters) are simply constant pressure applied to fluid inputs.

Pattern formation also occurs in granular materials, which have some striking similarities with our system. In both cases the fundamental particles are so large that thermal fluctuations are negligible. Also, granular systems can display a "jamming" phenomena, in which the particles get trapped in metastable configurations that are difficult to escape from. The pearl necklaces and zig-zag patterns in our system show an ability to get into jammed states of high stress. The joined droplets behave like a spring, continually trying to relieve the added strain within the system by trying to orient themselves in the center of the stream. This behavior is shown by multiparticle defects that propagate as waves through the pearl necklaces with a speed greater than the droplet stream (Figure 3.17 A). The propagation speed of the defects depends on the relative input oil and water pressures (Table 3.1). At lower oil and water pressures (~8.0 psi),

wave propagation is very slow and infrequently observed as strain release occurs locally in the form of minor rearrangements of the droplet packing configuration.

Water (psi)	Oil (psi)	Bulk Droplet Velocity (μm/sec)	Propagating Wave Velocity (μm/sec)
15.8	15	675	900
15	15	840	1000
14.5	15	860	1050
12	12.5	450	660
8	8	420	450

Table 3.1: Defect propagation speed in polyurethane crossflow device with water and hexadecane/2% span 80. Velocity measurements taken from 60 μm wide channel after the crossflow junction.

In conclusion, we have shown how instability can develop as a competition between shear forces and surface tension in a microfluidic device. The system is technically at low Reynolds number, but the equations of motion are nonlinear because the boundary between the two fluids is not static. Although we have outlined some of the basic physics leading to the vesicle-forming instability and subsequent pattern formation, it is clear that more work needs to be done to achieve a complete understanding of the system. Since geometric effects play a significant role in the pattern formation, one should be able to take advantage of the powerful microfabrication technology both to explore the consequences of this observation and to provide stringent tests of theoretical models.

3.4 A Variation on a Theme: Inline Droplet Generation

Upon further analysis of the microfluidic crossflow device, it became evident that crossflow is not essential for emulsified droplet formation. The deformation and breakup of liquid droplets through capillaries is well documented[58.59.60]. The parameters that govern the motion of a droplet through a capillary at low Reynolds number are the drop size relative to the tube size, the viscosity ratio of the discontinuous to continuous phase, and the capillary number, which is simply the inverse of equation (1)[61]. Droplet breakup occurs as the capillary number exceeds a critical value (Ca_c), in which the viscous forces and interfacial tension can no longer be balanced. Extending this analogy to the microfluidic realm, emulsification can be achieved simply by forcing the water stream into the center of the microfluidic channel, creating a slender, unstable thread of water that breaks up into droplets.

The in-line droplet generator channel designs were developed taking elements from flow cytometry and inkjet printer technology (Figure 3.19). Like a flow cytometer, in which laminar flow is used to focus the sample stream within the sheath buffer, the pressurized continuous oil phase in the inline device forms the boundaries of the water entering the central cavity. Unlike the crossflow device, in which the geometry of the channel determines the water profile at the point of droplet breakoff, the water is dynamically shaped by the oil phase in the inline device. Generating the initial droplets in the central cavity requires a destabilizing force. In inkjet printers, droplets are generated by several methods, including piezoelectric[62], thermal bubble[63], acoustic[64] and electrokinetic actuation[65]. In the in-line device, the co-flowing water stream is destabilized

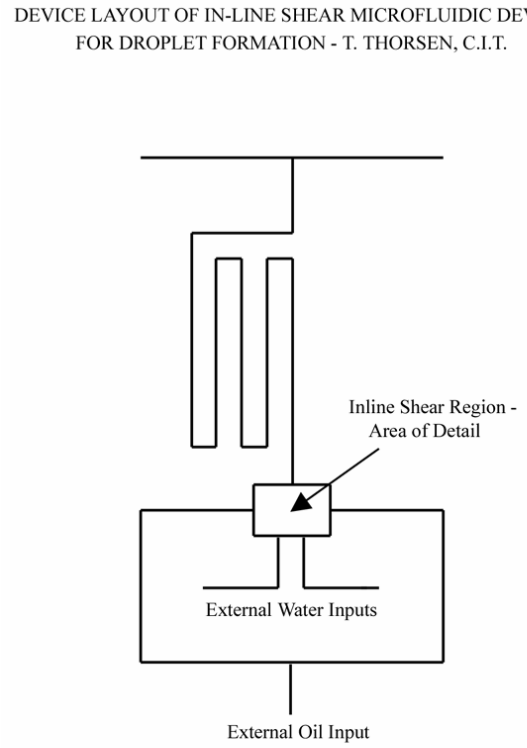

Figure 3.19: In-line microfluidic droplet generating device design.
Top Figure: Entire device layout
Bottom Figure: Enlargement of central cavity area

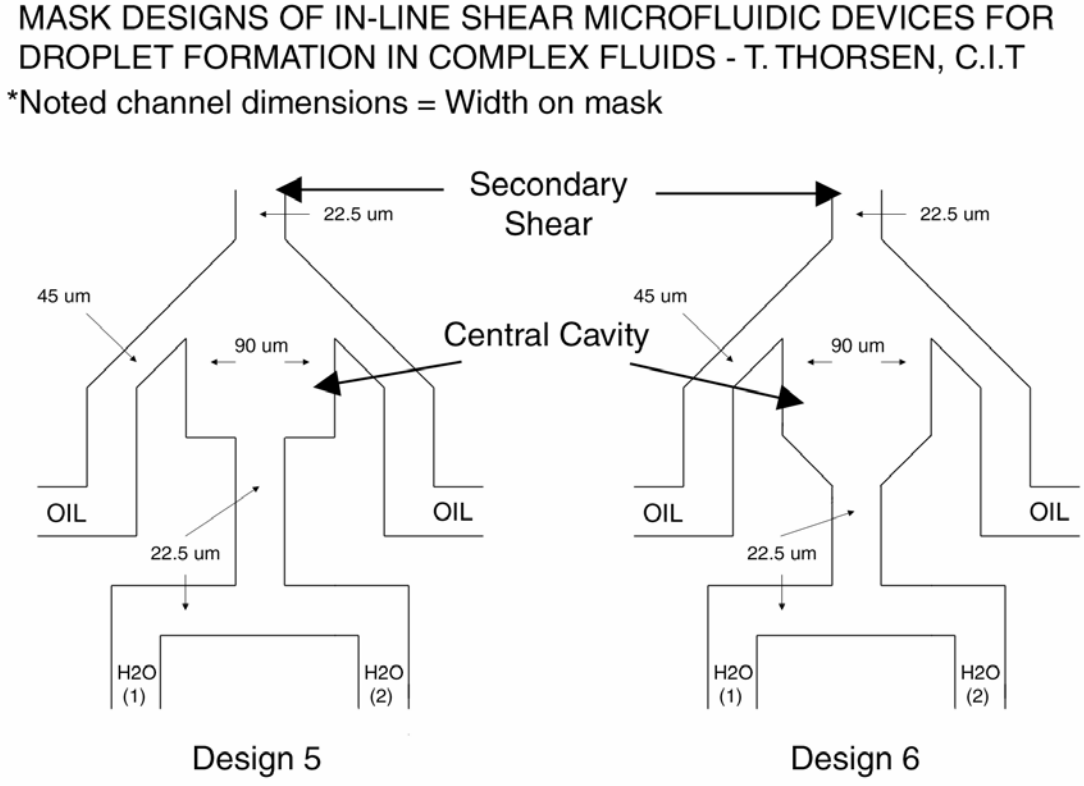

by the flanking oil streams that force it into an thread that breaks up in the central cavity.

The pattern of droplet generation in the central cavity is complex, depending on the channel geometry, the relative fluid pressures, and the viscosities of the oil and water phases. Under conditions using water and mineral oil, the droplets are generated in periodic bursts. The focused water stream retracts as several droplets are sheared off into the continuous phase (Figure 3.20). This behavior resembles front propagation the viscous Rayleigh capillary instability of a cylindrical interface[66]. Capillary instability

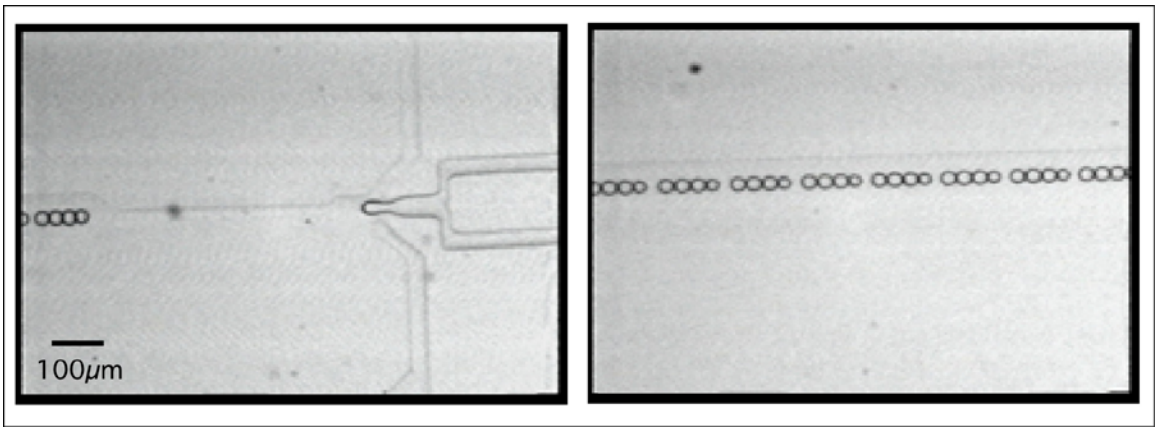

Figure 3.20: In-line Ebecryl 270 microfluidic device: water (17.6 psi) / mineral oil-2% Span 80 (18.2 psi). Droplet formation occurs in bursts in central cavity (left). Formed droplets flow as clusters toward outlet (right).

occurs as a liquid thread is subjected to destabilizing external forces, causing it to break up into small droplets. Front propagation of the Rayleigh instability, suggested by mathematical modeling studies of two immiscible fluids[67], occurs as the instability generated at a droplet tip propagates faster than the liquid thread can retract. The result of the instability is the sequential generation of several droplets. Experiments on the breakup and relaxation of static elongated droplets suspended in an outer fluid reveal that

this behavior depends on the relative viscosity of the two fluids[68]. Under conditions where the droplet viscosity (η^i) is much lower than the outer fluid viscosity (η^o), $\lambda = (\eta^i/\eta^o) = 0.001$, droplets break off before the end retracts, while at matched viscosities, retraction occurs before rupture. In both of these experiments, the Rayleigh instability is dampened and does not propagate through the droplet. In experiments with intermediate λ values ($.001 < \lambda < 1.0$), retraction is slow relative to the time for breakup and the instability is propagated down the droplet, generating several daughter droplets. The front propagation model may not be entirely appropriate to explain the droplet retraction behavior in the in-line microfluidic device, but the similarities are evident. In the in-line device, both oil and water streams are pressurized, unlike the static droplet model. However, the viscosity ratio of the water-mineral oil system, $\lambda = 0.04$, is within the range where front propagation is expected to occur. At higher λ values in the microfluidic in-line device, thread retraction appears to dominate and propagation of the Rayleigh instability is not observed. In an in-line microfluidic device using n-hexane as the discontinuous phase and dimethylformamide as the bulk phase, $\lambda=0.3$, monodisperse droplets are continually produced at the end of the hexane stream with a regular periodicity (Figure 3.21). The tip of the stream regularly contracts and expands, producing a single droplet each cycle.

The in-line droplet-generating devices, like the crossflow chips, were designed for HTS applications. As shown in Figure 3.19, two aqueous inputs are provided that mix only at the point of droplet formation due to the laminar flow conditions at the microfluidic scale. This design element, like the crossflow mixer, is useful for two component assay systems where the components need to be isolated prior to

compartmentalization, finding application in areas such as the screening of large mutagenized enzyme libraries.

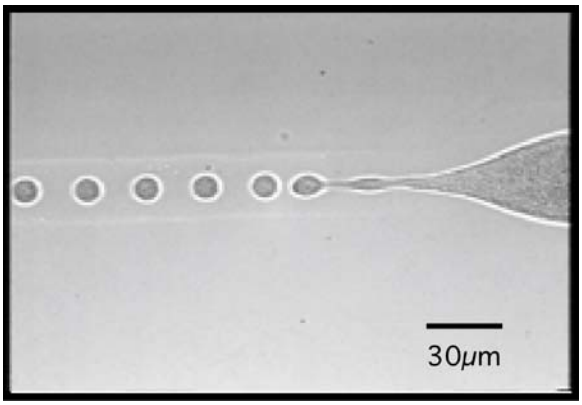

Figure 3.21: In-line Ebecryl 270 microfluidic device: n-hexane (8.0 psi)/ dimethylformamide-1% p123 block copolymer (10.0 psi). Uniform droplet generation observed at tip of hexane stream in central cavity.

3.5 Droplet Sorting

While a great deal of work went into designing and developing a high-throughput encapsulation microfluidic device, a technique to manipulate and sort the formed vesicles was clearly desirable for HTS applications. Electrokinetic techniques could not be utilized due to the insulating properties of the oils used as the continuous phase in the crossflow devices, and we were forced to consider other strategies. Two strategies were explored. The first, an optical valve, exploited the refractive index difference between the oil and water phases, using radiation pressure to repel the formed water droplets. The second, the development of integrated elastomeric valves, allowed the droplets to be sorted using pneumatic pressure.

3.5.1 Optical Valves

Introduction

In the 1970s, pioneering experiments were conducted by Arthur Ashkin at Bell Laboratories which used radiation pressure to manipulate dielectric particles[69]. By the early 1980s, Ashkin and co-workers had designed a laser apparatus capable of trapping a particle with a high dielectric constant in three dimensions, creating the first optical tweezer[70,71]. The radiation pressure generates piconewtons of force when it is reflected, refracted or absorbed by dielectric particles. Tweezing is the result of gradient forces of light incident on a dielectric particle. As a particle encounters a focused laser beam, it will either be trapped or repelled, depending on its index of refraction relative to the surrounding medium (Figure 3.22).

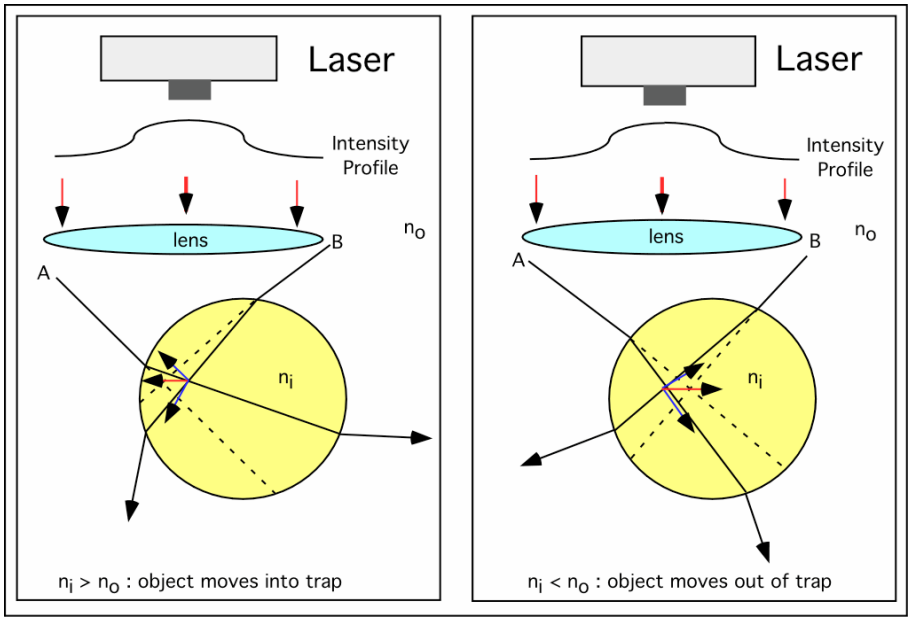

Figure 3.22: Optical trap dynamics. An object with a higher index of refraction than the surrounding media moves toward the focused beam (left) while an object with a lower index of refraction in repelled (right).

Preliminary experiments were conducted in the laboratory to determine if reverse vesicles could be repelled by an optical tweezer set-up. A crude emulsion consisting of water and mineral oil/2% Span 80 was made using the aforementioned propeller method. The index of refraction of the suspended water droplets (n = 1.33) is much lower than that of the surrounding mineral oil (n = 1.47), setting up the conditions for droplet repulsion by the optical tweezer. 20 μl of the crude emulsion was pipetted onto the center of a 24 x 50 mm No. 1 glass coverslip and covered with an additional coverslip. A dual beam optical tweezer apparatus constructed in our laboratory by Dr. Jens-Christian Meiners was used to apply the optical potential to the sample[72]. Two orthogonally polarized beams from an Nd:YAG laser (λ = 1064 nm) with an intensity of 80 mW each were focused with an immersion-oil microscope objective (Olympus PlanApo 60 x 1.4) into the sample plane. Using one of the focused beams, we were able to repel free-floating reverse vesicles with diameters ranging from 2 to 20 μm.

Device Design and Fabrication

While the preliminary results with the Nd:YAG optical tweezer were encouraging, we recognized the fact that such an apparatus would provide an inadequate amount of force to block water droplets in a *pressurized* oil stream. A laser with a much higher power output was clearly needed.

The optical valve was designed around an 808 nm laser diode in a TO3 package (SLI Corporation) with a maximum power output of 2.5 W. The device was assembled on a on a 6 x 6" aluminum breadboard (Figures 3.23 and 3.24)*. As the power output increases, laser diodes exhibit high divergence and astigmatism, requiring collimating optics to shape and focus the beam. A 0.68 NA IR aspheric lens (f = 3.10 mm) was used

to give the beam a more elliptical profile. A pair of focal length matched (f=75 mm) achromat lenses were also placed in the laser path to minimize the beam divergence as it traveled to the objective. A constant current driver was built to provide a stable current source for the laser diode (Appendix B). Diode lasers function by flowing current across a junction consisting of a sandwiched layer of semiconductive material. The laser diode is quickly destroyed by rapid current spikes or electrostatic discharge, making a good constant current source an essential component of the system. The constant current source was designed to provide a stable current source up to 2.5 A to the laser diode. A second source of laser failure is high temperature. High-power laser diodes require a thermoelectric (TE) cooler to keep the laser head at a stable operating temperature. The 808 nm 2.5W TO3 laser diode contains an independently powered TE cooler and a thermister. To maintain a stable laser head temperature, the thermister value was monitored on a meter (10kΩ = 25°C) while simultaneously adjusting the current inputs to the diode and TE cooler. Beam alignment was accomplished using an IR detector card (Garian) and an IR night vision scope (U.S. Army Metascope SU-43/U) at the minimum threshold current (0.35 A), which provided about 10mW of output power.

Initial functionality tests with the optical valve platform were carried out using 2 μm diameter aldehyde sulfate latex beads (Interfacial Dynamics Corp.) diluted 1:100 in 1x phosphate buffered saline (PBS), pH 7.0, with a 40x objective (Olympus, Plan NA 0.65). The beads, with a much higher index of refraction than water (1.59 vs. 1.33), should be trapped by the focused beam. Beads were introduced into a basic T-channel

---

[*] A complete parts list is available in Appendix A

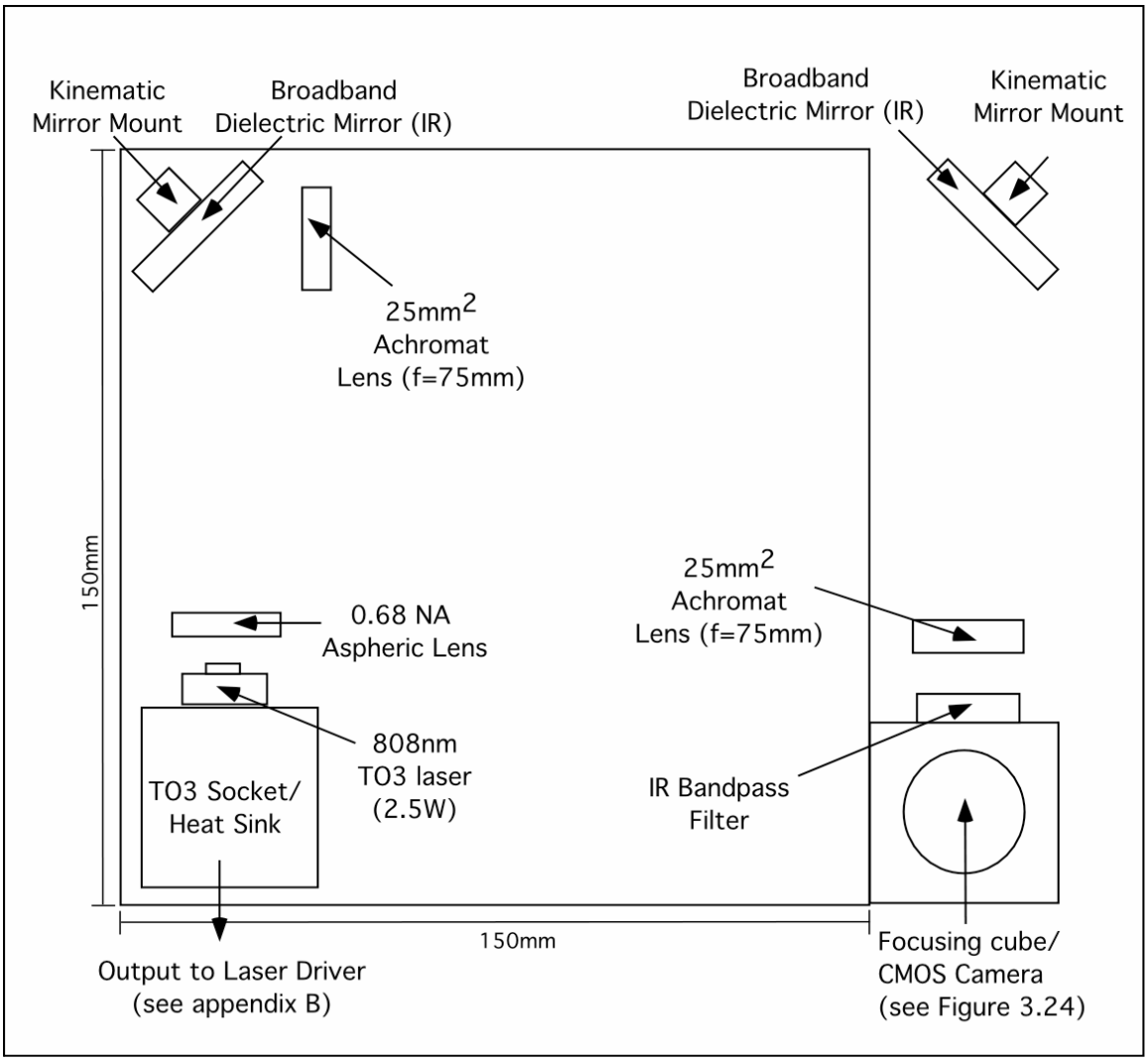

Figure 3.23: Central board layout of optical valve system. The output beam from the 808nm TO3 is shaped by the aspheric lens, while the pair of achromat lenses minimizes beam expansion. The reflected beam is directed into the focusing cube, where it passes through the objective and is focused into the sample plane.

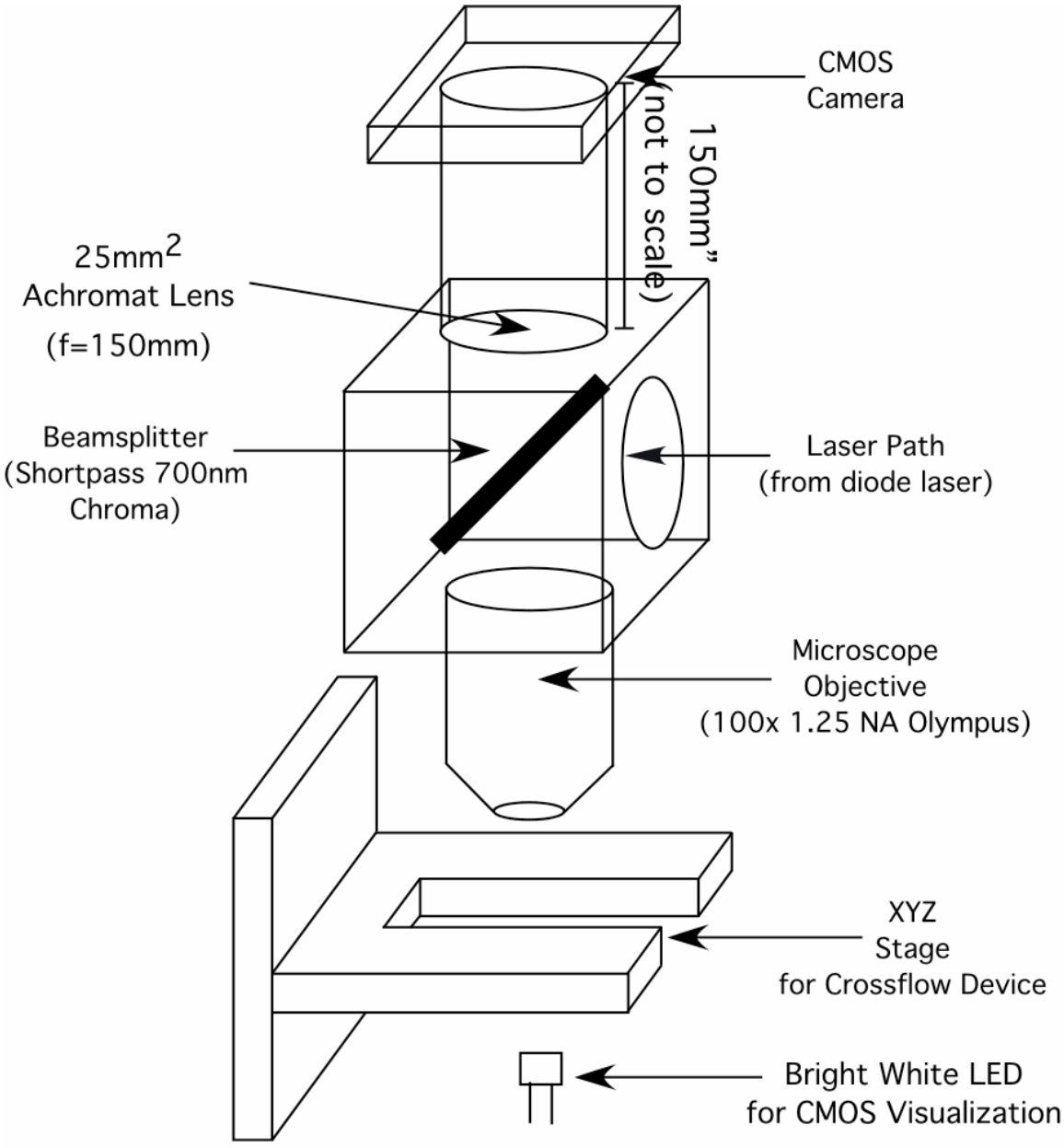

Figure 3.24: Optics/detector head of optical valve system. From the central board, the 808nm TO3 laser beam enters the focusing cube, where a beamsplitter reflects the 808 nm beam, passing it through the objective and into the sample plane. A bright white LED (5 mW) is used to illuminate the microfluidic device from below, providing a source of visible light for the CMOS camera.

Sylgard microfluidic device (channel dimensions – 100 μm (W) x 10 μm (H)) using capillary flow. Beads were trapped by the beam at 0.75 - 1.00 A input current (300 - 750 mW). The beam profile in the sample plane, a slightly elliptical bar (~200 μm x 5 μm), trapped the beads in a single file row. The beam intensity in the center of the trap was not uniform along its length, a characteristic of multimode, high power laser diodes. Once trapped, the beads began to migrate toward the region of highest intensity. Once trapped, the beads could be slowly dragged (~100 μm/second) through the channel.

The latex beads were used in a consecutive experiment to measure the trapping speed and the beam intensity profile in a microfluidic device under pressurized flow conditions. Dilute beads (1:100 in 1x PBS, pH 7.0) were introduced into a Sylgard T-channel microfluidic device under low pressure. The laser diode was driven at 1.2 A. A CCD camera (Phillips) was used to record the bead trapping efficiency over the tested pressure range and image data were saved to digital video tape for later analysis. The experiment showed that beads could only be trapped under very low flow velocities in the 100 μm wide channel (10 – 20 μm / second), suggesting that the laser intensity/ unit area in the sample plane was quite low (Figure 3.25).

Emulsion experiments with the laser diode were conducted using both bulk emulsions mounted on glass slides and crossflow-generated emulsions in polyurethane microfluidic devices. In an effort to improve the beam profile and the relative intensity of the laser at the sample plane, a 100x 1.25 NA objective replaced the 40x objective in the setup. Bulk emulsions (w/o) were prepared using mineral oil, hexadecane and decane

with 1% Span 80 using the propeller method. 10 µl of each emulsion was added to a glass slide and sealed with a No. 1 coverslip. At 1.00 A, the device was unable to deflect

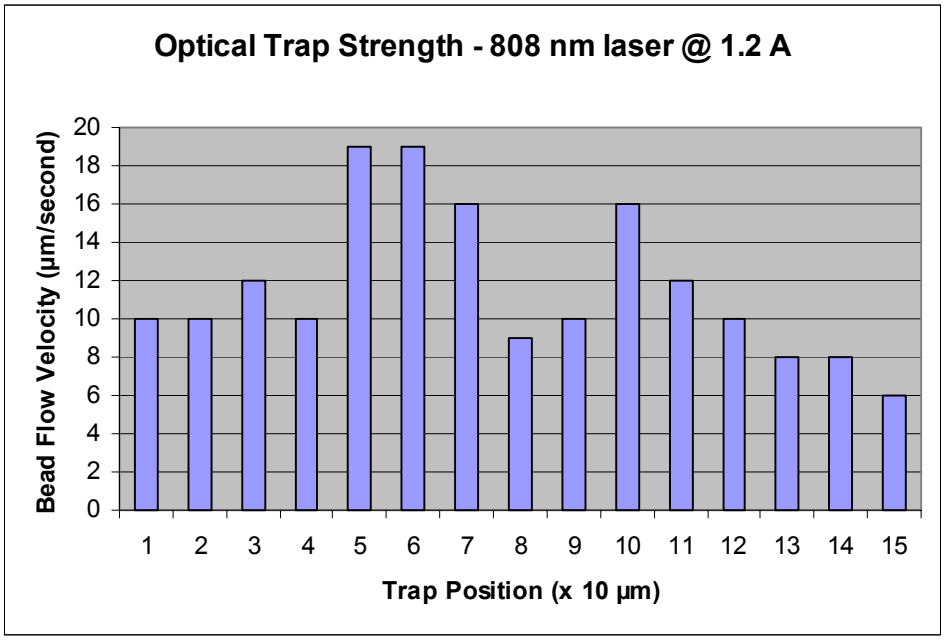

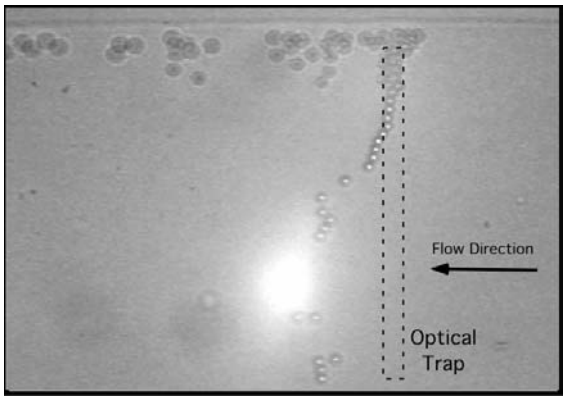

Figure 3.25: Trapping efficiency of 808 nm laser diode (@ 1.2 A) with latex beads/ 1x PBS in Sylgard microfluidic device

droplets in the mineral oil. Repulsion was clearly visible in the decane mixture. Slight repulsion was also observed in the hexadecane mixture at 1.00 A. At 1.25 A, repulsion in hexadecane was clearly visible. Droplets could be pushed around by moving the trap position using the XYZ stage. However, the laser diode was unable to repel droplets generated in the microfluidic devices. Reverse vesicles were generated using the three

oils and 1% Span 80 at ~10 psi. The pressure was then decreased to 1-2 psi to allow the droplets to slowly flow down the channels. At currents of 1.00 - 2.00 A, no droplet repulsion was observed in any of the oil mixtures.

Conclusions

A large effort went into constructing an optical valve and the supporting instrumentation for sorting water-in-oil droplets in a microfluidic device, but the final device was unsuitable for the application. In order to improve the device, the strength of the optical trap must be increased. While using a high power laser diode seemed like the best approach to create a strong repulsion barrier for the droplets, the power was attenuated by the wide beam profile (200 x 1 μm at the source). Better collimating optics combined with high NA objectives would help address this problem. Unlike trapping latex beads in water, which have quite different indices of refraction (1.59 vs 1.33, respectively), the values for water and the tested oils are much closer (1.33 vs 1.47), compounding the difficulty of repelling the droplets in a pressurized flow. Using oils with a higher index of refraction may offer a chemical solution for an improved optical valve.

3.5.2 Multilayer Soft Lithography: Elastomeric Valves

While the optical valve was not a success, another approach to gating microfluidic flow was being simultaneously investigated, the mechanical valve. Microscale mechanical valves and pumps fabricated from silicon had already been reported by several groups[73,74], but the meticulous assembly process combined with the stiffness of silicon made the technology impractical for rapidly prototyped microfluidic devices. While working with polymers like urethane and silicone to make microfluidic devices, we realized that these elastomers would make ideal microfluidic valves.

Device Design and Fabrication

The first monolithic microfluidic valve prototypes were made from silicone (GE RTV615). The devices were simple, containing a 100 x 10 μm microfluidic channel patterned from a wet-etched silicon wafer mold and a valve seat consisting of a cavity created by a computer chip placed over the channel during the curing process (Figure 3.26). Once the computer chip was removed from the cured device, a thin layer of silicone (~50-100 μm) remained over the top of the molded channel. When air pressure was applied to the cavity via syringe injection, the thin layer expanded, acting as a valve that collapsed the bottom channel.

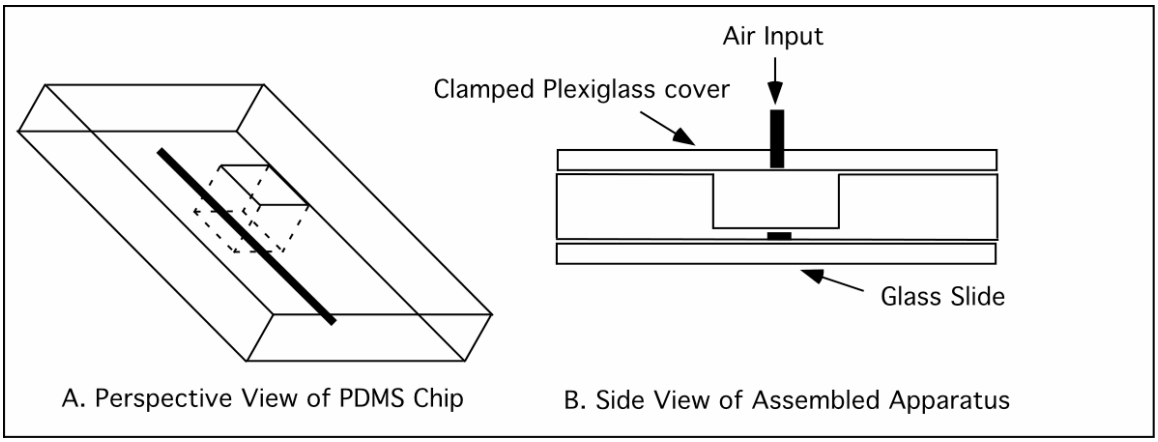

Figure 3.26: The first monolithic valve prototype developed in the Quake laboratory at Caltech. The flow channel mounted on the glass slide (black) is closed by applying air pressure to the valve seat left by the embedded computer chip.

Within months after the first prototype valve was fabricated from PDMS, Dr. Marc Unger and co-workers in our group developed a technique called "multilayer soft lithography" to fabricate monolithic valves and pumps[19]. Multilayer structures are made by bonding separately molded layers of silicone elastomer together to create a single

monolithic device. Using a two-part cure silicone, layer-layer bonding is achieved by varying the ratio of the components in each layer. For example, while the normal cure ratio for PDMS is 10:1 parts A:B, separate cured layers made from 20:1 and 5:1 can be bonded together by surface contact followed by a secondary baking step (Figure 3.27). Excess monomer and catalyst at the interface react to chemically crosslink the two layers. Valve structures are easily made by bonding a thick layer of patterned silicone to a layer spin-coated on a patterned silicon wafer. The spin coating process provides a method of precisely controlling the thickness of the silicone layer over the microchannels which function as valve structures in the assembled devices at the points where the top and bottom channels overlap. Efficient valve closure depends on microfluidic channel geometry. Rounded microfluidic channels, created by heating the patterned photoresist, close under pressure from above. Closure is incomplete in rectangular channels.

Multilayer soft lithography techniques were used to fabricate a two-layer Dow Corning Sylgard 184 crossflow device with integrated valves for droplet sorting. Sylgard was chosen as the material for the device because of its chemical compatibility with mineral oil and its elastomeric properties. A significant design modification was added to the device to accommodate chemical screening reactions where incubations of several minutes to a few hours are optimal (Figure 3.28A). The serpentine output channel at the crossflow junction was replaced with a large (~500 μm) high cavity to slow down the droplets and create an on-chip incubation chamber (Figure 3.28B). This design element not only created a more flexible on-chip screening environment, but also significantly reduced the footprint of the chip from 1 in^2 to 0.5 in^2. A control layer of valves was added

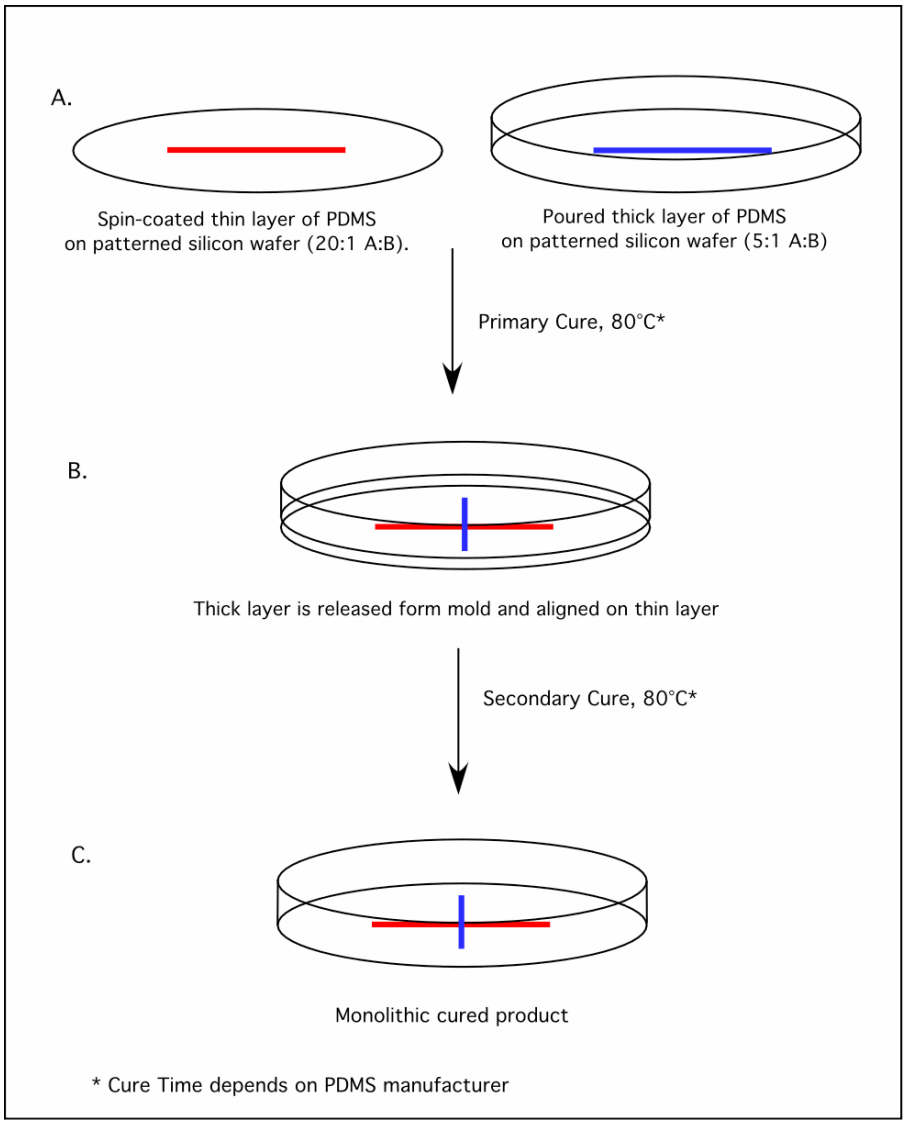

Figure 3.27: Multilayer soft lithography. Thick and thin layers of silicone with different component ratios bond together to create a monolithic microfluidic device. In the illustrated example, the red line represents the flow channel on the bottom face of the final device while the blue line represents the control channel. Inlet holes for the channels are punched for the thick layer after the primary cure and for the thin layer after the secondary cure. Like the original monolithic silicone valve prototype, the interfacial layer separating the overlapping channels is the functional valve.

for sorting droplets at the T-junction intersection at the end of the chip (Figure 3.28C). The devices were fabricated from the rounded 5740 photoresist molds. The incubation cavity was created by placing ~1 µl of 5740 resist over the center of the developed, but not hard baked, flow layer mold. The mold was then hard baked for 30 minutes at 120°C to round the flow channels and drive the solvent out of the resist forming the cavity.

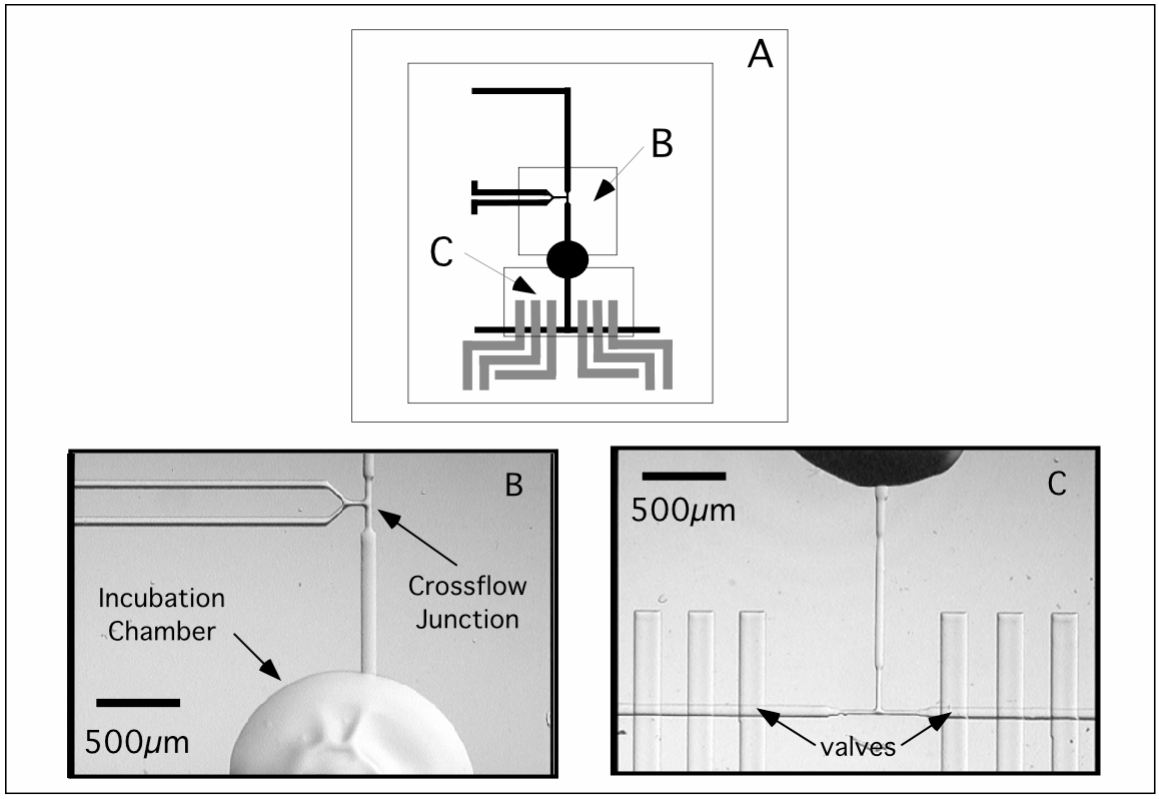

Figure 3.28: Schematic of silicone crossflow device with incubation cavity. A) Microfluidic chip design. Black layer - flow layer; Grey layer - control layer. B) High resolution image of actual chip showing crossflow junction and incubation chamber. C) High resolution of sorting junction in chip showing valve structures.

The Sylgard 184 crossflow devices were prepared in four steps: 1) The flow layer was spin-coated with 20:1 Sylgard 184 at 3000 rpm / 30 seconds while the thick layer of 5:1 Sylgard was poured on the control layer containing the valve structures. 2) After a 30 minute cure at 80° C, the thick layer was processed and aligned on the cured thin layer. Unlike typical multilayer microfluidic devices, the protruding incubation chamber prevented the alignment of the thick layer over the total area of the chip. To solve this problem, the thick layer was trimmed to small pieces containing the only the essential valve structures prior to layer-layer alignment. 3) As the device at this fabrication stage consisted of a thin flow layer and small regions of aligned valve structures, additional 5:1 Sylgard 184 was poured over the remaining exposed surface of the thin layer to the approximate height of the aligned thick layer prior to the secondary cure. This step was essential to provide a uniform thick layer over the flow layer for structural stability. The device was then cured for 1 hour at 80°C to facilitate layer-layer bonding. 4) Meanwhile, a thin layer of 5:1 Sylgard was spin coated at 5000 rpm for 30 second on a No. 1 coverslip (Corning glass) and cured for 80°C for 30 minutes. After the two-layer crossflow devices were cured, they were released from the mold, processed, and sealed channel side down on the coated coverslips. The spin-coated third layer is critical for creating flow channels that do not delaminate from the coverslip when subjected to the high pressures (15 - 20 psi) required to flow mineral oil through Sylgard. After a 2 hour tertiary cure, the three-layer devices were ready for testing.

Droplets were generated in the Sylgard 184 crossflow devices using mineral oil/ 1% Span 80 for the continuous phase and dH_2O for the disperse phase. Water and oil steams were balanced at the crossflow junction at ~12/15 psi water/oil-surfactant (w/o-s).

Water droplet formation was initiated by increasing the water pressure to 12.5 - 13.0 psi. Generated water droplets entered the "incubation" cavity, where they encountered a sharp drop in flow velocity (Figure 3.29A). After ~ 1 hour, the droplets had passed entirely through the cavity and re-entered the narrow (~60 μm wide) outlet channel, where they flowed toward the T-junction for valve-based sorting.

Initial sorting was performed by manually switching the valves while observing the droplets under 20x magnification. The elastomeric valves were actuated using pressurized air controlled by an external solenoid valve. When ~13-15 psi of air pressure was applied to the selected control channel, the interfacial membrane between the two channel layers (Figure 3.28C) was deflected down, closing the underlying flow channel. Manual valve switching rates of several Hz were carried out without any observable mechanical breakdown. The valves efficiently sorted the droplets at the T-junction (Figure 3.29B).

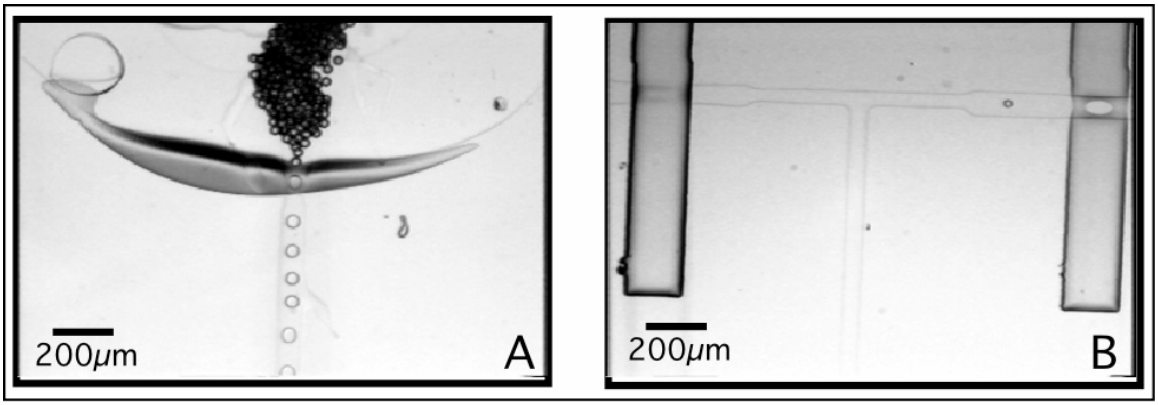

Figure 3.29: A) Water droplets entering incubation cavity of Sylgard 184 device. B) Sorting of droplets using elastomeric valves.

3.6 Detection: Development of a Fluorescence-Activated Droplet Sorter

Introduction

After we successfully demonstrated droplet sorting via elastomeric valves in the silicone microfluidic devices, the next logical step was to develop a platform to automate the process for high-throughput screening applications. Given the small volume of the individual droplets, fluorescence was proposed as an ultrasensitive indicator system for applications such as single-cell assays of enzymatic activity or protein/protein interactions.

The current, state-of-the art, fluorescence-based sorting system is the fluorescence-activated cell sorter (FACS). Capable of sorting up to 3 x 10^5 cells/ second, FACS systems have found applications in cytology, genetics, immunology, and microbiology[75,76]. As a tool for high-throughput screening applications, FACS has been used to sort combinatorial enzyme libraries[77]. The key components of traditional FACS systems are a pressurized liquid stream through which the sample is flowed, one or more lasers orthogonal to the stream that excite the fluorescent tagged particles, photodetectors to pick up the emitted light, and sorting hardware. At the sorting nozzle, the stream is broken up into discrete droplets and a charge is applied to positively selected droplets. The charged droplets are deflected by a pair of metal plates into a collection vial. However, convention FACS machines have several drawbacks that limit their utility in high throughput screening applications. Traditional FACS applications are affinity-based. Molecules such as antibodies or peptides specifically react with targets on the particle

surface. As the labeled particles are flowed through a common stream toward the detector element, the fluorescent tag must remain localized on the particle. Applications such as single enzyme assays where a soluble fluorescent product is generated can not be analyzed in this bulk environment. Most conventional FACS machines also require fairly large particles (10-30 μm diameter) to provide adequate signal/noise ratios for sorting. The ability to sort single particles on the bacteria-scale (1-2μm) is only available on the new high-end models.

Microfabricated sorting devices were first developed in our laboratory to sort DNA, beads, and cells. The first sorting devices used electroosmotic flow, in which the net fluid flow in the channel is driven by the migration of the positive ions in response to an electrical field. Under electroosmotic flow, directionality is accomplished in the microfabricated device by creating a net current through the buffer with a set of electrodes placed in the sample and output wells. This system has been tested using bacteria expressing green fluorescent protein and YOYO-1 stained DNA[10,11,78]. Sorting is accomplished by exciting the cells or DNA in a narrow detection region upstream of a narrow T-junction with a 488nm argon laser focused through the objective lens, which also collects the emitted light. The photocurrent from the detector is pre-amplified to voltage by a Burr-Brown OP128 op amp (10^7V/A), digitized, and processed by a computer running the analysis program, Labview. The computer sends out analog outputs (-5 V to 5 V), which are amplified and sent to the platinum electrodes in the wells. The final destination of the sorted cells or DNA depends on the net direction of the current after the fluorescent signal has been processed. The switching response time at the junction has been reported to be less that 1 msec[11].

The first elastomeric microfabricated FACS that sorted *E. coli* using integrated pumps and valves was developed by Anne Fu and colleagues in the Quake laboratory at Caltech[79]. Like its electroosmotic predecessor, the detector element was configured around a T-junction. Multilayer soft lithography techniques were used to create a set of integrated elastomeric valves on each side of the T-junction and a set of three valves upstream of the junction that acts as a peristaltic pump to flow the cells through the device when actuated sequentially. Using a water-cooled Argon laser (488nm), enrichment efficiencies of up to 89-fold were reported for eGFP expressing *E. coli* in a nonfluorescent control cell population.

The goal in the design and development of the microfabricated fluorescence-activated droplet sorter was to make a device that was significantly smaller than the previous sorters in the laboratory, eliminating large components present in the aforementioned elastomeric sorting device such as the inverted microscope and the bulky water-cooled laser system. The following sections detail the design and development of the sorter and, as a demonstration of its functionality, two-color sorting of dye-filled droplets in a multilayer elastomeric microfluidic device.

Design and Development

While microfluidics has dramatically reduced the analytical sample volume from microliters to picoliters, supporting control hardware such as computers, lasers, and microscopes are major obstacles to true device portability. With this concept in mind, the microfluidic droplet sorter was designed with a small footprint (12' x 9") on an aluminum optical breadboard, nearly an order of magnitude smaller than the space occupied by the previous prototypes in the laboratory using water-cooled lasers (Figure 3.30). The core

component of the droplet sorter is a solid state diode-pumped blue laser (Intelite - λ=473 nm). With dimensions of only 9.0 x 3.5 x 2.0", its 20 mW power output is comparable to a water-cooled argon ion laser several feet in length.

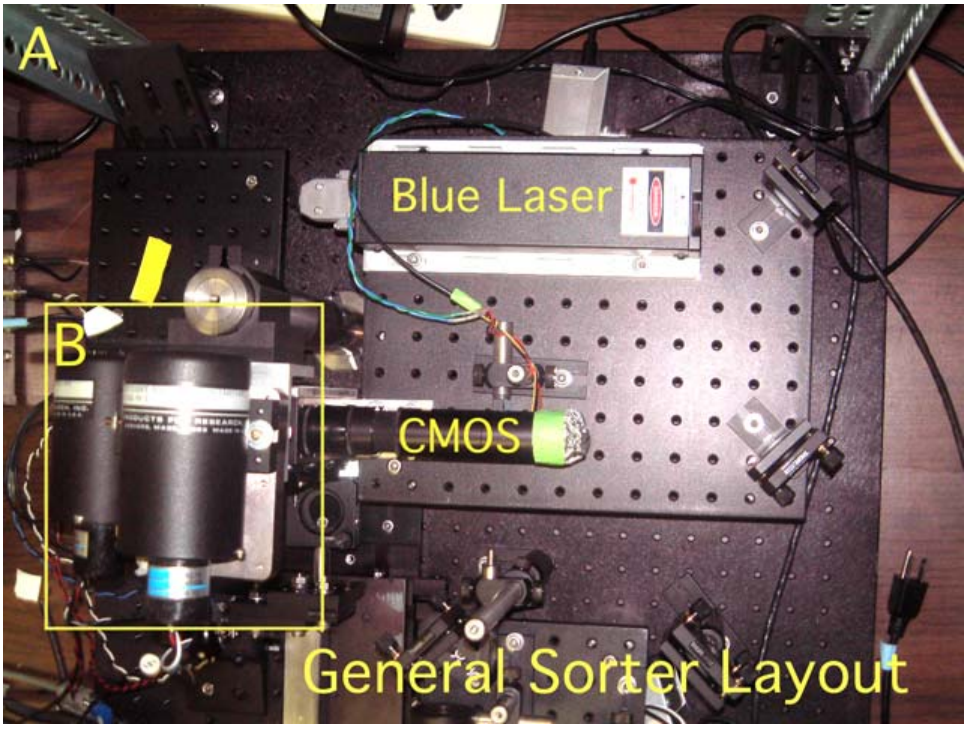

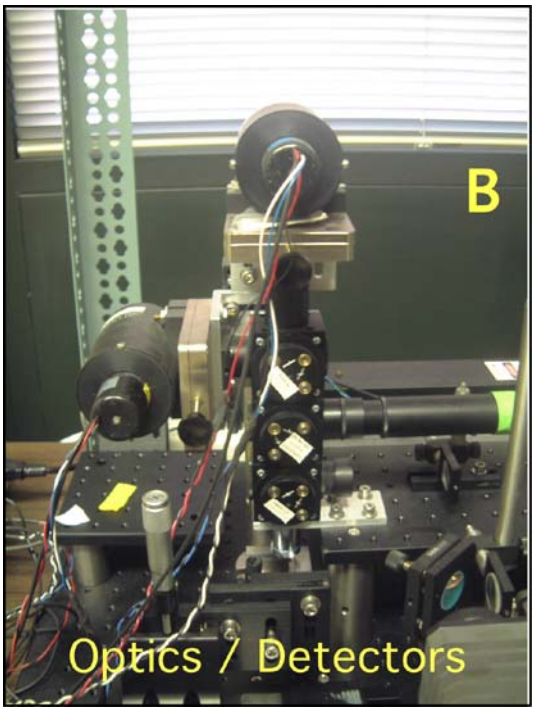

Figure 3.30: Microfluidic droplet sorter.
A) General sorter layout showing position of laser, CMOS camera, and optics/ detector head.
B) Side view of optics, filter cubes and PMT detectors.
*For a detailed schematic of the device components and layout, see Appendix B.

To operate the droplet sorter, the blue laser beam is reflected off a 500nm long-pass filter through the objective lens onto the sample plane of the crossflow microfluidic device actively generating droplets. Emitted photons from blue-light excitable red or green fluorophores in the droplets pass through the 500nm filter and are sent to both the CMOS camera for visualization and the 565 nm longpass filter that transmits the red photons while reflecting the green (Figure 3.31). The photons are detected by the photomultiplier tubes. Like previous microfluidic sorting devices,

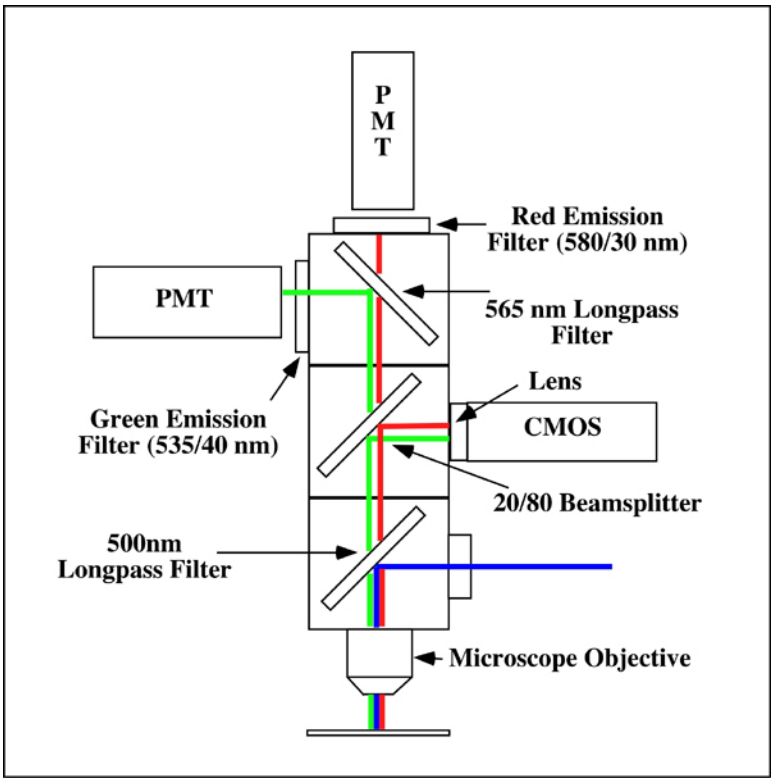

Figure 3.31: Functional diagram of droplet sorter. Blue laser light is focused onto the sample plane. Emitted green and red light is collected by the respective PMTs. The CMOS camera is for sample positioning.

the PMT current levels are converted to voltage, digitized, and processed by a computer running the analysis program, Labview. Droplet sorting is accomplished by setting the threshold voltage value for each PMT above which the sorting valves are actuated. For automated sorting, the computer sends a signal to a digital output card (National

Instruments PCI-DIO-32HS), which activates the solenoid valves that provide pneumatic pressure to the on-chip elastomeric sorting valves.

Two Color Droplet Sorting

As a functional demonstration of the device, the fluorescence-activated droplet sorter was used to sort 2-3μm diameter droplets filled with either green (fluorescein) or red (R-phycoerythrin) fluorescent dyes. Both dyes are excited by the 473nm blue laser and have appropriate distinct emission spectra for the two PMT detectors.

A Sylgard 184 microcavity crossflow device was primed with mineral oil/ 1% span 80 at the oil input, with fluorescein (130 μM in PBS, pH 7.2) and R-phycoerythrin (830nM in 0.1M sodium phosphate buffer, 0.1 M NaCl, pH 7.4). Flow was balanced at the crossflow junction at 14.2/18.0 psi (w/o-s), with the oil physically separating the two dye channels (Figure 3.32A). Single color-droplets were generated by adjusting the

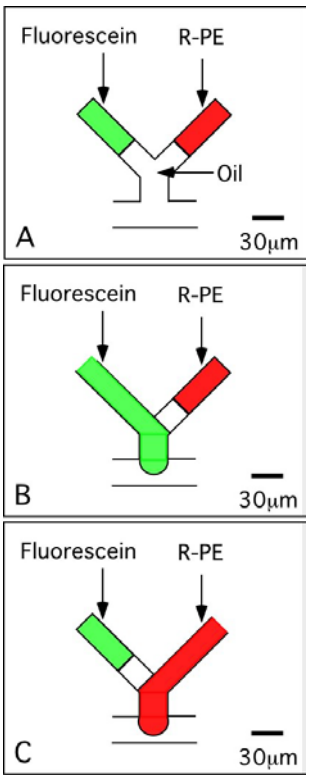

Figure 3.32: Single-color droplet formation at the crossflow junction. A) At equilibrium, the oil phase blocks both of the dye streams, preventing them from entering the crossflow junction B) As the pressure in the fluorescein channel is increased, droplets of fluorescein are generated at the junction while R-phycoerythrin (R-PE) flow is stagnant. C) Increasing the pressure of the R-PE input generates R-PE droplets at the junction.

relative pressures of the two dye streams, allowing only one stream to enter the crossflow region for droplet formation while the other stream is blocked and isolated by a plug of oil (Figure 3.32B,C). As switching between the two dye steams was accomplished manually, several hundred droplets were generated for each color type each time the relative water pressures were changed. Using this process, thousands of fluorescein/R-phycoerythrin droplets were generated with a rough population distribution of ~1:1. The formed droplets entered the microcavity, where they slowed down and formed a mixed cluster of droplets.

To sort the mixed droplet population, a detection region was set up ~100 μm upstream of the T-junction near the device outlets (Figure 3.33). The blue laser was

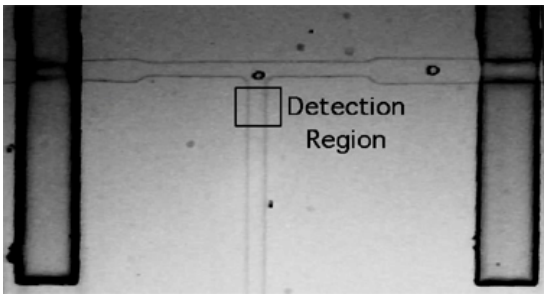

Figure 3.33: Detector region during the two-color droplet sorting process in a microcavity crossflow device.

tuned to ~15mW output power and focused down into the detection region with a 40x 0.65 NA objective (Olympus). As the fluorescent droplets passed through the detection region, the emitted light was collected by the PMTs, converted to voltage, and the resulting analog signal was fed into a National Instrument PC1200 board. A Labview based-program was written to analyze the input voltages from the two PMT channels. Based on set threshold values for each channel (+2.00 V of a 0 to +10 V scale), the program actuated the valves (actuation pressure=15 psi) to sort the droplets toward the respective output channels. Individual fluorescein droplets had average valves of +1 V in

the red channel and +4 V in the green channel, while, in R-PE droplets, the values were reversed (<1 V green, +4 V red). Droplet frequency passing through the detection region was low, with a single droplet or small cluster of droplets leaving the microcavity and passing through the region every few seconds. Sorting efficiency was measured both by looking at the PMT output values of the output material in the collection wells. As droplets formed a large aggregate in the output wells, PMT readings were not especially useful as neighbor droplets washed out the signal from improperly sorted droplets. Visual inspection of the output wells was carried under a 40x objective (0.65NA) on an inverted microscope (Olympus IX50) equipped with a mercury lamp. The wells were rapidly scanned using both green (Ex 480 nm ds 30/ Em 535 nm ds 40) and red (Ex 540 nm ds 25/ Em 605 nm ds 55) filter sets to look for improperly sorted droplets. Of the thousands of sorted droplets in each well, only a small fraction (~1-2%) were of the wrong dye type.

3.7 Conclusions

Creating and developing a microfluidic droplet generating device and its supporting instrumentation was in itself a dynamic process. The initial emulsification experiments emphasized the important relationship between emulsion stability and monodispersity. The crude, polydisperse emulsions produced by the propeller method evolved into stable, monodisperse droplets produced by the microfluidic crossflow devices. With dynamic microfluidic droplet formation as a viable method for encapsulating combinatorial chemical or biological libraries, it became necessary to develop technologies to actively manipulate the formed droplets.

While work on developing an optical valve to repel droplets was not successful, the project stimulated thought on alternatives to electroosmotic microfluidic flow switching methodology. Work on the development of monolithic elastomeric valves, first in polyurethane and later in PDMS, established a reliable on-chip method to sort droplets. Culminating with the development of the fluorescence-activated droplet sorter, an integrated microfluidic screening system emerged.

Chapter 4 - Microfluidic Crossflow: Biochemical Screening Applications

4.1 Introduction

The study of enzymatic reactions in reverse micelles is not new. In fact, since 1977, over 30 enzymes have been encapsulated and studied in this system[80]. Chemical reactions in reverse micelles can be analyzed using a variety of methods, including NMR, fluorescence, absorption, and calorimetry. In these experiments, the term "reverse micelle" has been confined to small vesicles, where the water-to-surfactant ratio, defined as w_O, is less than 15. Under these conditions, changing the water concentration can have a dramatic effect on the enzymatic catalysis rate. For several hydrophobic enzymes, such as α-chymotrypsin and lysozyme, optimal activity is not found at high w_O values, but rather at w_O values of 8-12[81,82,83]. In these examples, activity may be enhanced by interaction between the enzyme and the surfactant phase or the low water content in the reverse micelle core. Activity enhancement has not been limited to hydrophobic enzymes. A large activity enhancement in reverse micelles has also been reported for peroxidase[84] and acid phosphatase[85], in which electrostatic interactions between the enzyme and surfactant are thought to play a role.

Droplets with larger water-to-surfactant ratios (w_O >15) have frequently been referred to as reverse vesicles rather than reverse micelles. Vesicles generated by the microfluidic crossflow device using water/Span80/mineral oil, with micron-scale dimensions, fall within this category. As the water content in a vesicle increases, the

encapsulated water begins to behave like bulk water[86]. Under these conditions, enzymatic activity profiles are comparable to those observed in free solution. The first report of enzymatic activity in reverse vesicles was described in 1992 using polyphenol oxidase[87], where V_{max} was similar to that in water and twice that displayed in reverse micelles[88]. More recently, Tawfik and Griffiths reported the use of reverse vesicles for the transcription/translation of HaeIII methyltransferase, using substrate-tagged genetic material to specifically isolate encoding DNA strands from a 10-fold excess of genes encoding another enzyme[38]. These systems illustrate the potential of microcompartmentalization for high throughput screening processes.

In this section, the development and characterization of a model enzyme system in reverse vesicles generated by microfluidic crossflow is presented using recombinant p-nitrobenzyl (pNB) esterase expressed in *E. coli*. While the system was not entirely successful, with several problems encountered including substrate autohydrolysis and inefficient diffusion of the substrate across the cell membrane, the experiments provide important data for designing future emulsion-based assay systems.

4.2 Principle and Design

Using microfluidic crossflow, an assay was designed to measure recombinant enzyme activity at the single cell level. Cells expressing a recombinant enzyme and the appropriate substrate are injected into separate water channels that meet at the crossflow junction (Figure 4.1). As soon as the two water streams merge, they are immediately encapsulated into a droplet in the oil-surfactant stream. As the droplets flow down the channel toward the outlet, the substrate is converted to a detectable fluorescent product.

Under monodisperse droplet generating conditions, a PMT-based detector system can be used not only to compare endpoint activity between individual droplets at a fixed position in the outflow channel, but also to obtain single cell kinetic data for an enzyme population by taking measurements of droplets at multiple channel positions.

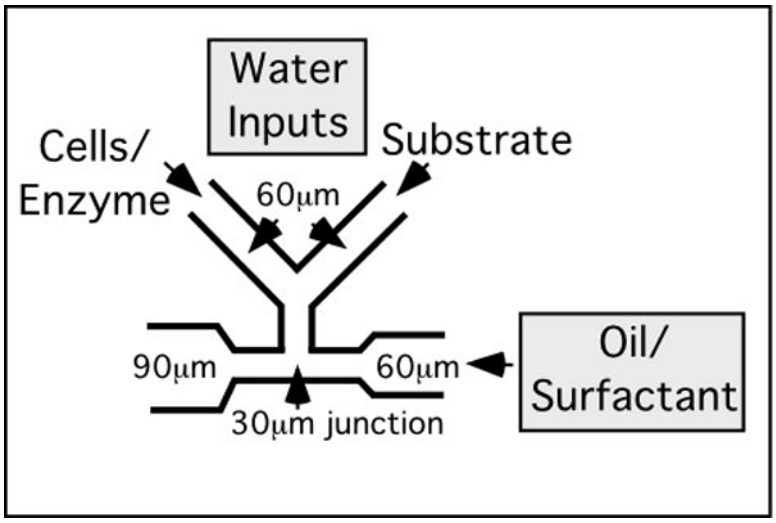

Figure 4.1: Microfluidic channel layout in a microfluidic crossflow for single cell catalysis measurements.

Several crossflow patterns were designed with serpentine outlet channels. The length and width of the channel where the droplets emerge from the crossflow junction were varied to create a long outlet path that served as an incubation chamber for the encapsulated enzyme and substrate. Single-layer devices were fabricated in Sylgard 184 from the photoresist molds of the patterns. With a 90 μm wide x 10 μm high output channel ~8 cm in length, formed droplets required ~20 minutes to reach the output well. Given adequate spacing between the monodisperse droplets at the crossflow junction, water droplets in mineral oil/2% Span 80 (13.0/15.0 psi w/o-s) traveled as a perfectly coherent stream from the crossflow junction to the outlet well (Figure 4.2). At higher relative water pressures, the generated droplets collided in the output channels, forming aggregates.

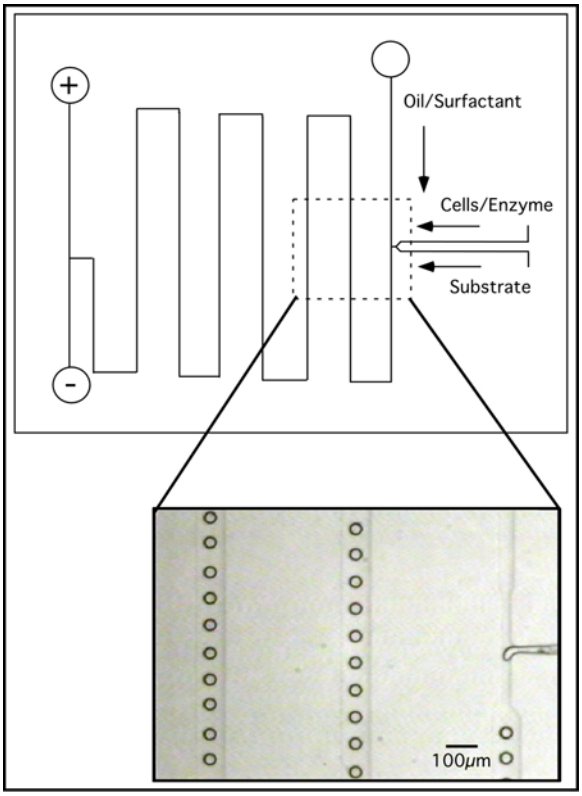

Figure 4.2: Serpentine channel design for biochemical screening chip. Monodisperse water droplets in mineral oil/2% Span 80 retain a coherent pattern as they flow towards the device outlet.

4.3 Model Enzyme System: P-Nitrobenzyl Esterase in *E. coli*

P-nitrobenzyl (pNB) esterase was chosen as a model enzyme system because it exhibits fast kinetics towards substrates like pNB-acetate (K_{cat}/K_m= 1.5 x 10^6 $M^{-1}s^{-1}$), is readily expressed in recombinant form and has commercially available substrates that are converted to fluorescent products. The pNB carboxy-esterase catalyzes rapid ester hydrolysis for simple organic esters, benzyl acetate and alpha-naphthyl acetate and deblocking (ester hydrolysis) of beta-lactam antibiotic PNB esters such as cephalexin-pNB and loracarbef-pNB[89]. The gene, originally isolated from *B. subtilis*, has been used in directed evolution studies to create enzyme variants that are more thermostable and active in organic solvents[90,91].

Expression was carried out in an *E. coli* host (TG1) as a cloned vector construct (pNB106R) under a temperature-sensitive λ promoter. Primary growth consisted of an overnight incubation of a plated colony in a shaker flask containing 10 ml Luria broth (LB) with 25µg/ml tetracycline at 30°C. The cells were then split 1:100 and grown for an additional 4.5 hours at 30°C. The culture temperature was then raised to 42°C for an additional 2.5 hours to induce synthesis of the recombinant esterase protein. While engineered for periplasmic expression, enzyme leakage into the extracellular medium was still observed. After induction, the cells were spun down at 735 x g, washed twice in PBS pH 7.0 to remove residual external enzyme, and resuspended in ice cold PBS in preparation for the on-chip assay.

A 0.5 mM stock of the substrate, fluorescein diacetate (FDA), was prepared by dissolving 2 mg FDA in 10 ml acetone. At neutral pH, pNB esterase cleaves FDA into the detectable fluorescein product (Figure 4.3). A working solution was made by diluting

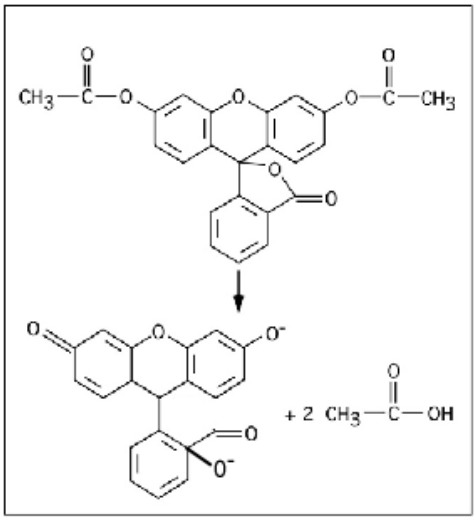

Figure 4.3: The conversion of fluorescein diacetate to fluorescein (λ_{ex} = 490 nm, $\lambda_{em\ (max)}$ = 518 nm). The reaction occurs via the cleavage of the ester bonds by pNB esterase.

the stock solution in PBS, pH 7.0, to a final concentration of 25 μM. The working solution, which contained 5% acetone (v/v), was formulated to shock the bacteria and facilitate

entry of the substrate into the cell. Five-minute endpoint spectrofluorometer-based experiments (Shimadzu RF-5301PC, λ_{ex}=490 nm, λ_{em}=514 nm) of washed and induced wild-type cultures in the presence of prepared substrate showed that small fractions of acetone (5-10% v/v) substantially improved the rate of product formation (up to twofold vs. substrate in PBS alone).

4.4 Encapsulation and Assay Mechanics

With all of the reagents prepared and optimized, crossflow experiments were initiated in crossflow devices. While the initial devices were fabricated from polyurethane (Ebecryl 270), later devices were also fabricated from Sylgard 184. The silicone-based devices proved to be superior, having lower background green fluorescence when observed under the mercury lamp (Ex 480 nm ds 30/ Em 535 nm ds 40) and lower cell adhesion levels to the channel walls. Using mineral oil/2% Span 80 for the continuous phase, the oil stream was balanced against the two separate aqueous inputs (containing washed cells and substrate respectively) as previously described for the two-color droplet sorting experiment (Chapter 3, Section 6). Balanced flow input pressures were generally within the range of 12-15 psi for the aqueous reagents and 15-20 psi for the oil phase. Crossflow was initiated by slightly decreasing the oil pressure to merge the two balanced water streams at the junction so that droplets containing ~50/50 (v/v) cell/substrate were generated at the breakoff point. Washed cells were initially diluted at

1:100 in PBS pH 7.0 so that each droplet (~30 pL) contained an average of one cell. When the input pressure of the substrate and cell solutions were balanced, very little mixing between the streams was observed under the laminar flow conditions present in the microfluidic device. As the droplets were sheared off at the junction, the cells became encapsulated with the substrate mixture (Figure 4.4). Mixing in the droplets was nearly instantaneous as the cells slowed down upon entering the wide output channel.

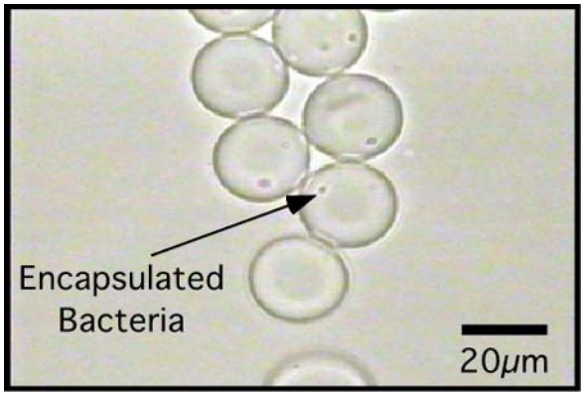

Figure 4.4: Encapsulated bacteria in droplets generated by microfluidic crossflow.

The crossflow assay was unreliable, as problems such as cell adhesion to the channel walls, substrate autohydrolysis, and pressure imbalances between the two aqueous inputs quickly made the microfabricated devices non-functional. The troubleshooting of these difficulties will be discussed in section 4.5. However, a few good examples of catalysis inside the formed droplets were still acquired (Figure 4.5). Droplets were visualized for fluorescent product approximately 10 minutes after encapsulation after they had flowed through 4 -5 loops of the wide serpentine output channel. The active cells took on a bright fluorescent green coloration as they accumulated fluorescein product during catalysis, making it easy to visually confirm their presence in droplets under a 60x / 1.4 NA oil immersion objective.

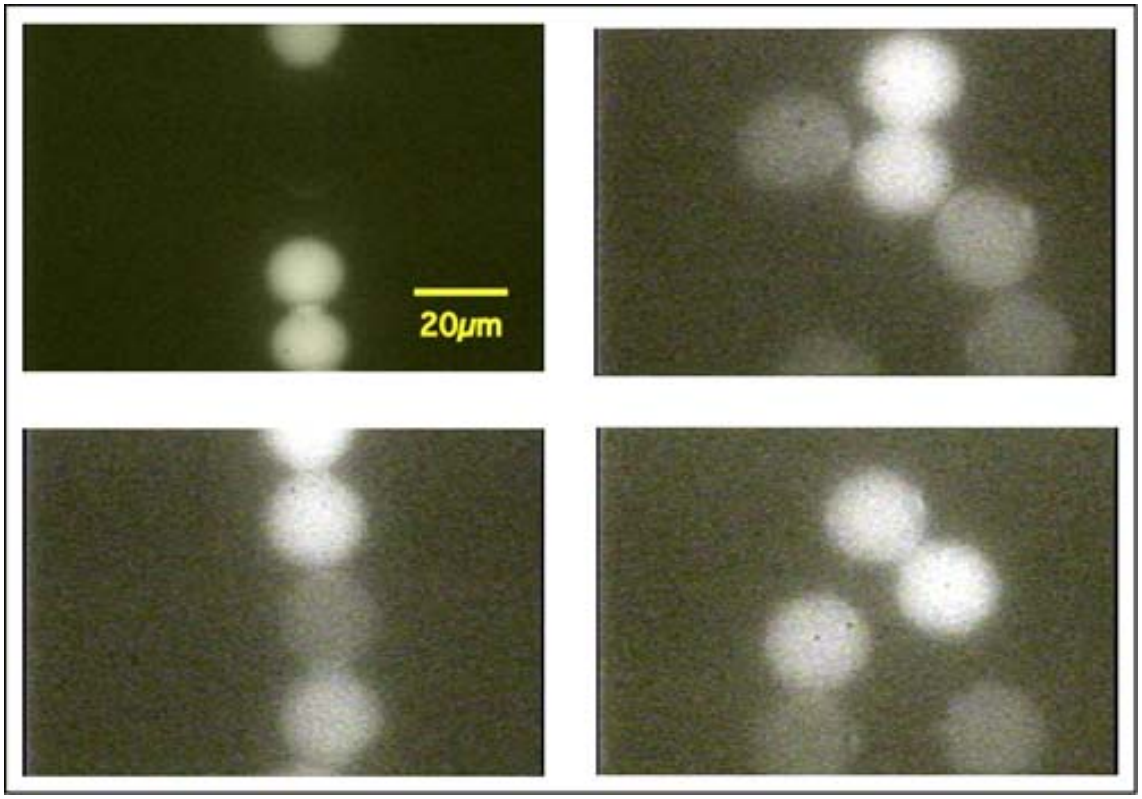

Figure 4.5: Monodisperse droplets containing *E. coli* expressing recombinant pNB esterase and fluorescein diacetate substrate. Droplets containing no cells are non-fluorescent while droplets containing one or more enzyme-expressing cells have converted the substrate into the fluorescent fluorescein product.

4.5 Droplet Assay Troubleshooting

While the mechanical aspects of the microfluidic droplet-generating device have been well characterized, its integration with biochemical systems still remains

problematic. Hundreds of crossflow devices were fabricated, injected with pNB esterase assay components, and ultimately discarded in an attempt to discover the perfect operating conditions. This section is intended to offer some insight into the troubleshooting process that evolved as the on-chip assay for pNB esterase was being developed.

4.5.1 Flow Balance

Establishing the flow balance between the two aqueous streams was a nontrivial process. A slight pressure imbalance between the streams led to instantaneous cross-contamination, as the contents of one aqueous channel rapidly flowed up the channel of the other aqueous input. Once cross-contaminated, background fluorescence levels in the droplets dramatically increased as the substrate was rapidly converted to product prior to encapsulation at the crossflow junction. To facilitate the flow balancing process, beads were added to the cell input solution to visually differentiate it from the substrate mixture and design work was done to optimize the channel geometry.

Micron-size bacterial cells were difficult to see at the low cell concentration used in the assay, making it extremely difficult to balance the aqueous inputs at the crossflow junction. Several types of beads were spiked into the cell solution as visual aides. The first experiments used 2.3μm diameter non-fluorescent latex beads (Interfacial Dynamics Corp.). A 10 μl aliquot of the bead stock solution (40 mg/ml in water) was added to 1ml of the diluted cell preparation. Flow was balanced at ~13.0 psi/ 15.0 psi (w/o-s) in a Sylgard 184 crossflow device with the standard dimensions illustrated in Figure 4.1, the two water streams were kept separated by the mineral oil/2% Span 80 phase. The oil pressure was slowly dropped to allow the two water streams to merge and droplet

formation was initiated. Under a 20x objective, it was easy to balance the two aqueous inputs with minimal backflow. However, over a period of a few minutes, the latex beads stuck to the channel walls at the junction interface, causing chaotic droplet formation and acting as a filter that trapped the bacteria in the stream just prior to encapsulation. Smaller beads gave better results. 100 nm red fluorescent microspheres (Duke Scientific) were tested in the crossflow devices using the same conditions. While a 1:100 dilution of these beads (10 mg/ml stock solution) could not be visualized by standard light microscopy, they were observed under a 60x oil immersion lens using the mercury lamp and a red filter set (λ_{ex} = 540 nm ds 25/ λ_{em} = 605 nm ds 55). The red fluorescent beads were chosen to have minimal spectral overlap with the fluorescein product generated in the assay. Flow balance at the junction was readily accomplished (Figure 4.6). Bead sticking to the channel walls was still observed, but not to the extent that it disrupted droplet formation.

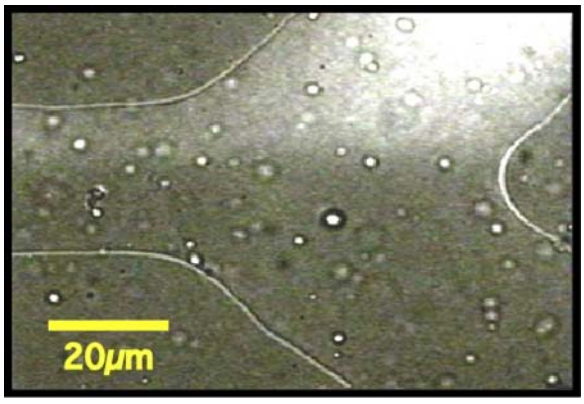

Figure 4.6: Flow balance at the crossflow junction between cells mixed with 0.1 μm red fluorescent beads (top channel) and substrate (bottom channel).

Channel geometry modifications were made at the crossflow junction to increase backflow resistance between the two aqueous streams. The 60 μm wide aqueous input channels were reduced to 22.5 - 30 μm while the junction region proximal to the shear point was widened to 60 - 80 μm (Figure 4.7). Narrower aqueous input channels, in

which the flow resistance was high, reduced the backflow in the system and made it easier to balance the aqueous streams at the junction.

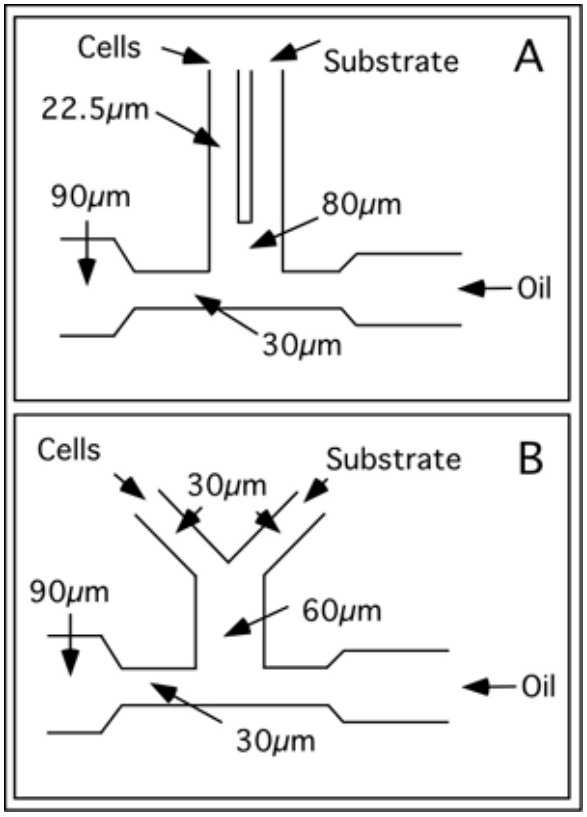

Figure 4.7: Restricted crossflow pattern designs to minimize crosstalk between the two aqueous input lines.

4.5.2 Cell Adhesion to PDMS

The second major problem with the assay was bacterial cell adhesion to the walls of the Sylgard 184 microchannels prior to encapsulation. Under assay conditions, the bacteria travel very slowly (50-100 μm/second down the aqueous input channel) as they flow toward the crossflow junction, because the flow rate of aqueous solution into the oil stream is very low (~ 50-100 pL/second at a droplet generation rate of 2 -3 Hz). Before reaching the crossflow junction, the majority of the bacteria suspended in a PBS solution stick to the channel walls.

To reduce bacterial adhesion, modifications were made to both the cell resuspension solution and the PDMS surface. Bovine serum albumin (BSA) and the non-ionic detergent Tween 20 were investigated as water-soluble blocking agents in the diluted cell mixture. Induced *E. coli* cells expressing pNB esterase were washed in PBS and diluted 1:500 in PBS containing either 2 mg/ml BSA or 0.1% Tween 20. Tests in the Sylgard crossflow devices under standard assay conditions showed that BSA had minimal effect on cell adhesion to the input microchannel, while cell adhesion in the Tween 20 mixture was several-fold lower. However, very low activity, if any, was observed in droplets containing either BSA or Tween 20, cells, and substrate. The inhibitory effects of the blocking agents were validated in bulk assays on the spectrofluorometer (Table 4.1). A significant drop in activity was observed in the presence of either Tween 20 or BSA. The data suggest that these blocking agents

Additive	RFU
none (5% Acetone, 50μm FDA)	27
2mg/ml bovine serum albumin	12.6
0.1% Tween 20	13.2
2mg/ml bovine serum albumin / 10% Acetone	25.3
0.1% Tween 20 / 10% Acetone	36.6
0.1% Tween 20 / 25% Bugbuster	44.6
2mg/ml bovine serum albumin/ 25% Bugbuster	46.6
10% Acetone	50
25% Bugbuster	97.3

Table 4.1: Surfactant and additive effects on whole cell *E. coli* expressing recombinant pNB esterase. 60-second endpoint assay on Shimadzu RF-5301PC (λ_{ex}=490 nm / λ_{am}=514 nm). No additive control solution contains 1:1 dilution of washed cells in PBS, pH 7.0, containing 5% acetone and 50 μm FDA.

non-specifically inhibit enzyme activity by blocking the diffusion of the substrate across the outer bacterial membrane. The addition of agents that shock the outer membrane, such as high acetone concentrations or the cell lysis agent, Bugbuster, reverse the inhibitory effect, giving support to the blocking hypothesis. Attempts to create a crossflow assay with 0.1% Tween 20 in the diluted cell mixture and 10-25% Bugbuster in the substrate mixture were unsuccessful. As a surfactant, Bugbuster dramatically changes the crossflow contact angle, generating polydisperse bursts of droplets (Figure 4.8).

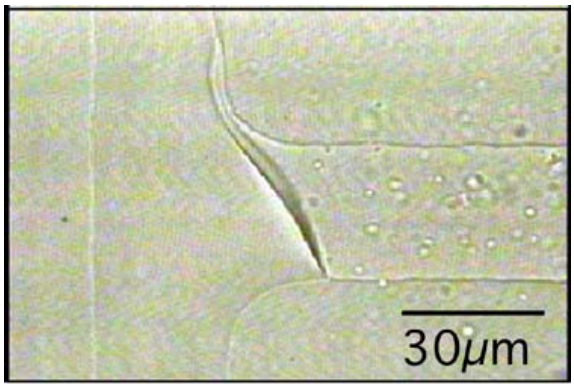

Figure 4.8: Bugbuster (12.5% v/v in PBS) sheared into mineral oil / 2% Span 80 in a Sylgard 184 crossflow device.

Attempts to alter the surface chemistry of the PDMS channels to prevent cell adhesion included HCl treatment of the channel surface and preparation of devices made with a small amount of MAKON 6, on oil-based surfactant. Both of these techniques were developed in our laboratory by Dr. Hou-Pu Chou and Dr. Anne Fu. HCl-treated Sylgard devices were made by injecting a solution of dilute HCl, pH 2.7, into the two-layer serpentine crossflow devices, filling all of the channels. After 1 hour at 37°C, the devices were flushed with water to remove residual HCl and dried at 80°C overnight. Crossflow tests under standard operating conditions showed no significant difference in

cell adhesion to the channel walls, chaotic droplet break, and wetting of the output channel walls, a phenomenon not observed with hdrophilic urethane after priming with oil/surfactant. Two-layer devices were also made with 0.2% MAKON 6 in both the 5:1 and 20:1 layers under standard fabrication conditions. Layer-layer bonding in the finished devices was incomplete and the surface was greasy. Mineral oil flowed through MAKON6-treated channels extracted the detergent, leaving a sludge on the channel surface.

4.5.3 Substrate Autohydrolysis

Detectable catalytic activity was generally only observable in the initial droplets formed in each experiment. Significant autohydrolysis was evident in the FDA substrate channel in time periods as short as 10 minutes, creating a stream of fluorescein that combined with the cell input stream and masked the catalytic activity of subsequently formed droplets. Working buffers with several pHs were tested. Fluorescein has a pKa of ~6.4, and it exhibits poor fluorescence in its protonated form, making a pH of 7 or higher essential for the assay. In buffers with a pH higher than 7.2, PBS, pH 7.4, and 0.1M Tris-HCl pH 8.0, autohydrolysis of the 50 μm FDA working solution was high, developing a visible green color in the substrate input well within minutes. In PBS, pH 7.0, the stability of the substrate was higher, but still evident after 10 - 15 minutes of reconstitution. As it often took up to 10 minutes to prime each device with the aqueous and oil solutions prior to initiating crossflow, substrate autohydrolysis invalidated most assays. Experiments were also carried out using another fluorescent molecule, resorufin acetate (Helix Research). Resorufin acetate is hydrolyzed by pNB esterase to its fluorescent derivative, resorufin ($\lambda_{ex\ (max)}$ = 563 nm / $\lambda_{em(max)}$ = 587 nm). In the

aforementioned buffers, autohydrolysis was even more pronounced for a 50 μm resorufin acetate solution than the corresponding fluorescein derivative. The hydrolyzed resorufin product also stuck to the substrate input channel, staining it with a bright fluorescent orange residue.

4.6 Conclusions

Working on the development of a microfluidic crossflow assay emphasized the difficult dynamic integration process between biochemical and micromechanical systems. Progress was made in making the crossflow device a true microfluidic mixer, capable of encapsulating picoliter volumes of two aqueous components exactly at the position where the two reagents combine. pNB esterase was chosen as a model enzyme on the basis of its recombinant expression in *E. coli*, its fast kinetics and the availability of sensitive, fluorescence-based detection reagents. While problems such as non-specific cell adhesion and substrate autohydrolysis plagued the assays, the results are not intended to discourage future research in this area. Improvements in areas such as surface chemistry technology and reagent stability will promote the development of cell-based, sensitive biochemical assays in this system.

Chapter 5 - Complex Addressable Microfluidic Arrays

5.1 Introduction

Primarily for high-throughput screening (HTS) applications, clever micro-patterning and compartmentalization systems for cells and proteins have been established by a variety of techniques. Examples include polydimethylsiloxane (PDMS) membranes with molded pores for deposition of cell and protein arrays onto glass substrates[92,93], patterning of chemicals and biomolecules by microcontact printing using elastomeric stamps[94,95], and high density nanoliter-scale assay plates[96].

As sample volumes decrease, integrated control systems become critical for manipulation of liquid volumes on the pico- to nanoliter scale. Several technologies have been developed for microfluidic metering[97], mixing[98,99], and compartmentalization[100]. On-chip valve structures for aqueous solutions include passive valves consisting of chemically derivatized hydrophobic patches[101] or small physical channel restrictions that prohibit capillary flow[102], and active elastomeric valves[19]. Active valves have the advantage of being individually addressable, having the capability of being turned on or off in any user defined pattern.

In this chapter, the design and development of high-density microfluidic chips that contain plumbing networks with thousands of mechanical valves and hundreds of individually addressable chambers are described. These fluidic devices are in some ways analogous to electronic integrated circuits fabricated with large scale integration (LSI) technology. A key component of these networks are fluidic multiplexors, which are combinatorial arrays of binary valve patterns that increase the processing power of a

network by allowing complex fluid manipulations with a minimal number of inputs. These integrated microfluidic networks have been used to construct the microfluidic analog of a comparator and a microfluidic memory storage device whose behavior resembles random access memory (RAM).

5.2 Microfluidic Large Scale Integration

In the first part of the 20century, engineers faced a problem commonly called the "Tyranny of Numbers": there is a practical limit to the complexity of macroscopically assembled systems[103]. Using discrete components such as vacuum tubes, complex circuits quickly become too expensive to build and operate. The ENIAC I, created at the University of Pennsylvania in 1946, consisted of 19,000 vacuum tubes, weighed thirty tons, and used 200 kilowatts of power. While the invention of the transistor by Bell Laboratories in 1947 replaced the bulkier vacuum tubes in circuits, connectivity remained a problem. Although engineers could in principle design increasingly complex circuits consisting of hundreds of thousands of transistors, each component within the circuit had to be hand-soldered, an expensive, labor-intensive process. Adding more components to the circuit decreased its reliability as even a single cold solder joint rendered the circuit useless.

In the late 1950s, Kilby and Noyce solved the "Tyranny of Numbers" problem for electronics by inventing the integrated circuit. By fabricating all of the components out of a single semiconductive material-initially germanium, then silicon-Kilby and Noyce created circuits consisting of transistors, capacitors, resistors and their corresponding interconnects *in situ*, eliminating the need for manual assembly. By the mid-1970s,

improved technology led to the development of large-scale integration (LSI): complex integrated circuits containing hundreds to thousands of individual components.

Microfluidics offers the possibility of solving similar system integration issues for biology and chemistry. However, devices to date have lacked a method for a high degree of integration, other than simple repetition. Microfluidic systems have been used to demonstrate a diverse array of biological applications, including biomolecular separations [104,105,106], enzymatic assays[107,108], polymerase chain reaction (PCR)[108,109], and immunohybridization reactions[110,111]. While these are excellent individual examples of scaled down processes of laboratory techniques, they are also stand-alone functionalities, comparable to a single component within an integrated circuit. The current industrial approach to addressing true biological integration has come in the form of enormous robotic fluidic workstations that take up entire laboratories and require considerable expense, space and labor, reminiscent of the macroscopic approach to circuits consisting of massive vacuum-tube based arrays in the early twentieth century.

There are two basic requirements for a microfluidic LSI technology: monolithic microvalves that are leakproof and scalable, and a method of multiplexed addressing and control. A candidate plumbing technology that allows fabrication of monolithic valves in silicone elastomer chips was described in Chapter 3. In this chapter, we describe a microfluidic multiplexing technology and show how it can be used to fabricate silicone devices with thousands of valves and hundreds of individually addressable reaction chambers.

5.3 Microfluidic Multiplexors

Microfluidic multiplexors are combinatorial arrays of binary valve patterns that increase the processing power of a network by allowing complex fluid manipulations with a minimal number of controllable pressurized inputs. While simple microfluidic arrays can be designed in which each fluid channel is controlled by its own individual valve control channel, this non-integrated strategy cannot be efficiently scaled up and faces similar problems encountered in pre-LSI electronic circuits. In contrast, multiplexors work as a binary tree (Figure 5.1) and allow control of n fluid channels with only $2\log_2 n$ interconnects. Multiplexors were fabricated using previously described

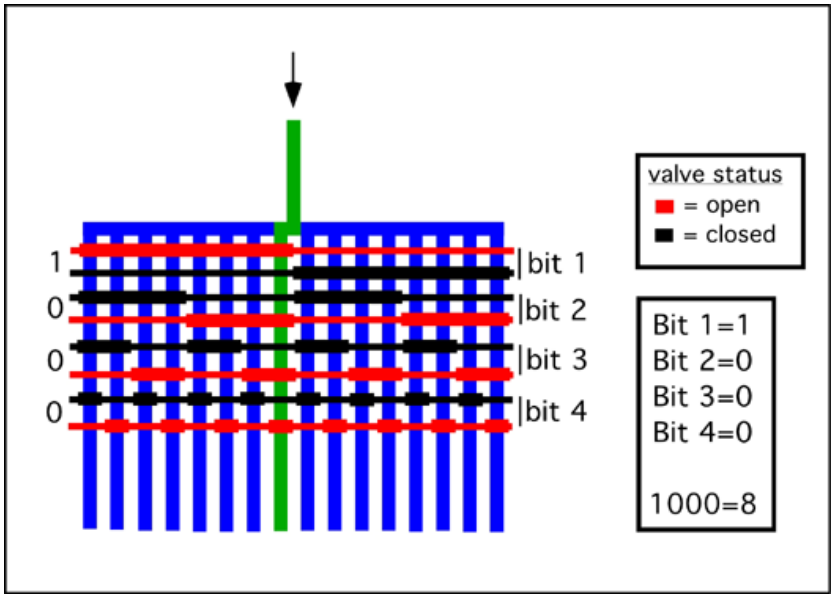

Figure 5.1: Multiplexor control in a multilayer elastomeric microfluidic device. Each open/closed valve configuration within the control layer opens a single flow channel. Valve closing pressure scales with the width of the control channel, allowing non-contiguous flow channels to be closed by the wide valves while flow channels under the narrow valves remain open.

multilayer soft lithography techniques. The two-layer monolithic silicone devices consist of a "control" layer containing the multiplexor channel network and a "flow" layer separated by a thin polymer membrane (~30 μm). The membrane at the intersection of the control and flow channels functions as a discrete valve, in which pneumatic pressure applied to the control channels causes the elastomeric membrane to deflect down, closing off the underlying flow channel. Simultaneous addressing of multiple non-contiguous flow channels is accomplished by fabricating control channels of varying width while keeping the dimension of the flow channel fixed (100 μm wide and 9 μm high). The pneumatic pressure in the control channels required to close the flow channels scales with the width of the control channel, making it simple to actuate 100 μm x 100 μm valves at relatively low pressures (~40kPa) without closing off 50 μm x 100 μm crossover regions. By using multiplexed valve systems, the power of the binary system becomes evident, with only 20 control channels required to specifically address 1024 flow channels. This allows a large number of elastomeric valves to perform complex fluidic manipulations within these devices, while the interface between the device and the external environment is simple and robust. Introduction of fluid into these devices is accomplished through steel pins inserted into holes punched through the silicone that connect the microfluidic control and flow channels with external fluid and pneumatic inputs. Unlike micromachined devices made out of hard materials with a high Young's modulus[112], silicone is soft and forms a tight seal around the input pins, readily accepting pressures of up to 300 kPa without leakage. Actuation of the valves in the control layer is accomplished through computer-controlled external miniature solenoid valves, making to easy to simultaneously address complex arrays of valves.

Multiplexor Mechanics - 1024 Well Serpentine Microfluidic Device

The first multiplexor-based microfluidic device was designed as an enrichment chip (Figure 5.2). The core of the chip functions as a high-density multichamber array, into which sample can be loaded, compartmentalized and analyzed. To load sample into the array region, a set of barrier valves is closed to isolate the array from the rest of the flow channel network. All valves are filled with water prior to actuation to prevent bubble formation in the flow channel that results that occurs when air passes through the elastomeric membrane between the control and flow layer channels. When the barrier valves are closed, the flow channel within the array adopts a serpentine form with a single sample input and a sample vent to purge the displaced air (Figure 5.3). After the

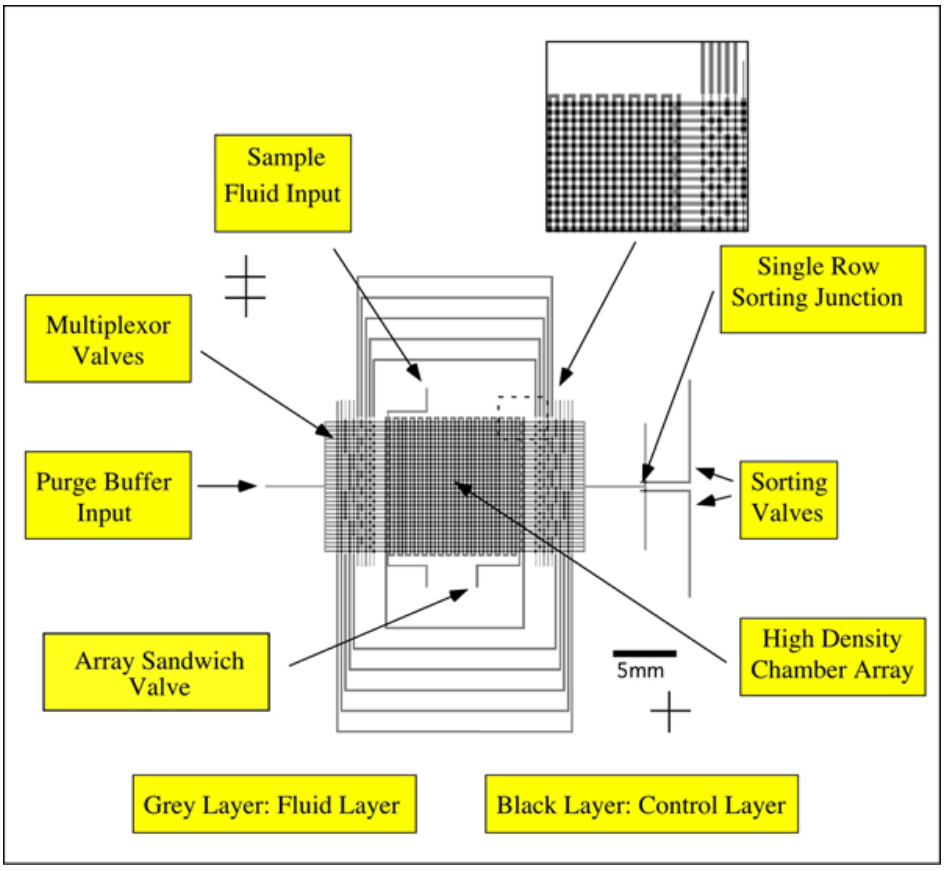

Figure 5.2: 1024 well serpentine chip schematic.

chip is filled with sample, the array sandwich valve is actuated at 12-15 psi, which compartmentalizes the 32 rows of sample into 1024 aliquots with volumes of ~80 pL (Figure 5.4).

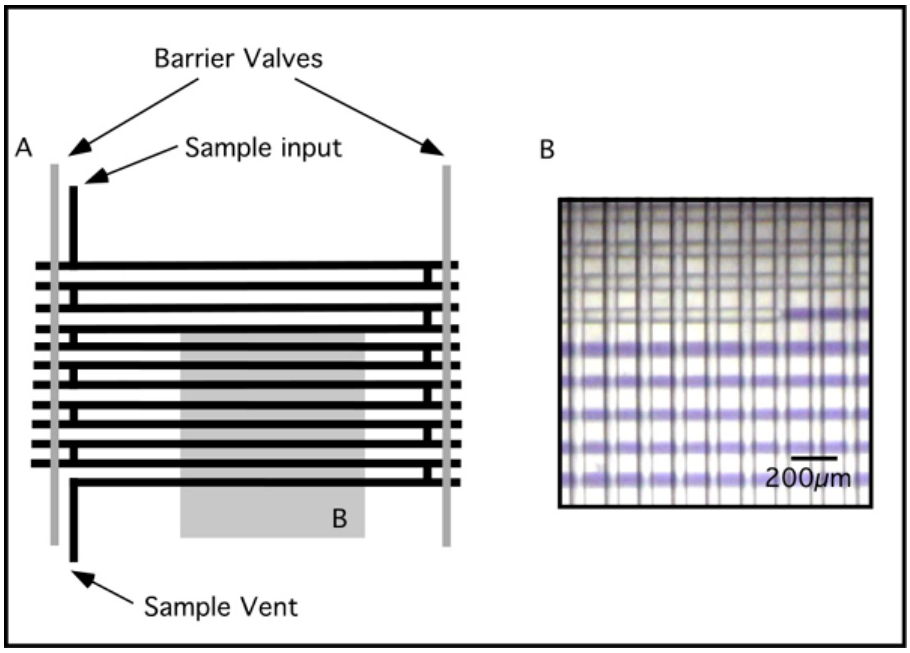

Figure 5.3: A) Detailed diagram of flow channel layout in high-density array region of serpentine chip illustrating flow path for sample loading when control layer barrier valves are closed. B) Illustration of sample loading mechanics in high-density array region using bromophenol blue. Vertical valves in photo are part of the non-actuated array sandwich valve (not visible in part A for simplification purposes).

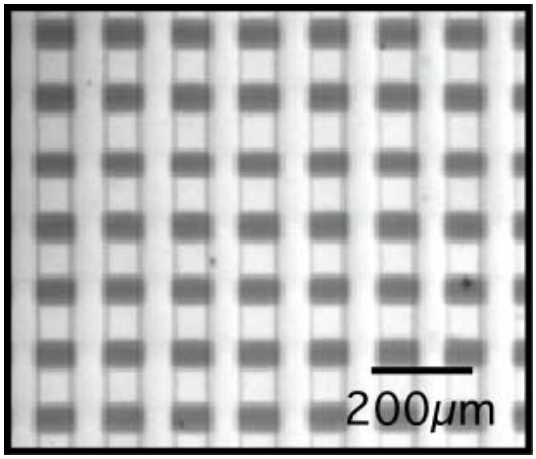

Figure 5.4: Compartmentalization of the sample into ~80 pL aliquots using the array sandwich valve in the serpentine chip.

The compartmentalized liquid can be used for applications such as *in vitro* protein synthesis or single-cell enzymatic assays (Chapter 6).

Sample recovery from the chip utilizes the multiplexor, which is used to isolate and recover a single row of sample within the 32 row matrix. Isolation of the contents of a single row proceeds as follows: 1) The array sandwich valve is released, mixing the contents of the compartmentalized sample within each row. 2) The purge buffer input is filled with pressurized solution (5 psi). Excess air trapped in the chip as a result of the filling process is outgassed through the elastomeric silicone. 3) All valves in the multiplexor complex are closed. The multiplexor valves are symmetrically arranged around both sides of the array to channel the purge stream to the selected row and direct the isolated sample material to the sorting junction at the output of the chip. 4) The barrier valve is opened. 4) A Labview-based program is used to operate the binary combination of multiplexor valves for a selected row, which instantly purges the contained sample material. An illustration of the multiplexor addressing process is shown in Figure 5.5, in which every other row in the matrix is sequentially purged.

The device functions as an enrichment chip, utilizing both the multiplexor and the sorting valves near the output. For applications involving screening for rare events, in which one compartment in the entire array is likely to contain a "positive" event, the isolation of the contents of the row that it resides in translates to a 32-fold enrichment vs. the original mixture. An example of this type of application is a directed evolution experiment using mutagenized enzyme libraries where only a small fraction of mutants are expected to be active against the selected substrate. The sorting valves are more limited it their application, as they require detection elements (such as a fluorescent tag)

to remain bound to the "positive" events within the purged sample row, which could then be detected and sorted by instruments like the fluorescence-activated droplet sorter.

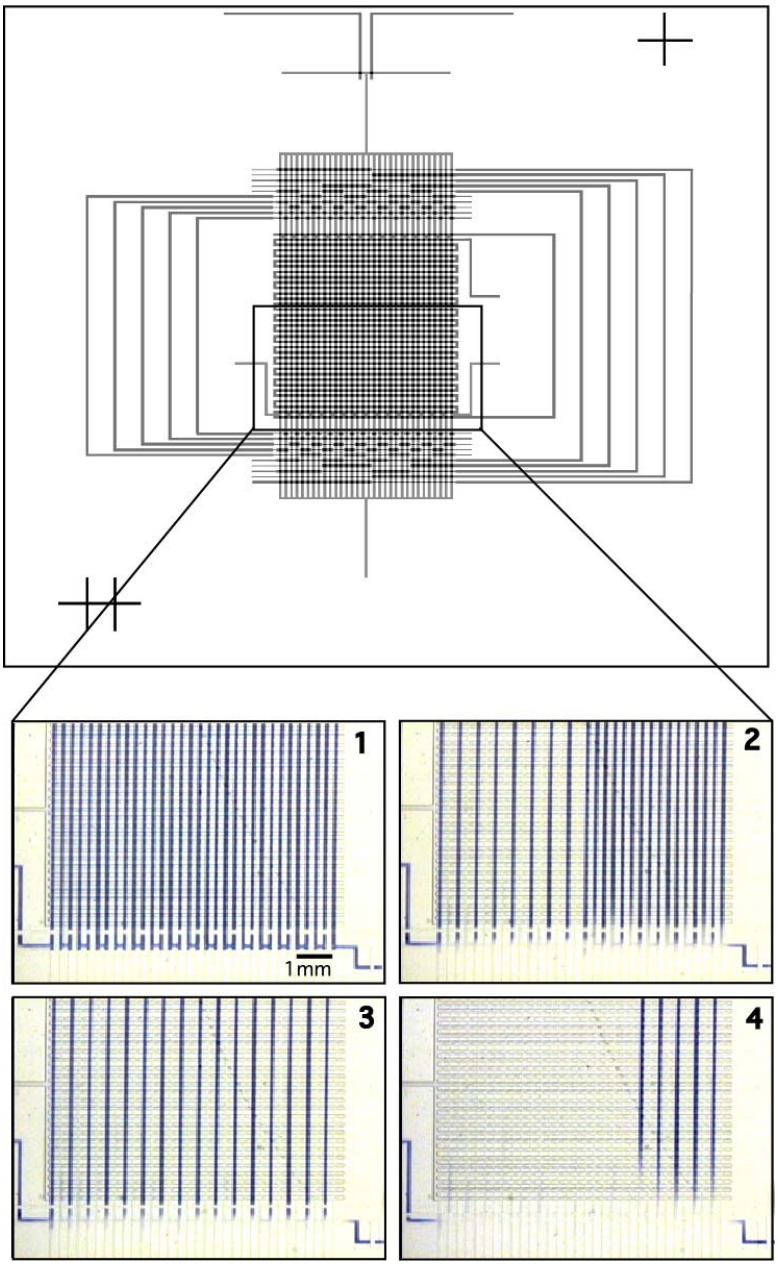

Figure 5.5: Sequential row purging of the high-density chamber array using multiplexor control. The bottom micrographs correspond to the highlighted area of the design schematic. Alternate sample rows in the array, filled with 2.4 mM bromophenol blue dye, are purged sequentially in the example.

5.4 Microfluidic Memory Storage Device

Using two multiplexors as fluidic design elements, a microfluidic memory storage device was designed with 1000 independent compartments and 3574 valves, organized as an addressable 25 x 40 chamber microarray (Figure 5.6). Unlike the serpentine chip predecessor, each compartment within the array can be individually addressed and the contents recovered. Sample is loaded into the device through a single input port, after which the control layer valves then act as gates to compartmentalize the array into 250 pL

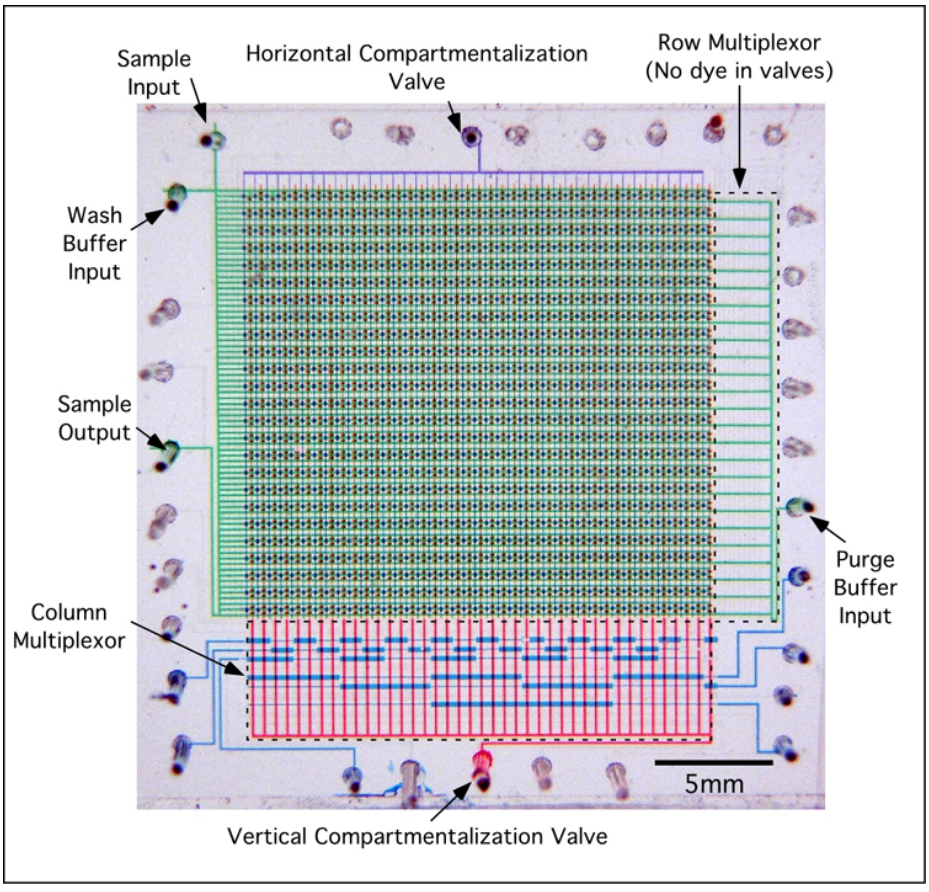

Figure 5.6: Microfluidic memory chip. Each compartment of the central array contains ~250 pL of liquid and is individually addressable.

chambers. Individual chamber addressing is accomplished through flow channels that run parallel to the sample chambers and use pressurized liquid under the control of the row and column multiplexors to flush the chamber contents to the output.

This device adds a significant level of complexity to previous microfluidic plumbing in that there are levels of control – the multiplexors actuate valve control lines, which in turn actuate the valves themselves. The design and mechanics of the microfluidic array are similar to random access memory (RAM). Each set of multiplexors is analogous to a memory address register, mapping to a specific row or column in the matrix. Like dynamic RAM, the row and column multiplexors have unique functions. The row multiplexor is used for fluid trafficking: it directs the fluid responsible for purging individual compartments within a row and refreshes the central compartments (memory elements) within a row, analogous to a RAM word line. The column multiplexor acts in a fundamentally different manner, controlling the vertical input/output valves for specific central compartments in each row. To operate the column multiplexor, the vertical containment valve on the control layer is pressurized to close off the entire array. The column multiplexor, located on the flow layer, is then activated, with its valves deflected upwards into the control layer to trap the pressurized liquid in the entire vertical containment valve array. A single column is selected by the multiplexor, and the pressure on the vertical containment valve is released to open the specified column, allowing it to be rapidly purged by pressurized liquid in a selected row (Figure 5.7).

To demonstrate the functionality of the microfluidic memory storage device, we loaded the central memory storage chambers of each row with dye (2.4 mM bromophenol blue in 0.1M sodium citrate buffer, pH 7.2) and proceeded to purge individual chambers

with water to spell out "CIT." Since the readout is optical, this device also functions as a fluidic display monitor (Figure 5.8). It is possible that microfluidics will complement liquid crystal display technology by using this sort of active plumbing control.

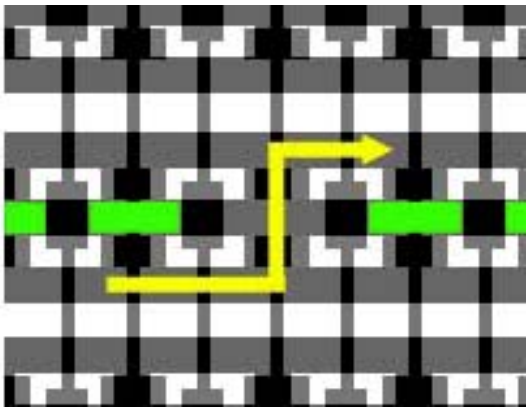

Figure 5.7: Mechanics of a single chamber purge within a single row of the microfluidic memory chip. Purging mechanics for a single chamber within a selected row of the chip. Each row contains three parallel microchannels. To purge a specific chamber: 1) Pressurized fluid is introduced in the purge buffer input. 2) The row multiplexor directs the fluid to the lower channel of the selected row. 3) The column multiplexor releases the vertical valves of the chamber, allowing the pressurized fluid to flow through the chamber and purge its contents.

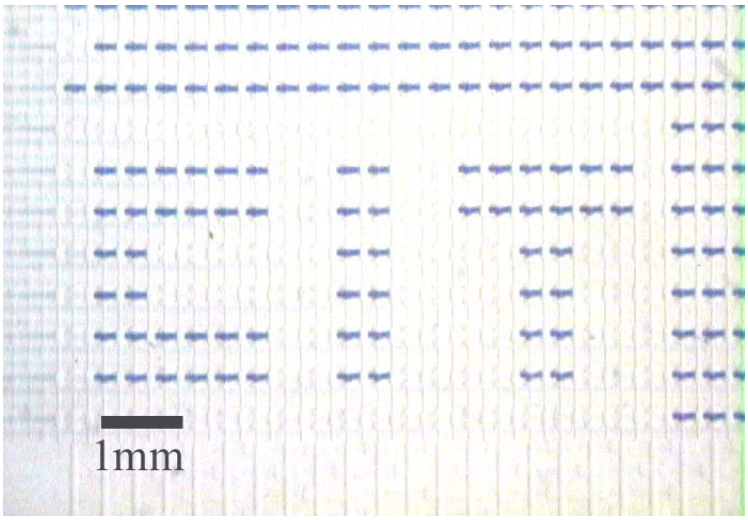

Figure 5.8: Demonstration of microfluidic memory display: Individual chambers are selectively purged to spell out "CIT."

5.5 Microfluidic Comparator

A second device, designed by Sebastian Maerkl in the Quake laboratory, was developed that contains 2056 valves and is capable of performing more complex fluidic manipulations (Figure 5.9). Two different reagents can be separately isolated, mixed and recovered using hundreds of subnanoliter compartments. The microchannel layout

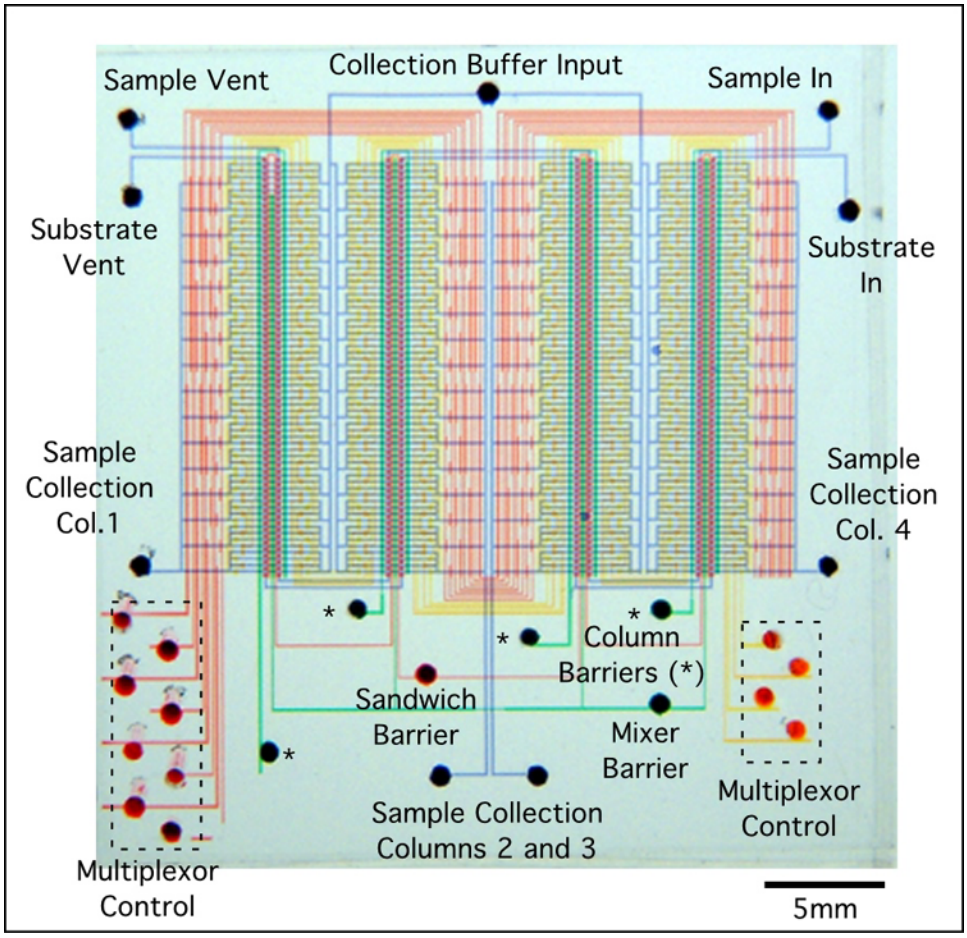

Figure 5.9: Microfluidic comparator chip (loaded with colored food dyes for channel visualization). The mixer barrier valve separates the sample and substrate within each column while the sandwich barrier valve partitions each column into 64 individual wells. Under the multiplexor control, purge buffer can be directed to isolate any individual compartment.

has four central columns in the flow layer consisting of 64 chambers per column, with each chamber containing ~750 pL of liquid after compartmentalization. Liquid is loaded into these columns through two separate labeled inputs under low external pressure (~20 kPa), filling up the array in a serpentine fashion. Barrier valves on the control layer function to isolate the sample fluids from channel networks on the flow layer used to recover the contents of each individual chamber, which function under the control of a multiplexor and several other control valves. The elastomeric valves are analogous to electronic switches, serving as high impedance barriers for fluidic trafficking. To demonstrate the device plumbing, the fluid input lines were filled with two dyes to illustrate the process of loading, compartmentalization, mixing and purging of the contents of a single chamber within a column (Figure 5.10). Each of the 256 chambers on the chip can be individually addressed and its respective contents recovered for future analysis using only 18 control connections to the outside world, illustrating the integrated nature of the microfluidic circuit.

We used this chip as a microfluidic comparator that measures the expression of a particular enzyme using a fluorogenic substrate system to provide an amplified output signal in the form of a fluorescent product. An electronic comparator circuit is designed to provide a large output signal when the input signal exceeds a reference threshold value. An op amp amplifies the input signal relative to the reference, forcing it to be high or low. In our microfluidic comparator, the non-fluorescent resorufin derivative, Amplex Red, functions as the reference signal. The input signal consists of a suspension of *E. coli* expressing recombinant cytochrome c peroxidase (CCP). CCP serves as a chemical

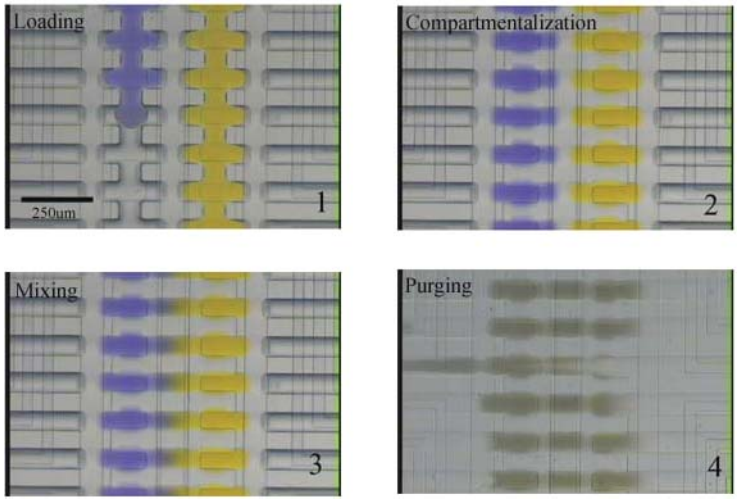

Figure 5.10: Comparator chip mechanics in chambers of single column. Elastomeric valves enable each of the 256 chamber on the chip can be independently compartmentalized, mixed, and purged.

amplifier in the circuit (Figure 5.11). The cells and substrate are loaded into separate input channels with the central mixing barrier closed in each column and compartmentalized exactly like the procedure illustrated for the blue and orange dyes. The cell dilution (1:1000 of confluent culture) creates a median distribution of ~0.2 cells/compartment, verified by optical microscopy. The barrier between the substrate and cell subcompartments is opened for a few minutes to allow substrate to diffuse into the

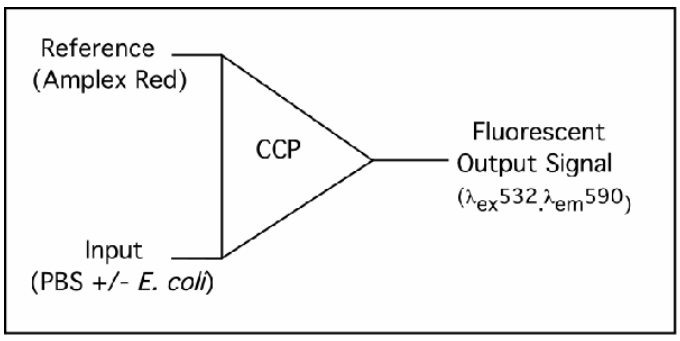

Figure 5.11: Microfluidic comparator diagram. When input signal contains CCP enzyme, non-fluorescent Amplex Red is converted to the fluorescent product, resorufin. In the absence of CCP, the output signal remains low.

compartments containing the cell mixture. The barrier is then re-closed to reduce the reaction volume and improve the signal/noise for the reaction. After a one-hour incubation at room temperature, the chip is scanned (λ_{ex}=532 nm, λ_{em}=590 nm ds 40) with a modified DNA microarray scanner (Axon Industries GenePix 4000B). The presence of one or more CCP expressing cells in an individual chamber produces a strong amplified output signal as Amplex Red is converted to the fluorescent compound, resorufin, by CCP while the signal in the compartments with no cells remains low (Figure 5.12). To verify that the output signal is a function of CCP activity, a control experiment using the same parameters was run using a mixture of *E. coli* expressing either CCP or enhanced green fluorescent protein (eGFP). The amplified output signal was only dependent on the number of CCP-expressing cells in an individual chamber (Figure 5.13).

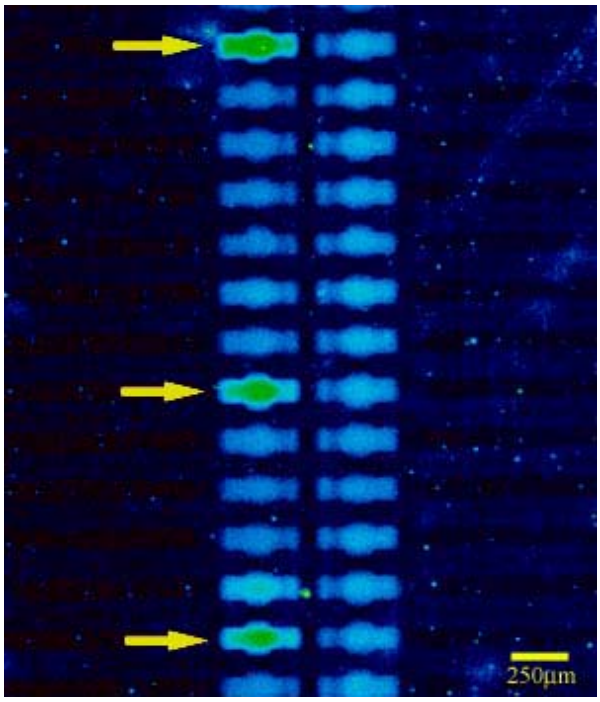

Figure 5.12: Chip in comparator mode. Left half of column: CCP expressing *E. coli* in PBS pH 7.2 after mixing reaction with Amplex Red. Arrows indicate chambers containing single cells. Converted product (resorufin) is clearly visible as green signal. Right half of column: Uncatalyzed Amplex Red substrate.

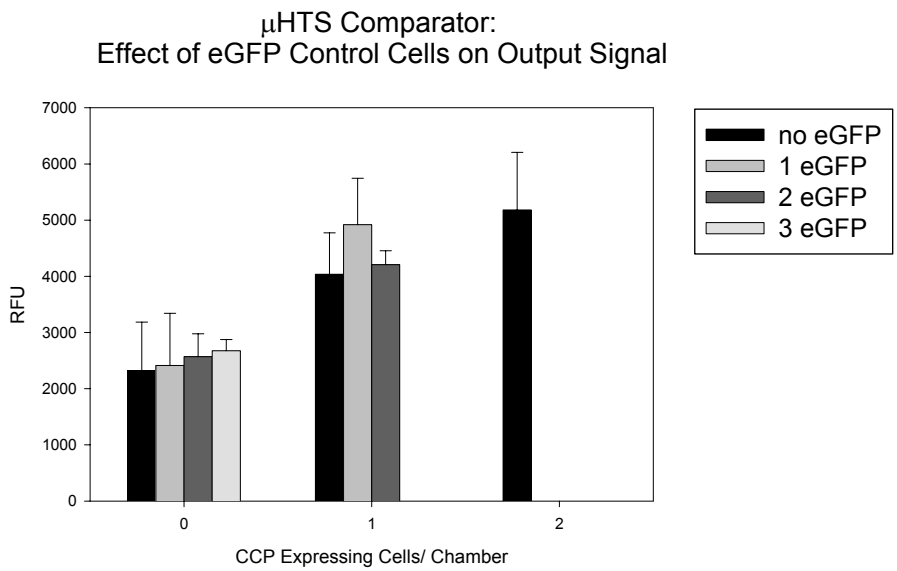

Figure 5.13: Microfluidic comparator chip: Effect of eGFP control cells and CCP cells on output signal. Resorufin fluorescence measurement (λ_{ex} = 532 nm, λ_{em} = 590 nm) in individual compartor chambers containing *E. coli* cells expressing either enhanced green fluorescent protein (eGFP) or cytochrome c peroxidase (CCP). As the number of CCP expressing cells/ chamber increased, chamber co-localization with GFP expressing cells decreased. Error bars represent one standard deviation from the median RFU.

Recovery from the comparator chip is accomplished simply by purging the contents of a chamber to a collection output. Each column in the chip has separate output, enabling a chamber from each column to be collected without cross-contamination concerns. To illustrate the efficacy of the collection process, a dilute PBS solution of *E. coli* expressing GFP was injected into the chip. After compartmentalization, each chamber contained ~0.5 bacteria. Using an inverted light microscope (Olympus IX50) equipped with a mercury lamp and GFP filter set, single GFP expressing cells were identified with a 20x objective and their respective chambers were individually purged.

The respective contents from each purged compartment were separately collected from the outputs using polyetheretherketone (PEEK) tubing, which has low cell adhesion properties. Isolations of single GFP-expressing bacteria were confirmed by the visualization of the collected cells under a 40x oil immersion lens using the appropriate green fluorescence filter set (λ_{ex} = 480 nm ds 30 / λ_{em} = 535 nm ds 40) and by observations of single colony growth on Luria broth (LB) plates innoculated with the recovered bacteria. GFP expression in the single-colony bacteria was also confirmed by fluorescent microscopy.

5.6 Conclusions

These examples show that complex fluidic devices with nearly arbitrary complexity can be fabricated using microfluidic LSI. The rapid, simple fabrication procedure combined with the powerful valve multiplexing can be used to design chips for many applications, ranging from high throughput screening applications to the design of new liquid display technology. The scalability of the process makes it possible to design robust devices with even higher densities of functional valve elements. Additional integration of this technology with on-chip detector components will create sophisticated analytical systems that will be compact, portable, and inexpensive.

Chapter 6 - Complex Microfluidic Arrays: Biochemical Assays

6.1 Introduction

The basic principles of miniaturized, parallel microarray-based protein assays were described more than a decade ago[113,114]. The explosive interest in protein-based HTS platforms is fueled by progress in genome-based sequencing projects[115,116] and the emerging field of proteomics. Other biological array-based platforms, like DNA/RNA microchips[117], have inspired the development of high-density, affinity-based protein screening devices.

Several protein-based microchips have been designed around ligand-binding assays[118-120]. Typically, proteins are attached to glass slides using crosslinking agents that react with the primary amines on the protein surface as well as by specific bimolecular reactions such a streptavidin-biotin and His-tag-nickel-chelate systems. Array generation is achieved by methods like hand spotting, pin-based robotic technologies, ink jet printers and stamping[121]. The challenge with developing array-based protein assays is creating efficient synthesis and deposition technologies while preserving the structure and function of the protein of interest. Proteins arrayed on solid support matrices are often denatured or adopt an unnatural conformation as a result of the drying process or interactions with the linker molecules that attach them to the substrate surface.

Complex microfluidic array devices, such as those described in Chapter 5, are particularly suited for protein-screening applications. Unlike solid-support spotting technologies, the proteins remain in buffered solutions that prevent drying or

denaturation. After compartmentalization, the proteins are well separated, minimizing cross-contamination between adjacent samples. Reagent volumes are also low, requiring nanoliters of substrate vs. milliliters required for bulk hybridization assays. The picoliter-sized compartments can be used as reaction vesicles for in vitro transcription/translation of protein libraries or to monitor protein expression and activity at the single cell level.

6.2 *In Vitro* Protein Synthesis in Picoliter Volumes

Microfluidic array devices provide an ideal, picoliter-scale environment for on-chip protein synthesis. *In vitro* transcription/translation kits, which are commercially available, can be used to synthesize proteins that are difficult to produce or toxic in whole-cell based systems, such as fusion proteins[122]. Cell-free systems can now be used to study the *in vitro* assembly of membrane proteins and viral particles, rapidly produce and analyze protein mutants, and enlarge the genetic code by incorporating unnatural amino acids[123]. As *in vitro* systems don't require recombinant hosts, problems related to cell culture conditions and heterogeneous protein expression at the single cell level are eliminated.

Enhanced Green Fluorescent Protein Expression - Serpentine Microfluidic Device

As a proof-of-concept experiment, enhanced green fluorescent protein (eGFP) was transcribed and translated in the array-based serpentine microfluidic device described in chapter 5. A commercial kit (Roche Rapid Translation System RTS 100, *E. coli* HY kit) based on *E. coli* lysate was used to synthesize eGFP using the provided control DNA construct (pIVEX 2.3 vector). The reagents were mixed on ice according to kit protocol and injected into the sample input of the serpentine microfluidic device, filling the central

grid region. A negative control (no DNA) was also set up and injected into a separate chip. The array sandwich valve was closed at ~15 psi and the compartmentalized mixture was incubated at 22°C for four hours. Each of the 1024 compartments in the chip, with volumes of ~80 pL of solution, contained ~2.0 x 10^5 DNA molecules. After four hours, the contents of the wells were visualized under a light microscope (Olympus IX50) with a 10X (0.35 NA) UPlan objective and a mercury lamp equipped with a green filter set (Ex 480 nm ds 30/ Em 535 nm ds 40) appropriate for GFP visualization. Images were captured using a cooled CCD camera (SBIG ST-7, SBIG Astronomical Instruments) with a 10 second exposure at 10°C. A strong fluorescent green signal was observed in the chip containing the eGFP DNA construct (Figure 6.1) while no signal was observed with the negative control chip. To look at the sensitivity of the assay, a titration experiment

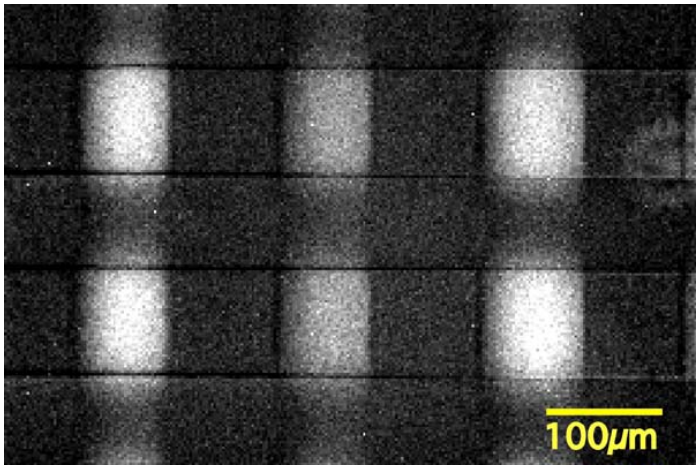

Figure 6.1: eGFP transcription/translation in the array-based 1024 well serpentine microfluidic device with ~2 x 10^5 eGFP DNA constructs/ 80 pL well (10 second exposure, SBIG-7 cooled CCD camera). Intensity variation due to mercury lamp alignment difficulties.

was conducted using the transcription/translation mixture and 10-fold dilutions of the eGFP DNA construct (ranging from ~2 x 10^5 to 20 copies per 100 pL). The mixtures were loaded into separate serpentine microfluidic chips and incubated at 22°C for four hours using the loading protocol described in Chapter 5. Detectable fluorescent signal over background was observable down to ~200 DNA molecules/compartment. At 20 copies/well, the signal was similar to background (no DNA).

While the detection of eGFP using a bacterial extract system was not sensitive down to a single molecule of DNA/ compartment in the described experiment, it is not unreasonable to believe that this goal can be achieved in an array-based microfluidic device in the near future. As protein synthesis using the Roche *in vitro* transcription/translation kit has been reported to occur for as long as 24 hours, the assay would benefit from a longer incubation period. The volume of each compartment can also be reduced by an order of magnitude by scaling down the channel dimensions. Functional valves as small as 20 x 20 μm have been fabricated in our laboratory by Dr. Anne Fu, suggesting that microfluidic arrays can be designed with compartment volumes of only a few picoliters.

6.3 Detection Systems for Array-Based Microfluidic Chips

Unlike the microfluidic crossflow devices, which utilize the fluorescence-activated droplet sorter to look at sequentially generated droplets, the array-based microfluidic chips need an "at-once" detection system to quantitatively measure the signal generated within all of the compartments. Rapid measurement is essential for

making endpoint comparisons between the compartments for time-sensitive assays such as enzymatic reactions.

Inverted Microscope / Mercury Lamp

While the inverted microscope equipped with the mercury lamp and the cooled CCD camera provided sensitive fluorescence measurements of small regions of the microfluidic devices (~1 mm^2 using a 10x objective (0.35 NA)), there are several problems inherent in this system for whole chip detection. The most significant are: 1) The field of view of the captured image is small relative to the array dimensions. Each image capture using the 10x objective contains 6 compartments. For the 1024 compartment on the serpentine chip, 171 separate images need to be obtained. Using lower magnification objectives reduces the light collection efficiency and sensitivity of the assay. 2) Fluorophore bleaching is very rapid using the mercury lamp (<1 second). As the images captured by the SBIG cooled CCD camera are cropped relative to the total field illuminated by the mercury lamp (taking the objective center of field of view), outlying compartments are bleached prior to image acquisition.

Fluorescence-Activated Droplet Sorter / Motorized Stage

A more practical scanning detection system was designed and constructed for the array-based chip using the microfluidic droplet sorter. A motorized XY stage (DynaOptics Motion) controlled by a Labview program and a DCX-PC100 motion control card (Precision MicroControl) was assembled to hold the microfluidic array devices, consisting of two single axis motorized stages and a micromachined mount for the array chips (Figure 6.2). The XY stage functions as a scanner by moving the chip under the droplet sorter objective lens to read out the signal in each of the compartments.

The stepper motors have a 50 m travel range (enough for a 2" x 2" chip), moving in 0.5 μm increments. A holder, designed to fit a 1 in^2 microfluidic chip, was attached to a kinematic mount to level the chip surface prior to scan initiation. A separate micrometer (Newport Corp.) was used as a Z-axis to focus the 40x objective within the array compartments. When only the main XY stage was used, motion was jerky when a chip was observed under a 40x (0.65 NA) objective, so an additional single-axis stage with a stepper increment of 0.1 μm (X-axis motor 2) was added for smooth scans across the compartmentalized rows within the array. A Labview program was written to control the

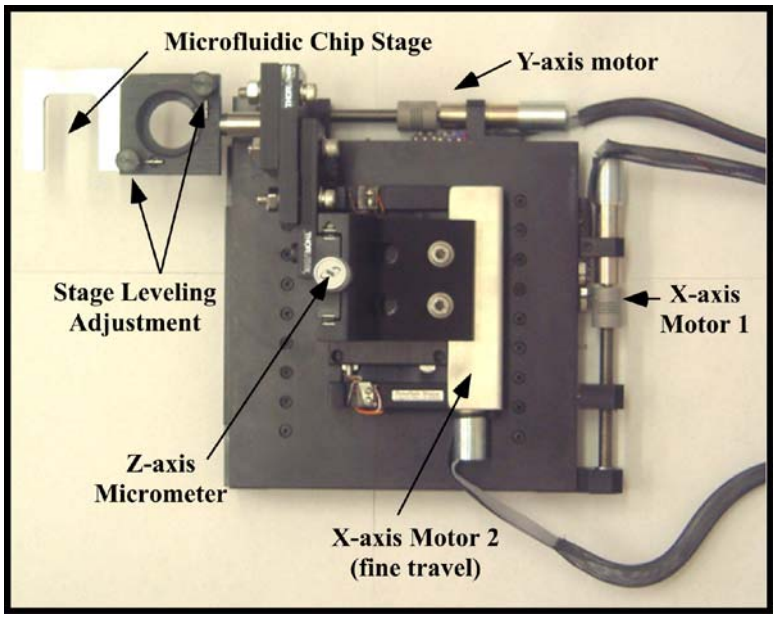

Figure 6.2: XY scanner stage layout. Motorized stage components (DynaOptics Motion) move the microfluidic chip mounted in the stage under the objective lens of the microfabricated droplet sorter.

travel distance of each axis and the pathway as each chamber in the array chip is interrogated. Raw analog voltage data from each PMT acquired during the scanning process was collected by an analog input card (PCI1200, National Instruments) and

compiled in Labview as a raw data file at an acquisition rate of 20 readings/ second. The sequential scan of all 32 rows in the serpentine chip took approximately 5 minutes.

To validate the compartment scanner, a serpentine chip was filled with 1 mm fluorescein in PBS pH 7.2 and compartmentalized by closing the sandwich valve array at ~ 14 psi. The Intelite blue laser output was set to 3.0 mW. The chip was scanned, with the analog output from each row of chambers binned (n=4) and saved as a single column of data. The final raw data file, organized as a 32-column matrix (corresponding to the number of rows in the chip), was imported into MathCad and converted into a color image file with the dynamic range set by the high and low voltage values (Figure 6.3).

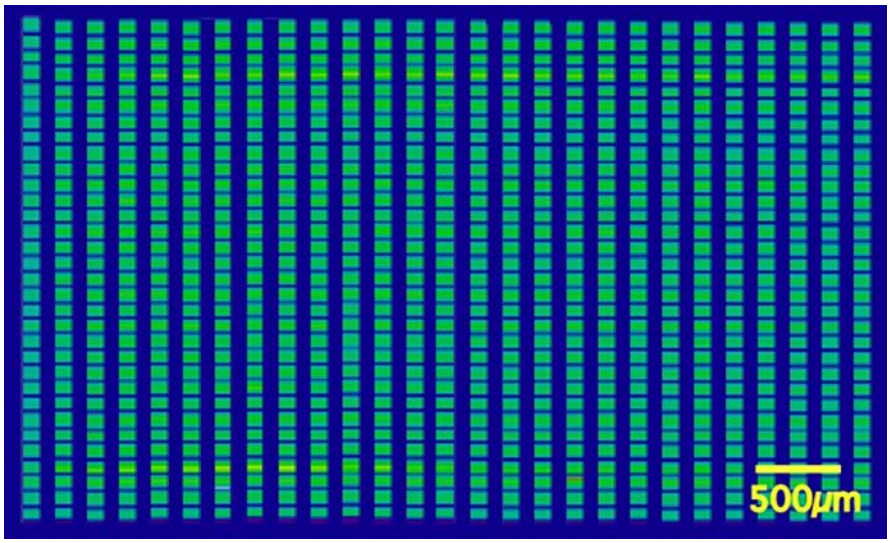

Figure 6.3: Image map of the array of fluorescein-filled compartments (1mm in PBS pH 7.2) in the serpentine microfluidic chip. Data acquired using the fluorescence-activated droplet sorter equipped with a motorized XY stage (DynaOptic Motion).

Well-to-well intensity variation was calculated by importing the image into an analysis program (Scanalytics One-D Gel Analysis). The intensity value of each well was

standardized by dividing the total intensity (peak integration) by the pixel width. The first-order standard deviation for the matrix ranged from 5 - 6.25%, depending on the smoothing algorithm used.

While the standard deviation and scanning speed were acceptable for the modified droplet sorter, it was very difficult to align the chips in the holder to match the programmed scanning pathway. If the array grid in the chip did not precisely map to the programmed XY coordinates, the scan pathway would deviate from the array. Precise chip alignment took up to 20 minutes in some experiments, an unacceptable condition for sensitive timepoint assays. With the arrival of the Axon GeneChip scanner, whose features will be discussed in the next section, no additional optimization work was done on this system.

Axon Genechip Scanner

The GeneChip scanner (Axon Instruments, Model 4000B), originally designed for scanning DNA microarrays, was modified for scanning microfluidic chips. The scanner consists of two diode lasers, a green laser (17 mW @ 532 nm) and a red laser (10 mW @ 635 nm), which are simultaneously rastered across the sample plane on a voice coil. The focal points of the two lasers are physically separated on the sample plane to avoid crosstalk between the two channels. Emitted light is collected by two PMTs fitted emission filters, 575nm df 35 and 670 nm df 40, which are optimal for the common DNA dyes, Cy3 and Cy5. The corresponding fluorescence image map is displayed real time during the scan using the supplied GenePix Pro software. A 5 micron resolution scan (1" x 1") is completed in less than 5 minutes. Unlike the motorized XY stage-based scanner,

the chip alignment is not important as a high resolution image of the entire sample surface is generated regardless of orientation.

6.4 CCP: Array-based Enzyme Library Screening

Background

An experiment was designed to compare the activity of a recombinant enzyme library at the single-cell level in the microarray chips with traditional microtiter plate-based assays used in high throughput screening protocols. Given the success of the microfluidic comparator experiment with cytochrome c peroxidase (chapter 5), CCP was selected as the model enzyme.

Cytochrome c peroxidase (CCP), an intracellular fungal peroxidase, was first isolated in brewer's yeast by Altschul et al. in 1940[124]. Found in the mitochondrial transport chain, CCP catalyzes the oxidation of ferrocytochrome c (CcII) to ferricytochrome c (CcIII) with the concurrent reduction of hydrogen peroxide. CCP has also be shown to catalyze several oxidative dehydrogenation and oxygen transfer reactions. As early as 1951, CCP was reported to oxidize guaiacol, pyrogallol, and ascorbate[125]. Over the last 30 years, CCP has been shown to oxidize other small compounds such as ferrocyanide[126] as well as several aniline and phenol derivatives[127].

CCP is an ideal enzyme for the microfabricated array chips because it is small, monomeric, and lacks disulfide bonds, making it easy to express in bacterial hosts. With its broad substrate specificity, several non-fluorescent substrates that convert to fluorescent products are also available for CCP, including Amplex Red, a resorufin ($\lambda_{ex\ (max)}$ = 571 nm, $\lambda_{em\ (max)}$ = 590 nm) derivative compatible with the GenePix scanner.

6.4.1 CCP Expression System

Yeast cytochrome c peroxidase (CCP) was obtained as a plasmid, pT7CCP, from Dr. D. Goodin at the Scripps Research Institute. This variant (CCP-MKT) contains an amino acid substitution at the second codon (Thr to Lys), which was found to have the highest bacterial expression level. However, the vector was not designed for random mutagenesis, having no pairs of unique restriction sites to clone in mutagenized CCP variants. A primers set was designed (forward: 5' - CGG CGA CAT ATG AAA ACG CTC GTT CAT G - 3'; reverse: 5' - GAG CTC GAA TTC CTA TAA ACC TTG TTC CTC TAA - 3') to clone the gene out of the original vector and introduce unique Nde I and Eco RI (underlined) restriction sites. Using the primer set, the gene was amplified out of the pT7CCP vector by PCR (polymerase chain reaction), restricted, and ligated into the multiple cloning site of the expression vector, pET26b+ (Novagen). The pET26b+ vector is a T7 promoter-based plasmid transcribed in hosts expressing the T7 RNA polymerase gene (λDE3 lysogen). The polymerase is under the control of a *lacUVA5* promoter, with expression induced by the chemical isopropylthiogalactoside (IPTG). Upon induction, T7 RNA polymerase is so active that genes under its control can comprise more than 50% of the total cell protein in a few hours. The pET26b+ construct was also selected because it contains an N-terminal *pelB* periplasmic localization sequence to retain the translated protein in the bacterial host and make it accessible to substrate systems that diffuse across the outer membrane of the gram-negative bacterial host. Intracellular protein expression is essential in microcompartmentalized single-cell bacterial assays, where secreted proteins increase the background noise in the system.

6.4.2 Random Mutagenesis - Library Construction

Random mutagenesis of the CCP enzyme was carried out using error-prone PCR. Primers (forward: 5' - CTT TAA GAA GGA GAT ATA CAT ATG - 3'; reverse: 5' - CTT GTC GAC GGA GCT CGA ATT C - 3') were used. The mutagenic PCR mixture consisted of 50 mM KCl, 10 mM Tris-HCl (pH 9.0), 0.2 mM GTP 0.2 mM ATP, 1.0 mM CTP, 1.0 mM TTP, 10 pmol of each primer, ~0.5 µg of pET26b+(CCP-MKT) plasmid, 7 mM $MgCl_2$, 0.25 mM $MnCl_2$, and 5U of *Taq* polymerase in a 100 µl volume. PCR was carried out in a thermocycler (MJ Research, PTC-200) for 30 cycles (94°C :1 minute, 50°C: 1 minute, 72°C:1 minute). The product was double digested with Nde I and Eco RI in two sequential reactions (37°C, 4 hours) due to buffer incompatibility. The sample was purified and eluted in 10 mM Tris-HCl, pH 8.0, between restriction digests and after the second digestion reaction using a column-based purification kit for PCR reactions (Qiagen, QIAquick PCR Purification Kit).

The pET26b+ backbone was prepared for ligation by double digesting the commercial pET26b+ vector with Nde I and Eco RI. The product was gel purified (Qiagen, QIAquick Gel Extraction Kit) and eluted in 10 mM Tris-HCl pH 8.0. The gel purified backbone was then dephosphorylated with 1U shrimp alkaline phosphatase (Roche) in 50 mM Tris-HCl, 0.1 mM $MgCl_2$, 0.01 mM ZnCl, 5% glycerol at 37°C for 10 minutes followed by heat inactivation at 65°C for 15 minutes. The dephosphorylated backbone was column purified (Qiagen, QIAquick PCR Purification Kit) and eluted in 10 mM Tris-HCl pH 8.0 to remove phosphatase buffer components that interfere with the ligation reaction. Ligation was carried out at 25°C using a 3:1 molar ratio of

insert:backbone using a commercial ligation kit (New England Biolabs, Quick Ligation Kit). After ligation, the library was immediately transformed into chemically competent *E. coli* (XLI0 gold) competent cells, a non-expression host, to generate the plasmid library and plated on LB-kanamycin plates. After overnight growth at 37° C, colonies were harvested by rolling 3 mm diameter sterile glass beads over the plate surface with 3 ml of LB media. The plasmid library was isolated from the resuspended cells using a commercial kit (Qiagen, Qiaprep Spin Kit) and used to transform *E. coli* BL21(DE3) chemically competent cells for the screening assays.

6.4.3 CCP Library Assay - Bulk vs. Microfluidic

Bulk assay (Microtiter Plate Screen)

Bulk activity assays were conducted for both wild type CCP and the corresponding 0.25 mM $MnCl_2$ mutant library based on single colony isolates grown as 3 ml cultures. Twenty colonies were selected from both freshly transformed wild type and mutant library plates (*E. coli* BL21(DE3)) grown overnight at 30°C. The colonies were picked with sterile pipet tips and grown in modified LB broth (30µg/ml kanamycin, 1mM thiamine, 1mM glycine, 0.5 mM δ-ALA) at 37°C / 275 rpm for 4 hours to mid-log phase, as measured by absorption at 600 nm (OD_{600} =0.5-0.7). The supplemental factors in the LB culture are essential to produce the protoporphyrin group in the center of the CCP enzyme. To control the protein expression level and prevent the formation of improperly folded protein inclusion bodies in the bacteria, the temperature was reduced to 30°C for induction. After the addition of 0.2 mM IPTG, the cultures were returned to the shaker for an additional 6 hours (275 rpm). 1 ml of each culture was spun down in a 1.7 ml

Eppendorf tube (3000 rpm / 3 minutes) to remove the supernatant, washed twice in 1 ml PBS pH 7.2, and resuspended in 1 mL PBS. Substrate was prepared by adding 10 µl of 10 mM Amplex Red stock solution (in DMSO) to 1 mL PBS pH 7.2 containing 880 µM H_2O_2.

A microtiter-plate assay format was used to measure the activity of each culture. 10 µl of each washed culture and 90µl of substrate were added to wells of a black-bottom microtiter plate for fluorescence assays (Dynex, Microfluor 2). After incubation for 30 minutes at room temperature in the dark (due to the light sensitive nature of the Amplex Red substrate), the wells were read on a fluorometric microtiter plate reader (Molecular Devices, Gemini XS spectrofluorometer, λ_{ex}=560, λ_{em}=590). An activity profile was plotted, comparing the wild-type CCP and mutant enzyme cultures (Figure 6.4).

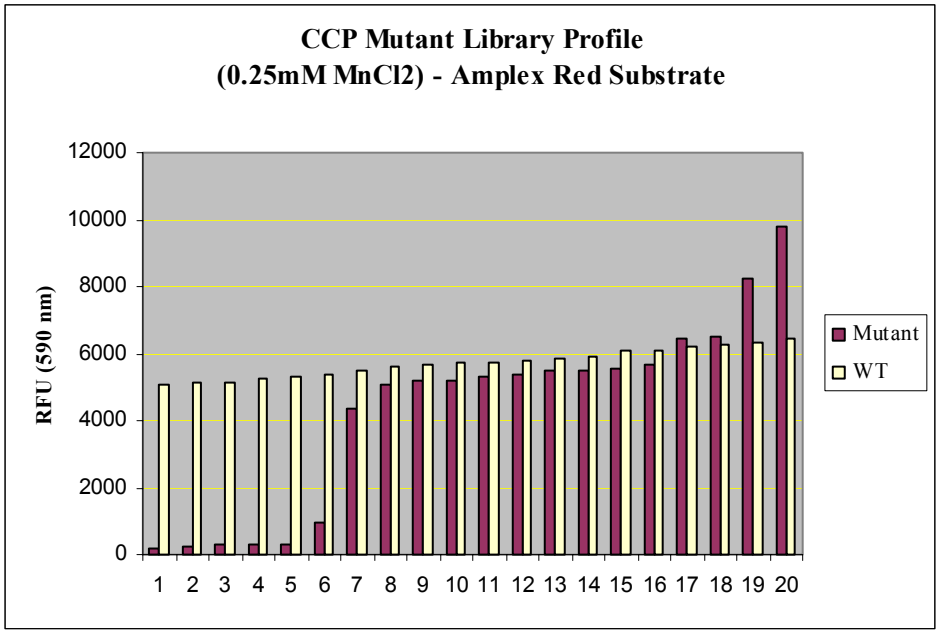

Figure 6.4: Activity profile of wild-type cytochrome c peroxidase (CCP) single colonies vs. CCP mutants generated by error-prone PCR (Amplex Red substrate).

Statistical analysis of the two populations revealed a fairly tight distribution of the activity profile for the wild-type CCP enzyme while the mutant population had a broad distribution with significant fraction of inactive clones. The wild type population had a median fluorescence value of 5725 RFU with a first-order standard deviation of 434 RFU (C.V. = 7.5%) while the corresponding values for the mutant population were 5264 and 2886 (C.V.= 67.2%). Background fluorescence (substrate only, no cells) in the assay was negligible at ~49 RFU.

Microfluidic Assay (Serpentine Array Chip Screen)

The microfluidic chip assays were designed to measure single-cell enzymatic activity levels within a cell population. Freshly transformed wild- type CCP and mutant library plates (*E. coli* BL21(DE3)), grown overnight at 30°C, were harvested using 3 ml of LB media and 3 mm sterile glass beads to remove all of the colonies on each plate (~1000 colonies / plate). Harvesting of plated transformants was done instead of simply transforming into broth to avoid biasing the population diversities of the cultures in favor of growth mutants. The harvested cell resuspensions were diluted 1:10 (due to high cell density) in modified LB medium (30μg/ml kanamycin, 1mM thiamine, 1mM glycine, 0.5 mM δ-ALA) plus 0.2 mM IPTG. The cell cultures were then induced for 6 hours in the shaker (30°C, 275 rpm). The cells were then washed and resuspended in PBS per the method described for the bulk CCP assay and put on ice. Substrate was prepared by adding 10 μl of 10 mM Amplex Red stock solution (in DMSO) to 1 mL ice cold PBS pH 7.2 containing 880 μM H_2O_2.

1024-well serpentine array chips were used to analyze the enzymatic activity of the wild type CCP and mutant libraries at the single-cell level. Washed wild-type and

mutant CCP cultures were separately diluted 1:500 in 1 ml ice-cold substrate and quickly injected into the central array regions of individual serpentine chips at 5 psi. The array sandwich valves were closed at ~15 psi and the compartmentalized mixtures were incubated at 22° C for 1 hour in the dark. After the incubation, the compartmentalized arrays in the chips were scanned with the GenePix scanner at 532 nm (Figure 6.5).

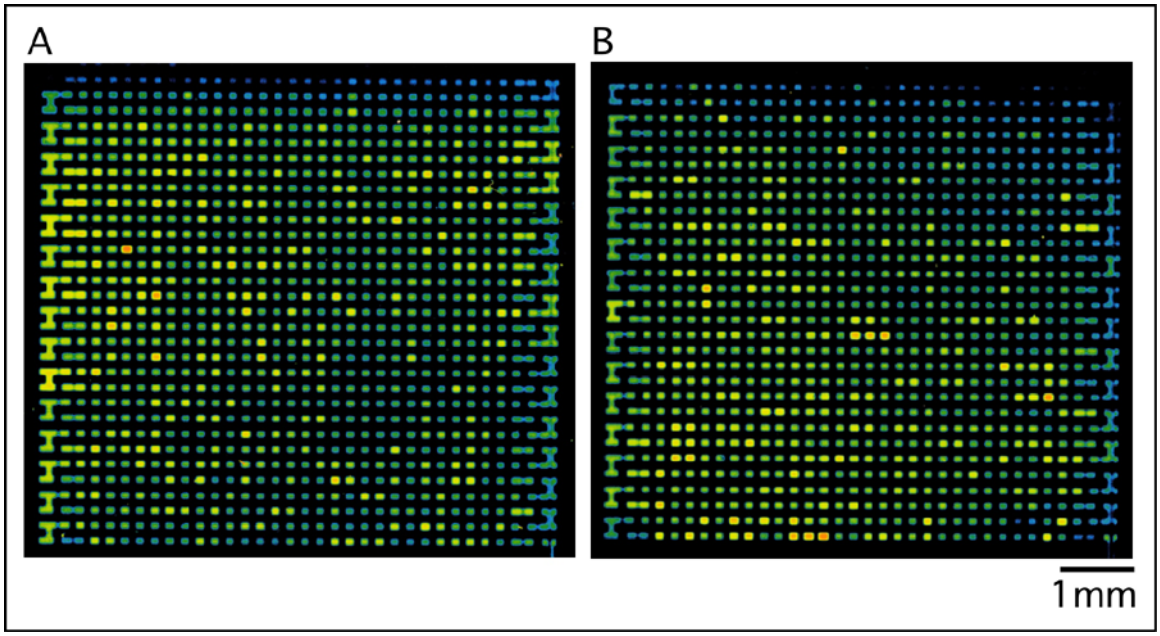

Figure 6.5: GenePix array scans of (A) compartmentalized CCP wild type cells and (B) 0.25 mM $MnCl_2$ CCP mutant library in Amplex Red substrate mix (880 µm H_2O_2, 100 µM Amplex Red, PBS pH 7.2) after 60 minute incubation at 20°C. Scan wavelength - 532 nm; Emission filter - 575nm df 35; Laser power - 1.7 mW; PMT power 600 W.

To correlate activity in each compartment with cell number, the bacteria in each compartment of the arrays were counted with a 60 x oil immersion lens (1.4 NA, Olympus) under the light microscope. The resulting data was used to create profiles of cell number vs. activity for the wild type CCP and mutant populations (Figures 6.6 and 6.7)

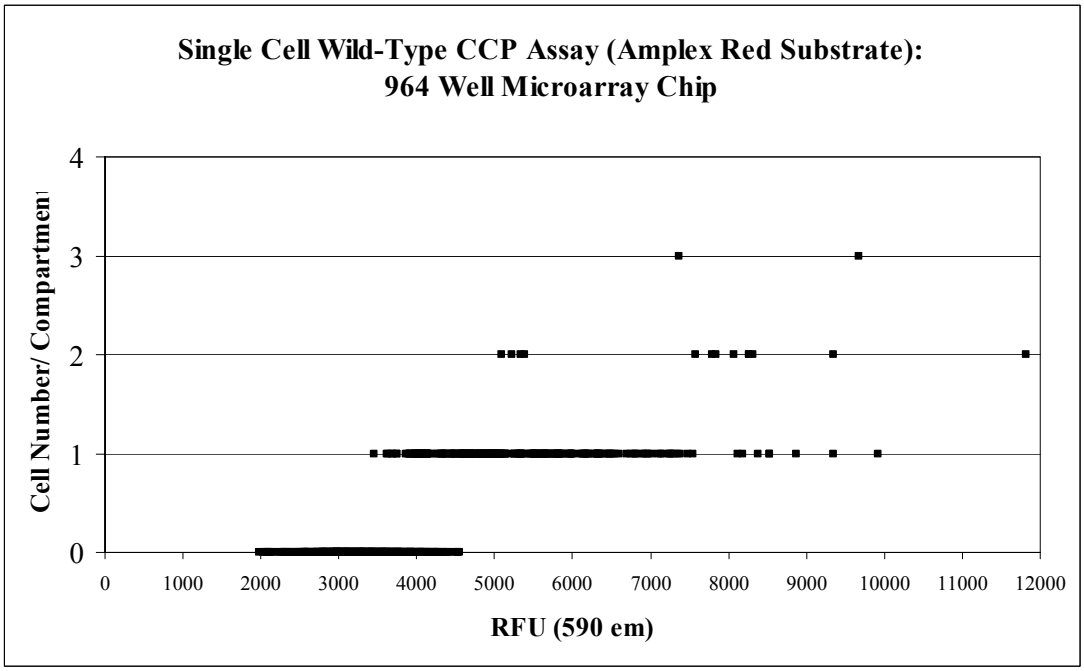

Figure 6.6: Cell number vs. activity profile for wild-type CCP in the 1024-well serpentine microarray chip.

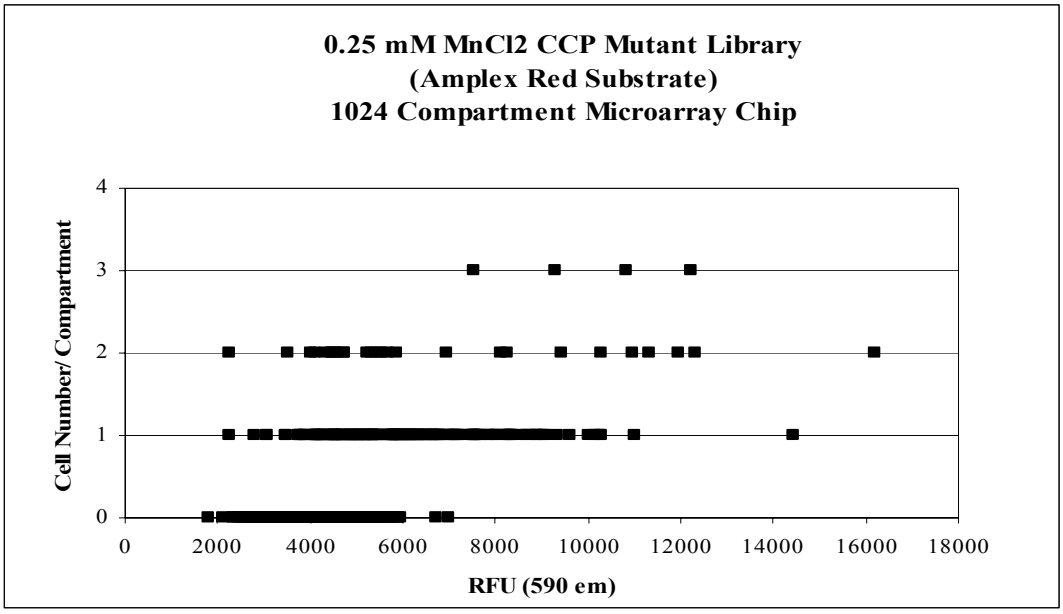

Figure 6.7: Cell number vs. activity profile for the 0.25 mM $MnCl_2$ randomly mutagenized CCP library in the 1024-well serpentine microarray chip.

Statistical analysis of the serpentine chip array assays revealed activity profiles for wild type CCP enzyme and the mutant library that were quite different than the respective microtiter plate profiles (Table 6.1). The primary difference between the

1024 Compartment Serpentine Chip - Amplex Red Assay

Wild-Type CCP	0 cells (n=611)	1 cell (n=240)	2 cells (n=13)
Average RFU	3283	5344	8233
Median RFU	3263	5097	7954
Standard Deviation	479	1127	3118
C.V.	14.60%	21.10%	37.90%

Average cells/compartment = 0.33

Mutant CCP Library	0 cells (n=560)	1 cell (n=276)	2 cells (n=26)
Average RFU	4472	5990	6932
Median RFU	4568	5814	5504
Standard Deviation	728	1545	3421
C.V.	16.30%	25.80%	49.40%

Average cells/compartment = 0.40

Table 6.1: 1024 compartment serpentine microfluidic chip assay (1 hour incubation at 22°C; Substrate - 100 μm Amplex Red, 880 μm H_2O_2 in PBS pH 7.2). Statistical analysis of raw resorufin product fluorescence levels (λ_{em} = 590 nm) in individual compartments (by cell number) comparing wild-type CCP (CCP-MKT variant) with 0.25 mM $MnCl_2$ mutant CCP library.

microtiter plate and the serpentine chip assays is the high background fluorescence in the chip (0 cells/ compartment). As the cells are resuspended in the substrate prior to loading and compartmentalization in the serpentine chip, the substrate becomes contaminated with free CCP enzyme, which creates background fluorescence in the cell-free

compartments during the incubation period. Subtracting the median background fluorescence from each cell-containing compartment prior to statistical analysis reveals a better representation of the true activity of the intracellular CCP activity at the single-cell level (Table 6.2).

1024 Compartment Serpentine Chip - Amplex Red Assay
Median Background Fluorescence Subtracted

Wild-Type CCP	1 cell (n=240)
Average RFU	2080
Median RFU	1826
Standard Deviation	1125
C.V.	54.10%

Average cells/compartment = 0.33

Mutant CCP Library	1 cell (n=276)
Average RFU	1421
Median RFU	1246
Standard Deviation	1595
C.V.	112.00%

Average cells/compartment = 0.40

Table 6.2: 1024 compartment serpentine microfluidic chip assay (1 hour incubation at 22°C; Substrate - 100 μm Amplex Red, 880μm H_2O_2 in PBS pH 7.2). Statistical analysis of single cell background-corrected resorufin product fluorescence levels (λ_{em} = 590 nm) in individual compartments of the serpentine chip comparing wild type CCP (CCP-MKT variant) with 0.25 mM $MnCl_2$ mutant CCP library.

The histogram plot of the background-subtracted wild-type and mutant CCP single cell activity levels in the microarray chip (Figure 6.8) is comparable to the bulk microtiter

profile shown in Figure 6.4, with ~25% of the single cell CCP mutants at or below the respective median background fluorescence level.

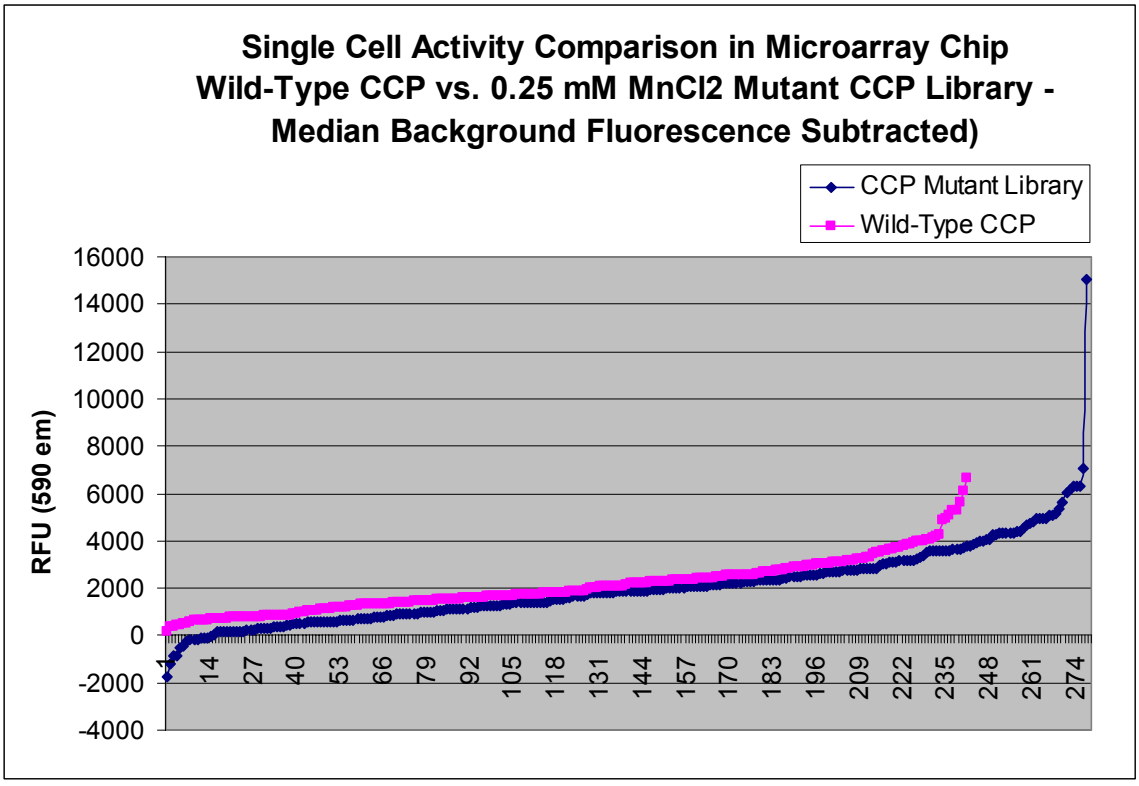

Figure 6.8: Single cell activity comparison for the wild-type CCP and the 0.25 mM $MnCl_2$ randomly mutagenized CCP library. Median background fluorescence levels were subtracted for each respective population.

Discussion

A comparison of the coefficient of variation (C.V.) values between the microtiter plate assay and the serpentine chip (with background subtraction) shows significantly more variation at the single-cell level than the population level in the microtiter plate. This result is not surprising as single bacterial cells have a polydisperse size distribution. Taking the ratio of the mutant library to wild-type CCP C.V. levels gives values of 8.96

for the microtiter plate vs. 2.07 for the compartments in serpentine chip containing a single cell. With higher wild-type CCP C.V. values at the single-cell level, the assay sensitivity drops and it becomes more difficult to identify mutants with activity levels only marginally higher than the wild-type enzyme. Wild-type single-cell CCP assays (background subtracted) in partitioned single compartments (~300 pL) of the comparator microfluidic chip had similar C.V. values (Table 6.3), ranging from 41.3 - 79.3%. The single-cell microfluidic assay sensitivity could be substantially improved by correcting for the relative cell size by staining the cells with second fluorescent dye or co-expression of a protein like GFP that has a non-overlapping emission spectra with the assay product. However, the scanning technology also needs to be improved to implement bacterial size calibration. The minimum pixel size is 5μm on the GenePix scanner, much larger than single gram-negative bacteria (1 μm wide x 2 μm long).

6.5 Conclusions

Increasing biocomplexity created by explosive advances in genomics and proteomics in the last decade has established the need for HTS technologies to transform the vast collections of data generated from these systems into organized knowledge[128]. Microarray-based microfluidic chips are poised to fill this role, using ultra-low sample volumes and multiplexing technology to provide high-density, addressable screening platforms for both *in vitro* and cell-based applications.

Microfluidic array chips reduce sample volumes from microliters to picoliters, making a good detection system an essential part of the screening platform. In this

chapter, several candidate technologies were discussed, ranging from an optical microscope equipped with a sensitive CCD camera to the commercial GenePix array scanner. While the optical microscopy setup provided an ultra-sensitive method for

WT CCP Data (comparator chip) -Set 1 (3/19/02) 6 hour induction, PMT = 600V	1 cell (n=56)
Average RFU	1228
Median RFU	1225
Standard Deviation	1022
C.V.	79.30%
WT CCP Data (comparator chip) -Set 1 (3/20/02) 6 hour induction, PMT = 600V	**1 cell (n=19)**
Average RFU	1024
Median RFU	1183
Standard Deviation	701
C.V.	68.50%
WT CCP Data (comparator chip) -Set 3 (3/23/02) 4 hour induction (PMT = 600V)	**1 cell (n=72)**
Average RFU	579
Median RFU	540
Standard Deviation	381
C.V.	65.70%
WT CCP Data (comparator chip) -Set 4 (3/28/02) 6 hour induction (PMT = 800V)	**1 cell (n=87)**
Average RFU	10110
Median RFU	9761.5
Standard Deviation	4122
C.V.	41.30%

Table 6.3: Microfluidic comparator chip assay (1 hour incubation at 22°C; Substrate - 100 µm Amplex Red, 880µm H_2O_2 in PBS pH 7.2). Statistical analysis of background-corrected resorufin product fluorescence levels (λ_{em} = 590 nm) in individual compartments containing single *E. coli* single cell expressing wild type CCP (CCP-MKT variant).

looking at a select number of individual compartments in the chips, the scanning systems were able to rapidly create fluorescence intensity maps of the entire arrays. As

microfluidic technologies continue to mature, system integration is likely to occur, combining Micro-Electrical-Mechanical Systems (MEMS) technology with microfluidics to make portable, low-cost HTS devices.

Library analysis at the single-cell level presents its own set of challenges. Expression level variability becomes not only dependent on the amino acid sequence of the recombinant enzyme, but also on enzyme content at the single cell level and the stage of the cell in its growth cycle. The effect of these additional factors is to add noise to the "fitness landscape" of an enzyme, an *n*-dimensional plot of sequence vs. activity[129]. This additional noise, which is averaged out in microtiter plate-bases assays that measure the average activity of an individual colony, makes selection of mutants with small improvements in activity more difficult to identify. However, array-based chips, which can rapidly screen thousands of bacteria, may be able to identify "super" mutants in a large mutagenized recombinant protein library (10^5 - 10^7) that may never be found by techniques that only sample a small fraction of the library diversity.

Although tremendous progress has been made in designing integrated, high-density microfluidic array chips consisting of thousands of picoliter-scale compartments, it is only the foundation for an exciting new platform having applications in a wide range of fields such as biochemistry, mechanical engineering, public health, and pharmacology. The main advantages of these new devices are rapid prototyping, sub-microliter consumption of reagents and sample, and disposability. While much of the research is still at the proof-of-concept stage, this technology has the potential to transform chemical analysis in the same way that miniaturization transformed computing, making tools that are smaller, more integrated, less expensive, and a lot faster[130].

Appendix A

Component List for Optical Valve:

1. Aluminum Breadboard- 6" x 6"

   Thorlabs: Part number MB6

2. 4" mounting posts

   Thorlabs: Part number P4A

3. 808nm TO3 package laser diode

   SLICorp: Part number SLI-CW-TO3-C1-808-2M-PD

4. TO3 mount/heat sink (connects to TO3 package pin-out)

   Unknown source; obtained from Dr. Kerry J. Vahala at Caltech

5. Angle bracket mount for TO3 mount/heat sink

   Thorlabs: Part number AB90

6. 0.68 NA aspheric lens

   Thorlabs: Part number C330TM-B

7. Aspheric lens adapter

   Thorlabs: Part number S1TM09

8. Post assembly for aspheric lens mount and achromat lens mounts

   Thorlabs: Part numbers TR3, RA90, TR2, B1A

9. Broadband dielectric mirrors

   Thorlabs: Part number BB1-R2

10. Kinematic mirror mount assembly

    Thorlabs: Part numbers KM1, B1AS

11. Achromat lenses (f=150mm) - 25mm diameter

    Edmund Optics: Part number 32-494

12. IR bandpass filter

    Edmund Optics: Part number 46051

13. Threaded cage plate for bandpass filter mount

    Thorlabs: Part number CD02

14. Mounting cube assembly

    Thorlabs: Part numbers C4W(1), B1C(3)

15. Aluminum right angle bracket for cube mount (1x1" on side)

    Self-fabricated in machine shop to specifications

16. 100x 1.25 NA achromat objective

    Olympus America

17. 6" extension tube for CMOS

    Thorlabs: Part number SM1E60

18. CMOS camera (chip package with power and video out connects)

    Beamsplitter (700 nm short pass) -25 x 50mm

    Chroma Technology: Part number 700CPSP

19. Beamsplitter mount

    Fabricated in machine shop to specifications

20. Aluminum chip stage (chip holder) - mounts to XYZ linear stage

    Self-fabricated in machine shop

21. XYZ linear stage

    Newport: Cat # 460A-XYZ

Appendix B

Schematic for Solid-State FACS:

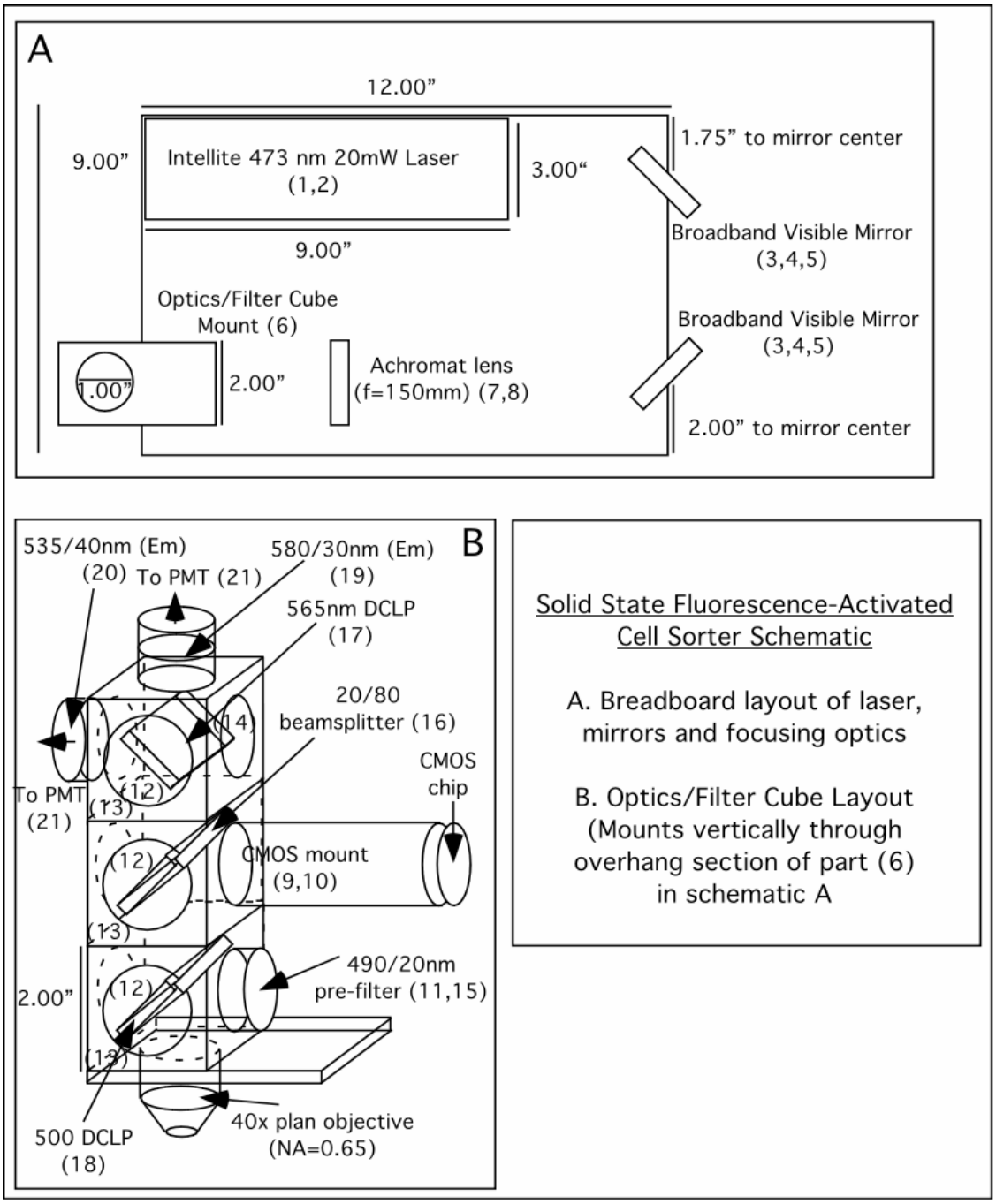

Component List for Solid-State FACS:

1. Intellite solid-state diode-pumped blue laser (λ=473nm)

   Intellite: Part number BSF73-20P

2. Aluminum plate for heat sink/ height adjustment of laser beam

   2024 aluminum (9.00" x 3.50" x 0.25")

   Mounting holes - .250"

3. Kinematic mirror mount

   Thorlabs: Part number KM1

4. Base plate

   Thorlabs: Part number B1AS

5. Broadband visible mirror - 01" diameter

   Thorlabs: Part number BB1-R1

6. Bracket for cube/ lens mount

   2024 aluminum - 0.25" stock

   2.00" x 4.00" x 0.25"

   1.00" through hole 1.00" on center from one end

   0.25" mounting holes to breadboard

7. Achromat lens (f=150 mm) – 25 mm diameter

   Edmund Optics: Part number 32-494

8. Lens mount for 1" optics

   Thorlabs: Part number LMR1

9. 1" adjustable focus tube

   Thorlabs: Part number SM1V10

   Achromat lens (f=125 mm) – 25 mm diameter

   Edmund Optics: Part number 32-491

10. 2" lens tube

    Thorlabs: Part number SM1L20

11. 490/20nm bandpass pre-filter (25mm diameter)

    Chroma Technology

12. Kinematic mounting platform

    Thorlabs: Part number B4C

13. Mounting Cube (2.00" square)

    Thorlabs: Part number C4W

14. Blank cover plate (1.00" diameter)

    Thorlabs: Part number B2C

15. 0.50" lens tube

    Thorlabs: Part number SM1L05

16. 20/80 beamsplitter (25 x 50 mm)

    Chroma Technology

17. 565 nm DCLP (25 x 50mm)

    Chroma Technology

18. 500 nm DCLP (25 x 50mm)

    Chroma Technology

19. 580/30 nm emission filter (25mm diameter)

    Chroma Technology

20. 535/40 nm emission filter (25mm diameter)

    Chroma Technology

21. Photomultiplier tube

    Hamamatsu: Part number C6271

Bibliography

[1] L. Mere *et al*. Miniaturized FRET assays and microfluidics: key components for ultra-high throughput screening. *Drug Discov. Today* **4**, 363 (1999)

[2] D. Walt. Bead-based fiber-optic arrays. *Science* **287**, 451 (2000)

[3] A. W. Czarnik. Encoding methods for combinatorial chemistry. *Curr. Opin. Chem. Biol.* **1**, 60 (1997)

[4] B. J. Battersby and M. Trau. Novel miniaturized systems in high-throughput screening. *Trends Biotech*. **20** (4), 167 (2002)

[5] S. A. Sundberg *et al*. Microchip-based systems for target validation and HTS. *Drug Discov. Today* **5**, 223 (2000)

[6] Z. H. Fan *et al*. The high-throughput screening infrastructure: the right tools for the task. *J. Biomol. Screening* **4**, 143 (1999)

[7] B. Eckstrom, G. Jacobsen, O. Ohman, and H. Sjodin. International Patent WO 91/16966. (1990)

[8] R. M. McCormick, R. J. Nelson, M. G. Alonso-Amigo, D. J. Benvegnu, and H. H. Hooper. Microchannel Electrophoretic Separations of DNA in Injection-Molded Plastic Substrates. *Anal. Chem*. **69**, 2626 (1997)

[9] L. Martynova, L. E. Locasico, M. Gaitan, G. W. Kramer, and R. G. Christiansen. Fabrication of Plastic Microfluid Channels by Imprinting Methods. *Anal. Chem*. **69**, 4783 (1997)

[10] H-P. Chou, C. Spence, A. Scherer, and S. R. Quake. A microfabricated device for sizing and sorting DNA molecules. *Proc. Natl. Acad. Sci.* **96**(1): 11 (1999)

[11] H-P. Chou, C. Spence, A. Scherer, and S. R. Quake. A microfabricated device for sizing DNA and sorting cells. *Proc. SPIE* **3258**: 181 (1998)

[12] H. Becker and C. Gartner. Polymer microfabrication methods for microfluidic analytical applications. *Electrophoresis* **21**, 12 (2000)

[13] Y. Kodera and B. J. McCoy. Distribution kinetics of polymer thermogravimetric analysis: A model for chain-end and random scission. *Energy and Fuels* **16** (1): 119 (2002)

[14] J. M. O'Reilly and F. E. Karasz. Specific heat studies of transition and relaxation behavior in polymers. *J. Poly. Sci. C* **14**, 49 (1966)

[15] J. Jancar. Structure-property relationships in thermoplastic matrices. *Adv. Polymer Sci.* **139**: 1 (1999)

[16] T. H. Lane. Silica, silicon, and silicones...unraveling the mystery. Dow Corning Corporation (1995)

[17] G. M. Whitesides, E. Ostuni, S. Takayama, X. Jiang, and D. E. Ingber. Soft lithography in biology and chemistry. *Ann. Rev. Biomed. Eng.* **3**: 335 (2001)

[18] White paper - Vulcanization/Curing of Silicone Rubber - HVI Workshop. *General Electric Corp.* (2001)

[19] M. A. Unger, H-P. Chou, T. Thorsen, A. Scherer, and S. R. Quake. Monolithic Microfabricated Valves and Pumps by Multilayer Soft Lithography. *Science* **288**:113 (2000)

[20] M. K. Chaudhury and G. M. Whitesides. Direct Measurement of interfacial interactions between semispherical lenses and flat sheets of polydimethylsiloxane and their chemical derivatives. *Langmuir* **7**:1013 (1991)

[21] M. K. Chaudhury and G. M. Whitesides. Correlation between surface free energy and surface constitution. *Science* **255**: 1230 (1992)

[22] H. Ng, I. Manaszloczo, and M. Shmorhun. Moldability studies for the reaction injection molding of dicyclopentadiene. *Polymer Eng. Sci.* **34** (11): 929 (1994)

[23] White paper - Urethane Acrylate Oligomers. *Sartomer* (2001)

[24] J. Walia. Understanding the processes and benefits of Nitrogen inerting for UV curable coatings. *RadTech* (2000)

[25] J. P. Fouassier and J. F. Rabek. Radiation Curing in Polymer Science and Technology. *Elsevier Applied Science, Vol. II*. p.242 (1993)

[26] B. J. Battersby and M. Trau. *Trends Biotech*. **20** (4): 167 (2002)

[27] M. Beggs. HTS - where next? *Drug Discovery World*. **2** 25 (2001)

[28] K. Macounova, C. R. Cabrera, and P. Yager. *Anal Chem*, **73** (7): 1627 (2001)

[29] M. Abrantes, M. T. Magone, L. F. Boyd, and P. Schuck. *Anal Chem*, **73** (13): 2828 (2001)

[30] E. T. Lagally, I. Medintz, and R. A. Mathies. *Anal Chem.* **73** (3): 565 (2001)

[31] J. Wang, A. Ibanez, M. P. Chatrathi, and A. Escarpa. *Anal Chem.* **73** (21): 5323-5327 (2001)

[32] N. C. Wrighton *et al*. Small peptides as potent mimetics of the protein hormone erythropoetin. *Science* **273**, 458 (1996)

[33] C. L. Chirinos-Rojas *et al*. A peptidomimetic antagonist of TNF-alpha-mediated cytotoxicity identified from a phage-displayed random peptide library. *J. Immunol*. **161**: 5621 (1998)

[34] N. Cohen, S. Abramov, Y. Dror and A. Freeman. *In vitro* enzyme evolution: the screening challenge of isolating the one in a million. *Trends Biotech*. **19** (12): 507 (2001)

[35] M. Olsen *et al*. Function-based isolation of novel enzymes from a large library. *Nature Biotech.* **18**, 1071 (2000)

[36] N. Maurer, D. B. Fenske, and P. R. Cullis. Developments in liposome drug delivery systems. *Expert Opin. Biol. Therapy* **1** (6): 923 (2001)

[37] H. Hauser. Spontaneous vesiculation of uncharged phospholipid dispersions consisting of lecithin and lysolecithin. *Chem Phys Lipids* **43** (4):283 (1987)

[38] D. S. Tawfik and A. D. Griffiths. Man-made cell-like compartments for molecular evolution. *Nature Biotechnol*. **16** (7): 652 (1998)

[39] J. Bibette, F. L. Calderon, and P. Poulin. Emulsions: Basic Principles. *Rep. Prog. Phys*. **62**: 969 (1999)

[40] D. W. R. Gruen and D. A. Haydon. The absorption of N-alkanes into bimolecular lipid layers - theory and experiment. *Pure and Applied Chem.* **52**, 1229 (1980)

[41] P. G. Nilsson and B. Lindman. Water self-diffusion in non-ionic sufactant solutions - hydration and obstruction effects. *J. Phys. Chem.* **87**, 4756 (1983)

[42] S. Omi. K. Katami, A. Yamamoto, and M. Iso. Synthesis of polymeric microspheres employing SPG emulsification technique. *J. Appl. Polymer Sci*. **51** (1): 1 (1994)

[43] S. Omi. Preparation of monodisperse microspheres using Shirasu porous glass emulsification technique. *Colloids Surf. A*. **109**, 97 (1996)

[44] S. Peng and R. A. Williams. Controlled production of emulsions using a crossflow membrane. *Part. Part. Syst. Charact*. **15**, 21 (1998)

[45] M. C. Cross and P. C. Hohenberg. Pattern-formation outside of equilibrium. *Rev. Mod. Phys.* **65**: 851 (1993)

[46] J. P. Gollub and J. S. Langer. Pattern formation in non-equilibrium physics. *Rev. Mod. Phys.* **71**: S396 (1999)

[47] For two interesting exceptions, see R. H. Liu *et al*. *J. Microelectromech. Sys.* **9**:190 (2000) and D. Bokenkamp *et al. Anal. Chem.* **70**: 232 (1998)

[48] J. P. Brody, P. Yager, R. E. Goldstein, and R. H. Austin. Biotechnology at low Reynolds numbers. *Biophys. J*. **71** (1996)

[49] G. M. Whitesides and A. D. Stroock. Flexible methods in microfluidics. *Physics Today (online)* **54**: 6 (2001)

[50] G. Mason. New fundamental concepts in emulsion rheology. *Curr. Opin. Colloid In.* **4**: 231 (1999)

[51] P. B. Umbanhowar, V. Prasad, and D. A. Weitz. Monodisperse emulsion generation via drop break off in a coflowing stream. *Langmuir* **16**, 347 (2000).

[52] T. Kawakatsu, T. *et al.* Effect of microchannel structure on droplet size during crossflow microchannel emulsification. *J. Surf. Deterg.*, **3**, 295-302 (2000)

[53] T. G. Mason and J. Bibette. Shear rupturing of droplets in complex fluids. *Langmuir* **13**, 4600 (1997).

[54] T. Nakashima and M. Shimizu. *Kagaku Kogaku Ronbunshu*, **19**, 984 (1993).

[55] S. J. Peng and R. A. Williams. Controlled production of emulsions using a crossflow membrane part I: Droplet formation from a single pore. *Chem. Eng. Res. Des.* **76**: (A8) 894 (1998)

[56] L. D.Landau and E. M. Lifshitz. *Fluid Mechanics* (Pergamon Press, London, ed. 1, 1959), p. 233. [first edition]

[57] G. I. Taylor. The formation of emulsions in definable field of flow. *Proc. R. Sc. A*. **146**, 501 (1934)

[58] C.-W. Park and G. M. Homsy. Two-phase displacement in Hele-Shaw cells: Theory. *J. Fluid Mech*. **139**, 291 (1984)

[59] A. Borhan and J. Pallanti. Breakup of drops and bubbles translating through cylindrical capillaries. *Phys. Fluids* **11** (10): 2846 (1999)

[60] M. J. Martinez and K. S. Udell. Axisymmetric creeping motion of drops through circular tubes. *J. Fluid Mech*. **210**, 565 (1990)

[61] W. L. Olbricht and D. M. Kung. The deformation and breakup of liquid drops at low Reynolds number flow through a capillary. *Phys. Fluids*. **4** (7): 1347 (1992)

[62] Collection of papers in IBM Journal, **21** (1), (1977)

[63] P. A. Torpey and R. G. Markham. Thermal inkjet printhead, Xerox Corporation, U.S. Patent No. 4638337, January 1987

[64] S. A. Elrod. Capillary wave controllers for nozzleless droplet injectors. Xerox Corporation, U.S. Patent No. 4878461, May 1988

[65] S. Kamisuki *et al*. A low power, small electrokinetically driven commercial inkjet head. *Proc. IEEE Micro Elect. Mech. Sys.* Heilderberg, Germany, p.63 (1998)

[66] T. R. Powers. D. Zhang, R. E. Goldstein and H. A. Stone. Propagation of a topological transition: the Rayleigh instability. *Phys. Fluids*, **10**(5): 1052 (1998)

[67] T. R. Powers and R. E. Goldstein. Pearling and pinching: propagation of Rayleigh instabilities. *Phys. Rev. Lett*. **78**, 2555 (1997)

[68] H. A. Stone, B. J. Bentley and L. G. Leal. An experimental study of the transient effects in the breakup of viscous drops. *J. Fluid Mech.* **173**, 131 (1986)

[69] A. Ashkin. Acceleration and trapping of particles by radiation pressure. *Phys. Rev. Lett*. **24**:156 (1970)

[70] A. Ashkin. Applications of laser radiation pressure. *Science* **210**:1081 (1980)

[71] A. Ashkin, J. M. Dziedzic, J. E. Bjorkholm, and S. Chu. Observation of a single-beam gradient force optical trap for dielectric particles. *Opt. Lett.* **11**:288 (1986)

[72] J-C. Meiners and S. Quake. Direct Measurement of Hydrodynamic Cross Correlations between Two Particles in an External Potential. *Phys. Rev. Lett.* **82**(10): 2211 (1999)

[73] A. Emmer, M. Jansson, J. Roeraade, U. Lindgerg, and B. Hok. Fabrication and characterization of a silicon microvalve. *J. Microcol. Separ.* **4** (1): 13 (1992)

[74] R. Zengerle, J. Ulrich, S. Kluge, M. Richter, and A. Richter. A bi-directional silicon micropump. *Sens. Actua. A* **50** (1-2): 81 (1995)

[75] M.J. Fulwyler. Flow cytometry and cell sorting. *Blood Cells* **6**(2):173 (1980)

[76] K.L. Johnson. Basics of flow cytometry. *Clin. Lab. Sci*. **5**(1):22-4 (1992)

[77] M. J. Olsen *et al*. Function-based isolation of novel enzymes from a large library. *Nature Biotech*. **18** (10): 1071 (2000)

[78] A. Y. Fu, C. Spence, A. Scherer, F. H. Arnold, and S. R. Quake. A microfabricated fluorescence-activated cell sorter. *Nature Biotech.* **17**: 1109 (1999)

[79] A. Y. Fu, H-P. Chou, C. Spence, F. H. Arnold, and S. R. Quake. An integrated microfabricated cell sorter. *Anal. Chem.* **74** (11): 2451 (2002)

[80] P. L. Luisi, M. Giomini, M. P. Pileni, and B. H. Robinson. Reverse micelles as hosts for proteins and small molecules. *Biochim. Biophys. Acta*. **947**: 209 (1988)

[81] S. Barbaric and P. L. Luisi. Micellar solubilization of biopolymers in organic solvents. *J. Am. Chem. Soc.* **103**: 4239 (1981)

[82] C. Grandi, R. E. Smith and P. L. Luisi. Micellar solubilization of bioploymers in organic solvents - activity and conformation of lysozyme in isooctane reverse micelles. *J. Biol. Chem.* **256**: 837 (1981)

[83] P. D. I. Fletcher *et al*. Reactivity of alpha-chymotripsin in water-in-oil microemulsions. *Colliod Surfaces* **10**, 193 (1984)

[84] K. Martinek *et al*. Micellar enzymology. *Eur. J. Biochem.* **155**: 453 (1986)

[85] A. V. Levashov *et al*. Superactivity of acid-phosphatase entrapped into surfactant revesed micelles in organic solvents. *Dokl. Akad. Nauk SSSR*. **289**: 1271 (1986)

[86] P. H. Poon and M. A. Wells. Physical studies of egg phosphatidylcholine in di-ethyl ether water solutions. *Biochemistry* **13**: 4928 (1974)

[87] A. Sanchez-Ferrer and F. Garcia-Carmona. Reverse vesicles as a new system for studying enzymatic activity in organic solvents. *Biochem. J.* **285**: 373 (1992)

[88] R. Bru, A. Sanchez-Ferrer, and F. Garcia-Carmona. The effect of substrate partitioning on the kinetics of enzymes acting in reverse micelles. *Biochem. J.* **285**: 373 (1992)

[89] Y. R. Chen, S. Usui, S. R. Queener, and C. A. Yu. Purification and properties of a p-nitrobenzy esterase from *B. subtiliis*. *J. Indist. Micro*. **15**: 10 (1995)

[90] J. C. Moore and F. H. Arnold. Directed evolution of a para-nitrobenzyl esterase for aqueous-organic solvents. *Nature Biotech*. **14**:458 (1996)

[91] L. Giver *et al*. Directed evolution of a thermostable esterase. *Proc. Natl. Acad. Sci.* **95** (22): 12809 (1998)

[92] E. Ostuni, R. Kane, C. S. Chen, D. E. Ingber, and G. M. Whitesides. Patterning mammalian cells using elastomeric membranes. *Langmuir* **16** (20): 7811 (2000)

[93] L. Griscom , P. Degenaar, B. LePioufle, E. Tamiya, and H. Fujita. Cell placement and neural guidance using a three-dimensional microfluidic array. *Jap. J. Applied Physics* **40** (9A): 5485 (2001)

[94] C. D. James *et al.* Patterned protein layers on solid substrates by thin stamp microcontact printing. *Langmuir* **14** (4): 741 (1998)

[95] J. Lahiri, E. Ostuni, and G. M. Whitesides. Patterning ligands on reactive SAMs by microcontact printing. *Langmuir* **15** (6): 2055 (1999)

[96] L. Mere *et al*. Miniaturized FRET assays and microfluidics: key components for ultra-high-throughput screening. *Drug Discovery Today* **4** (8): 363 (1999)

[97] K. Hosokawa, T. Fujii, and I. Endo. Handling of picoliter liquid samples in a poly(dimethylsiloxane)-based microfluidic device. *Anal. Chem*. **71** (20): 4781 (1999)

[98] A. D. Stroock *et al.* Chaotic mixer for microchannels. *Science* **295** (5555): 647 (2002)

[99] T. J. Johnson, D. Ross, and L. E. Locascio. Rapid microfluidic mixing. *Anal. Chem.* **74** (1): 45 (2002)

[100] T. Thorsen, R. W. Roberts, F. H. Arnold, and S. R. Quake. Dynamic Pattern Formation in a Vesicle-Generating Microfluidic Device. *Phys. Rev. Lett.* **86**: 4163 (2001).

[101] H. Andersson, W. van der Wijngaart, and G. Stemme. Patterned self-assembled beads in silicon channels. *Electrophoresis* **22** (2): 249-257 (2001)

[102] J. Zeng *et al*. Design Analyses of Capillary Burst Valves in Centrifugal Microfluidics. *Tech. Proc. Micro. Total Anal. Syst*. 493 (2000)

[103] T. R. Reid. *The Chip: How Two Americans Invented the Microchip and Launched a Revolution*, New York: Simon and Schuster, 1984

[104] A. G. Hadd, S. C.Jacobson, and J. M. Ramsey. Microfluidic assays of acetylcholinesterase inhibitors. *Anal. Chem.* **71** (22): 3407 (1997)

[105] D. J. Harrison *et al*. Micromachining a miniaturized capillary electrophoresis-based chemical analysis system on a chip. *Science* **261** (5123): 895 (1993)

[106] P. C. H. Li and D. J. Harrison. Transport, manipulation, and reaction of biological cells on-chip using electrokinetic effects. *Anal. Chem.* **69** (8): 1564 (1997)

[107] A. G. Hadd, D. E. Raymond, J. W. Haliwell, S. C. Jacobson, and S. C. Ramsey. Microchip device for performing enzyme assays. *Anal. Chem.* **69** (17): 3407 (1997)

[108] E. T. Lagally, I. Medintz, and R. A. Mathies. Single-molecule DNA amplification and analysis in an integrated microfluidic device. *Anal. Chem*. **73** (3): 565 (2001)

[109] J. Khandurina *et al*. Integrated system for rapid PCR-based DNA analysis in microfluidic devices. *Anal. Chem*. **72** (13): 2995 (2000)

[110] E. Eteshola and D. Leckband. Development and characterization of an ELISA assay in PDMS microfluidic channels. *Sens. Actua. B*. **72** (2): 129 (2001)

[111] J. Wang, A. Ibanez, M. P. Chatrathi, and A. Escarpa. Electrochemical enzyme immunoassays on microchip platforms. *Anal. Chem*. **73** (21): 5323 (2001)

[112] L. Buchaillot, E. Farnault, M. Hoummady, and H. Fujita. Silicon nitride thin films Young's modulus determination by an optical non destructive method. *Jpn. J. Appl. Phys. 2* **36**, L794 (1997)

[113] M. Templin *et al*. Protein microarray technology. *Trends Biotech.* **20** (4): 160 (2002)

[114] R. P. Elkins *et al*. Multispot, multianalyte immunoassay. *Ann. Biol. Clin. (Paris)* **48**: 655 (1990)

[115] E. S. Lander *et al*. Initial sequencing and analysis of the human genome. *Nature* **409**: 860 (2001)

[116] J. C. Venter *et al*. The sequence of the human genome. *Science* **291**: 1304 (2001)

[117] G. Ramsay. DNA chips: state-of-the-art. *Nature Biotech.* **16**: 40 (1998)

[118] G. MacBeath and S.L. Schreiber. Prinitng proteins as microarrays for high-throughput function determination. *Science* **289**: 1760 (2000)

[119] B. Schweitzer *et al*. Immunoassays with rolling circle DNA amplification: a versatile platform for ultrasensitive antigen detection. *Proc. Natl. Acad. Sci. USA* **97**: 10113 (2000)

[120] P. Arenkov *et al*. Protein microchips: use for immunoassay and enzymatic reactions. *Anal. Biochem.* **278**: 123 (2000)

[121] R. S. Kane, S. Takayama, E. Ostuni, D. E. Ingber, and G. M. Whitesides. Patterning proteins and cells using soft lithography. *Biomaterials* **20**: 2363 (1999)

[122] G. A. Martin, R. Kawaguchi, A. DeGiovanni, M. Fukushima, and W. Mutter. High-yield, in vitro protein expression using a continuous-exchange, coupled transcription/translation system. *Biotechniques* **31** (4): 948 (2001)

[123] L. Jermutus, L. A. Ryabova, and A. Pluckthun. Recent advances in producing and selecting functional proteins by using cell-free translation. *Curr. Opin. Biotech.* 9 (5): 534 (1998)

[124] A. M. Altschul, R. Abrams, and T. R. Hogness. Cytochrome c peroxidase. *J. Biol. Chem*. **136**: 777 (1940)

[125] B. Chance. *Enzymes and Enzyme Systems*, p.93 (1951)

[126] A. F. W. Coulson, J. E. Erman, and T. Yonetani. Studies on cytochrome c peroxidase. XVII. Stoichiometry and mechanism of the reaction of compound ES with donors. *J. Biol. Chem*. **246**: 917 (1971)

[127] J. Roe and D. B. Goodin. Enhanced oxidation of aniline derivatives by two mutants of cytochrome c peroxidase at tryptophan 51. *J. Biol. Chem*. **268**: 20037 (1993)

[128] J. Khandurina and A. Guttman. Microchip-based high-throughput screening analysis of combinatorial libraries. *Curr. Opin. Chem. Biol.* **6**: 359 (2002)

[129] M. Smith. Natural selection and the concept of a protein space. *Nature* **225**, 563 (1970)

[130] A. P. Sassi, Q. F. Xue, and H. H. Hooper. Making analysis in the life sciences faster through miniaturization. *Amer. Laboratory* **32** (20): 36 (2000)